NASA TECHNICAL NOTE

NASA TN D-6332
C. 1

NASA TN D-6332

THERMAL BUCKLING ANALYSIS FOR STIFFENED ORTHOTROPIC CYLINDRICAL SHELLS

by L. K. Chang and Michael F. Card

Langley Research Center
Hampton, Va. 23365

NATIONAL AERONAUTICS AND SPACE ADMINISTRATION • WASHINGTON, D. C. • APRIL 1971

1. Report No. NASA TN D-6332	2. Government Accession No.	3. Recipient's Catalog No.
4. Title and Subtitle THERMAL BUCKLING ANALYSIS FOR STIFFENED ORTHOTROPIC CYLINDRICAL SHELLS*		5. Report Date April 1971
		6. Performing Organization Code
7. Author(s) L. K. Chang** and Michael F. Card		8. Performing Organization Report No. L-7021
		10. Work Unit No. 722-02-10-02-23
9. Performing Organization Name and Address NASA Langley Research Center Hampton, Va. 23365		
		11. Contract or Grant No.
		13. Type of Report and Period Covered Technical Note
12. Sponsoring Agency Name and Address National Aeronautics and Space Administration Washington, D.C. 20546		
		14. Sponsoring Agency Code

15. Supplementary Notes

*Part of the information herein was presented at the AIAA/ASME 11th Structures, Structural Dynamics, and Materials Conference.

**NRC-NASA Resident Research Associate, now at Argonne National Laboratory, Argonne, Ill.

16. Abstract

A theory for thermal buckling of an orthotropic, multilayered, stiffened cylindrical shell is presented. The theory includes the effects of eccentricity of layers and stiffening, and deformations prior to buckling. It is sufficiently general to account for discrete rings and averaged properties of longitudinal stiffening, as well as arbitrary temperature distributions through the thickness of the shell and depth of the stiffeners. Two computer programs are described corresponding to solutions for buckling obtained by using finite differences and determinant plotting or modal iteration.

Computed results for thermal buckling of unstiffened and ring-stiffened shells are presented and are in reasonable agreement with published results. The interaction of thermal loading and axial compression in two large-diameter stiffened shells representative of a launch vehicle interstage and a preliminary supersonic transport fuselage design is investigated. Results indicate that buckling can occur in both structures at a realistic temperature under thermal loading alone.

17. Key Words (Suggested by Author(s)) Thermal buckling Cylindrical shells Stiffened orthotropic shells	18. Distribution Statement Unclassified — Unlimited

19. Security Classif. (of this report) Unclassified	20. Security Classif. (of this page) Unclassified	21. No. of Pages 87	22. Price* $3.00

THERMAL BUCKLING ANALYSIS FOR STIFFENED
ORTHOTROPIC CYLINDRICAL SHELLS*

By L. K. Chang** and Michael F. Card
Langley Research Center

SUMMARY

A theory for thermal buckling of an orthotropic, multilayered, stiffened cylindrical shell is presented. The theory includes the effects of eccentricity of layers and stiffening, and deformations prior to buckling. It is sufficiently general to account for discrete rings and averaged properties of longitudinal stiffening, as well as arbitrary temperature distributions through the thickness of the shell and depth of the stiffeners. Two computer programs are described corresponding to solutions for buckling obtained by using finite differences and determinant plotting or modal iteration.

Computed results for thermal buckling of unstiffened and ring-stiffened shells are presented and are in reasonable agreement with published results. The interaction of thermal loading and axial compression in two large-diameter stiffened shells representative of a launch vehicle interstage and a preliminary supersonic transport fuselage design is investigated. Results indicate that buckling can occur in both structures at a realistic temperature under thermal loading alone.

INTRODUCTION

Advanced aerospacecraft of the seventies, such as space shuttles and hypersonic aircraft, will probably experience severe thermal environments during flight. A renewal of interest in thermal stress and thermal buckling problems is anticipated, since it is unlikely that thermal protection can completely eliminate stresses and deformations arising from thermal gradients in stiffening frameworks, bulkheads, and covers. Thermal buckling problems in unstiffened shells have been investigated in references 1 to 8. Results for stiffened and sandwich shells are given in reference 3 and references 9 to 12. An excellent summary of existing thermal buckling analyses and experiments is given in reference 13. A review of these references, however, indicates that further studies of thermal buckling in stiffened, multilayered shells are needed.

Recent advances in computer technology together with derivations of more consistent buckling theories (refs. 14 to 17) permit the development of buckling analyses which accurately account for thermal stresses and deformations in stiffened shells. The purpose of the present paper is to present an analysis for thermal buckling of stiffened cylindrical shells, to describe two computer programs based on solutions for buckling, and to report the results of thermal buckling calculations for unstiffened and stiffened cylindrical shells.

The analysis was developed by extending the theory of reference 17. The theory is sufficiently general to account for the averaged properties of longitudinal stiffening and multiple orthotropic layers with differing coefficients of expansion as well as arbitrary temperature gradients through the thickness of the shell and depth of the stiffeners. A general outline of the theory is given and buckling solutions suitable for rapid computer calculations are presented. Two computer programs based on determinant plotting and modal iteration are described. Results of computations for unstiffened and ring-stiffened cylindrical shells under thermal loads are compared with results from existing buckling theory. Results are presented to demonstrate the effects of interactions of axial compressive loads and thermal loads on buckling of large-diameter cylinders typical of those which might be considered for an interstage structure of a launch vehicle and a fuselage of a supersonic transport.

SYMBOLS

The units used for the physical quantities in this report are given both in U.S. Customary Units and in the International System of Units (SI). A table of conversion factors is given in appendix A. The relationship between these two systems of units can be found in reference 18.

A   cross-sectional area of stiffener

A_i, B_i, C_i 4×4 matrices defined after equation (C16)

C_{ij} extensional stiffness of stiffened shell wall (eqs. (B10))

D_{ij} bending stiffness of composite shell wall (eqs. (B10))

E   Young's modulus

E_x, E_y Young's moduli of orthotropic layer of shell

G	shear modulus
G_{xy}	shear modulus of orthotropic layer of shell
I	moment of inertia of stiffener about its centroid
J	torsional constant for stiffener
K_{ij}	stiffnesses associated with coupling between bending and extension (eqs. (B10))
M	buckling-moment variation with x as defined by equations (C13)
$M_x, M_y,$ M_{xy}, M_{yx}	moment resultants for stiffened shell
M_{Tx}, M_{Ty}	thermal moment resultants in multilayered shell
M_{Ts}, M_{Tr}	thermal moment resultants in stringers and rings, respectively
N	number of rings
N_x, N_y, N_{xy}	stress resultants for stiffened shell
$\hat{N}_x$	magnitude of applied compressive load at ends of cylinder
N_{Tx}, N_{Ty}	thermal stress resultants in multilayered shell
N_{Ts}, N_{Tr}	thermal stress resultants in stringers and rings, respectively
R	radius of cylinder (to reference surface)
T	change in temperature
T_{cr}	skin temperature change at buckling
U, V, W	buckling-displacement functions of x defined by equations (C13)
Z	curvature parameter for ring-stiffened cylinder bay, $\dfrac{l^2}{Rt}\sqrt{1 - \mu^2}$

3

$$\left(Z_A\right)_i = \begin{Bmatrix} \xi \\ w_A \end{Bmatrix}_i$$

$$Z_i = \begin{Bmatrix} U \\ V \\ W \\ M \end{Bmatrix}_i$$

a	length of cylinder
d	stringer spacing
$\bar{e}$	distance from reference surface of cylinder to surface on which $\hat{N}_x$ acts
f	function
g	shape factor for exponential temperature variation (eqs. (B5) to (B7))
h	height of stringer or ring
i	integer
k	total number of finite-difference intervals along length of cylinder
l	ring spacing
n	number of full waves in cylinder buckling pattern in circumferential direction
p	pressure (positive for external pressure)
p_o	sea-level atmospheric pressure
t	thickness of isotropic cylindrical shell
$\bar{t}$	effective wall thickness of stiffened isotropic cylinder, $\dfrac{A_s}{d} + t$
u,v,w	displacements of stiffened shell at reference surface in x-, y-, and z-direction, respectively

4

x,y,z orthogonal curvilinear coordinates (see fig. 1)

$\bar{z}$ distance from centroid of stiffener to reference surface (see fig. 1), positive if stiffener lies on external side of reference surface

Λ_{ij} structural coefficients defined after equations (C15)

Π_s strain energy of composite shell wall (shell plus stiffeners)

Π_L potential energy of loading

α coefficient of linear thermal expansion

α_x,α_y coefficients of linear thermal expansion for orthotropic layer of shell

$\beta_{sk},\beta_r,\beta_s$ temperature distribution factors (see eq. (C1))

$\beta_1,\beta_2,\ldots\beta_7$ structural coefficients in equations (C4) and (C6)

$\gamma_{sk},\gamma_r,\gamma_s$ temperature distribution factors (see eq. (C1))

γ_{xy} shearing strain

Δ distance between adjacent finite-difference stations

$\delta(x - jl)$ Dirac delta function defined so that $\displaystyle\int_{-\infty}^{\infty} f(x)\ \delta(x - jl)\ dx = f(jl)$ where $\delta(x - jl) = 0$ when $x \neq jl$

δ_{iH} Kronecker delta, equal to zero when $i \neq H$ and equal to 1 when $i = H$

ϵ_x,ϵ_y normal strains

$\kappa_x,\kappa_y,\kappa_{xy}$ changes in curvature

μ Poisson's ratio for isotropic material

μ_x,μ_y Poisson's ratios for extension of orthotropic layer of shell

5

$$\xi = w_A''$$

σ normal stress

τ shear stress

Subscripts:

A   prebuckling state

B   small changes away from prebuckling state which occur at buckling

H.   integer denoting finite-difference station at which ring is located

cr   at buckling

i   index of finite-difference station

max   maximum

r   rings (circumferential stiffening)

s   stringers (longitudinal stiffening)

sk   skin

Superscripts:

i   layer index

t   total strain in composite shell

    A subscript preceded by a comma indicates partial differentiation with respect to the subscript.

    Primes denote total derivatives with respect to x.

BUCKLING THEORY

Assumptions

The theory employed herein is an extension of the theory of reference 17. The cylinder considered (see fig. 1) is composed of a multilayered orthotropic shell, stiffened by uniform, equally spaced rings and stringers, all having linearly elastic properties. The elastic constants of the multilayered shell are taken as those given in reference 19. Individual layers of the shell are assumed to be such that their principal axes of orthotropy are alined with the principal directions of loading. The stringers are assumed to be closely spaced so that their elastic properties may be averaged over the stringer spacing. The effects of the rings are not averaged but instead the rings are considered to be located along the length of the shell at uniform spacings. The effects of the individual (discrete) rings are accounted for through the introduction of the Dirac delta or impulse function as described in references 17 and 20. The cylinder is assumed to be loaded by compressive and/or pressure loadings (mechanical loading), and is subjected to thermal stresses.

In considering thermal stresses and deformations, the usual assumptions of engineering thermal-stress studies are adopted in that coupling between heat transfer and deformation is ignored. Thermal effects are accounted for by specifying axisymmetric temperature distributions in the shell and stiffening elements. The theory is sufficiently general to include arbitrary temperature variations through the thickness of the shell and depth of the stiffening elements. The effects of axisymmetric temperature variations along the length of the shell are accounted for in an approximate manner.

The theory was derived by specifying strain energy expressions corresponding to nonlinear Donnell-von Karman displacements in the shell and stiffeners, and by applying the method of minimum potential energy to obtain equilibrium equations and associated boundary conditions. These equations were separated by a perturbation procedure into equations governing axisymmetric behavior prior to buckling and equations governing behavior at buckling. A complete development of the theory is contained in appendix B. Since similar developments have appeared in the literature (for example, refs. 17 and 21), only pertinent equations are presented.

In the derivation of the governing equations, the ends of the stiffened cylinder were considered to be free to expand longitudinally ($u \neq 0$). With this assumption, thermal buckling is a consequence of circumferential compressive stresses introduced by radial restraint at the boundaries ($w = 0$) and restraints resulting from differences in expansion between the stiffeners and the shell.

Governing Equations

Prebuckling.- The equation governing the prebuckling behavior of a multilayered stiffened cylinder subject to axisymmetric thermal and mechanical loadings derived from the present theory (see appendix B (eq. (B21))) can be written as

$$\left(D_{11} - \frac{K_{11}^2}{C_{11}}\right)w_A'''' + \left[\frac{2}{R}\left(\frac{K_{11}C_{12}}{C_{11}} - K_{12}\right) + \hat{N}_x\right]w_A'' + \frac{1}{R^2}\left(C_{22} - \frac{C_{12}^2}{C_{11}}\right)w_A$$

$$= \frac{1}{R}\left[N_{Ty} + N_{Tr} + \frac{C_{12}}{C_{11}}\left(\hat{N}_x - N_{Ts} - N_{Tx}\right)\right] + N_T(x) - p \tag{1}$$

The equation is a linear, fourth-order, ordinary differential equation in w_A, the radial displacement of the cylinder prior to buckling. The coefficients of w_A involve the structural stiffnesses of the composite shell wall (including stiffeners) D_{ij}, C_{ij}, and K_{ij} which are associated with bending, extension, and coupling between extension and bending, respectively. Because rings are treated as discrete members, the circumferential extensional stiffness C_{22} is a function of x, the axial coordinate. Thus, equation (1) contains involved variable coefficients and requires numerical techniques for solution. The magnitude of the applied axial compressive load $\hat{N}_x$ appears on the left-hand side of equation (1) as $\hat{N}_xw_A''$, a term which represents the contribution of nonlinear von Karman strain-displacement terms to the prebuckling analysis.

The right-hand side of equation (1) involves loading terms resulting from temperature gradients in the stiffened shell structure (terms with subscript T) and the applied external pressure p. The thermal loads N_{Tx}, N_{Ty}, N_{Ts}, and N_{Tr} are results of temperature gradients through the thickness of the shell and depth of the stiffening elements, whereas $N_T(x)$ contains terms associated with exponential variations of temperature along the length of the stiffened shell. The effect of thermal gradients and mechanical loadings is both to stress the cylinder and change its shape prior to buckling. The total effect can be accounted for by finding w_A and its derivatives by solving equation (1) for suitable boundary conditions and applied loadings.

Buckling.- The equations governing the buckling behavior of a stiffened shell derived from the present theory (see eqs. (B22)) can be written as

$$N_{x_{B,x}} + N_{xy_{B,y}} = 0 \tag{2a}$$

$$N_{xy_{B,x}} + N_{y_{B,y}} = 0 \tag{2b}$$

$$-M_{x_{B},xx} + M_{xy_{B},xy} - M_{yx_{B},xy} - M_{y_{B},yy} + \frac{N_{y_{B}}}{R} + \hat{N}_{x}w_{B,xx} - N_{x_{B}}w_{A}''$$

$$- N_{y_{A}}w_{B,yy} - 2N_{xy_{A}}w_{B,xy} = 0 \tag{2c}$$

Equations (2a) and (2b) involve the stress resultants associated with extension $\left(N_{x_{B}}\right.$ and $\left.N_{y_{B}}\right)$ and shear $\left(N_{xy_{B}}\right)$ during buckling. Equation (2c) involves the moment resultants $\left(M_{x_{B}}, \ M_{y_{B}}, \ M_{yx_{B}}, \text{ and } \ M_{xy_{B}}\right)$ and contains some of the effects of deformations and stresses in the axisymmetric prebuckling state (terms with subscript A). In form, equations (2) reduce to more familiar classical buckling equations if the term $N_{x_{B}}w_{A}''$ is omitted in equation (2c). The classical buckling theory contains the effects of prebuckling loads $\left(\hat{N}_{x}, \ N_{y_{A}}, \text{ and } \ N_{xy_{A}}\right)$ but not prebuckling deformations $\left(w_{A}' \text{ and } \ w_{A}''\right)$.

The effects of thermal gradients appear in equations (2) in two ways. First, the buckling stress and moment resultants are functions of w_{A}' so that terms corresponding to thermal prebuckling deformations appear in equations (2a), (2b), and (2c). Secondly, a direct thermal-stress term appears as $N_{y_{A}}w_{B,yy}$ in equation (2c). This term represents the effects of circumferential stresses introduced by differences in expansion due to thermal gradients or variation in thermal properties in the stiffened shell wall. In many existing theories for thermal buckling, the direct thermal-stress term is retained, whereas the less obvious effects of thermal deformations are omitted.

Numerical Solutions

The complexity of equations (1) and (2) requires the use of numerical techniques. Solutions to the equations governing prebuckling as well as buckling behavior were obtained by omitting the applied torsional loadings $\left(N_{xy_{A}}\right)$ and employing finite differences. Both sets of equations were formulated as a system of second-order difference equations which are documented in appendix C. The prebuckling equations (eqs. (B18) and (B21)) were solved by matrix algebra by exploiting Gaussian elimination. Buckling loads were extracted from the equations governing buckling (eqs. (C15) and (C16)) by either of two methods: determinant plotting or modal iteration. In the determinant plotting solution, either the applied axial compressive load $\hat{N}_{x}$, the pressure p or a base temperature T_{A} can be used as a buckling parameter. For the modal iteration solution, T_{A} must be the buckling parameter. The parameter T_{A} is related to temperature changes between the cylinder shell and stiffeners and the boundaries of the stiffened cylinder.

The two numerical solutions have been incorporated into computer programs entitled BAMSOC I and BAMSOC II (Buckling Analysis of Multilayered Stiffened Orthotropic Cylinders). The programs were written in FORTRAN IV for the Control Data 6600 computer. Input variables and sample problems are given in appendix D. The cards and computer listings for these programs can be obtained from COSMIC, University of Georgia, Athens, Georgia 30601.

APPLICATIONS OF ANALYSIS

By use of the present analysis, the thermal buckling behavior of four types of cylindrical shells was investigated: unstiffened, ring stiffened, stringer stiffened, and ring and stringer stiffened. Unstiffened and ring-stiffened shells were studied in order to relate results from the present theory to published results from less complex theories. The behavior of two large-diameter shells — one stringer stiffened, the other ring and stringer stiffened — was also studied. The interaction of thermal and mechanical loading in these two structures was investigated in order to assess the sensitivity of contemporary aerospace designs to thermal buckling.

Unstiffened Cylinders

A solution for buckling of unstiffened cylinders subjected to uniform temperature has been presented by Hoff in reference 1. In the reference, calculations of the thermal buckling temperature were made for a steel cylinder with a radius-thickness ratio of 300 and a length-radius ratio of about 0.3. The boundary conditions employed corresponded to those of simple support $\left(N_{x_B} = v_B = w_B = M_{x_B} = 0\right)$. The cylinder was found to buckle at an unusually high temperature.

In calculations using the present theory, both the determinant plotting solution and the modal iteration solution were employed in an attempt to find a buckling temperature for the cylinder. The modal iteration solution would not converge. Further investigation was conducted with the determinant plotting solution, but no buckling temperature could be found within a practical temperature range.

The basic difference between the present theory and that of reference 1 lies in the treatment of the effects of deformations and stresses in the shell prior to buckling. In the theory of reference 1, the effects of thermal stresses introduced by restraints offered by the boundaries of the cylinder are accounted for by introducing circumferential thermal stresses into Donnell's buckling equation. In the Donnell equation, however, the effects of rotations and changes in rotations $\left(w_A' \text{ and } w_A''\right)$ in the cylinder prior to buckling are ignored. The present theory accounts for thermal effects in a more consistent fashion, and as previously discussed, contains additional terms in the buckling equations which

are associated with shell prebuckling rotations. In order to make computations for the steel cylinder on a more comparable basis, these additional terms were suppressed in buckling calculations. Thermal buckling predictions were then in excellent agreement with the results of reference 1. It must be concluded that the additional terms of the present theory tend to alleviate the effects of the boundary restraints; thus, the buckling temperature of this cylinder is beyond a practical range of interest.

An approximate solution for buckling of clamped, unstiffened cylinders subjected to uniform temperature is presented by Sunakawa in reference 6. The solution is based on a theory which includes the prebuckling displacement effect just discussed. The clamped boundary conditions for buckling implied in the solution are $N_{x_B} = 0$, $v_B = 0$, $w_B = 0$, and $w_{B,x} = 0$. Thermal buckling predictions for the steel cylinder previously described were performed by using the same clamped boundary conditions in the present theory. Results for the nondimensional buckling temperature difference αT_{cr} and the number of circumferential waves n in the buckling mode are as follows:

	Present theory	Theory of reference 6
αT_{cr}	0.01440	0.01255
n	46	44

It can be seen that the present theory yields a buckling temperature which is about 15 percent higher than that predicted by reference 6 with similar circumferential mode shapes. The differences in buckling predictions are attributed to lack of convergence of the one-term Galerkin solution of reference 6. Convergence of the present solution was investigated by varying the number of finite-difference stations and was found to be satisfactory when 100 finite-difference stations were employed.

Ring-Stiffened Cylinders

A theoretical model for buckling of ring-stiffened cylinders has been proposed by Anderson in reference 10. In Anderson's theory, the ring-stiffened cylinder is idealized by considering the behavior of a skin bay in the central regions of an infinitely long cylinder. Thermal stresses caused by temperature differences between the skin and rings are found for the bay by assuming that no rotation occurs at the rings. The circumferential stresses are then introduced into Donnell's buckling equation for an unstiffened, isotropic shell. Boundary conditions (at the rings) during buckling are assumed to be those corresponding to conventional simply supported or clamped boundaries.

In contrast, the present theory treats a cylinder of finite length. Thermal stresses and deformations prior to buckling are found for a cylinder supported at its ends in

conventional fashion, but with intermediate, discrete stiffening rings. Rotation of the rings may occur during thermal loading. Thermal stresses and deformations for a discretely stiffened shell are introduced consistently into the buckling equation. Boundary conditions during buckling are enforced only at the ends of the cylinder so that the continuity conditions at each ring are natural consequences of the structural stiffnesses of the ring and shell at the line of attachment.

<u>Comparison with reference 10.</u>- In order to compare Anderson's predictions with the present results, an analytical investigation was made of the thermal buckling behavior of ring-stiffened cylinders with proportions similar to the test cylinders of reference 11. These cylinders were internally stiffened with equally spaced Z-shaped rings having the dimensions shown in figure 2. Geometric and mechanical properties employed in the present calculations are indicated in table I. In the investigation, the rings and boundaries of the cylinder were considered to be at room temperature, whereas the cylinder skin was heated to a constant temperature. The nonuniform temperature in the stiffened cylinder produces circumferential thermal stresses that cause buckling of the cylinder skin between rings. The cylinder was assumed to be simply supported at its ends with the boundary conditions $N_{x_B} = 0$, $v_B = 0$, $w_B = 0$, and $M_{x_B} = 0$.

For the comparison, the length, radius, and thickness of the cylinder were held constant for all the computations. The number of rings in the cylinder (and hence the ring spacing l) was varied to study the effects of the bay curvature parameter $Z\left(\dfrac{l^2}{Rt}\sqrt{1-\mu^2}\right)$ on thermal buckling characteristics. The results of reference 10 suggest that somewhat unusual behavior occurs for small Z in ring-stiffened cylinders. The overall cylinder length a was much shorter than that of the test cylinders of reference 11. The particular value selected (see fig. 2) was based on considerations of the number of rings and finite-difference stations required to investigate small values of Z.

Results of the theoretical buckling predictions from reference 10 and the present theory are compared in figure 3. The nondimensional skin-buckling temperature αT_{cr} is shown as a function of Z. Results from the present theory are shown as discrete points corresponding to calculations with a finite number of rings. The solid curve has been faired through the points to indicate trends. The dashed curves on the figure are based on results presented by Anderson (ref. 10) for simply supported and clamped cylinder bays with rigid rings. A correction which accounts for flexibility of the rings is suggested in the reference. When the rings are considered to be flexible, circumferential thermal stresses near the rings are less than those computed for rigid rings; therefore, the thermal buckling temperatures are higher. For the present cylinders the correction amounts to an increase of about 7 to $7\frac{1}{2}$ percent above the values shown in figure 3.

In figure 3, it can be seen that results from the present theory are in reasonable agreement with Anderson's results for clamped cylinder bays when Z is greater than 15. The numerical differences shown for this range of Z are about 5 percent. For smaller Z, a larger disparity exists. Studies of prebuckling stress distributions based on the present theory suggest that the idealizations used by Anderson to obtain thermal stresses are reasonably accurate. It is believed, therefore, that the analytical differences shown in figure 3 stem mainly from the additional thermal deformation terms in the present buckling theory, and the effective ring boundary conditions during buckling. The present results suggest that when Z is greater than 15, the cylinder rings offer nearly clamped support to the skin bays during buckling. Furthermore, both the present theory and that of reference 10 suggest that the thermal buckling temperature becomes independent of ring spacing for this range of Z. The theoretical differences and unusual behavior for cylinders with smaller Z is probably associated with the interaction of closely spaced rings.

Thermal-mechanical interactions.- A further topic of interest in the thermal buckling behavior of ring-stiffened cylinders is the interaction between thermal and mechanical loading. The behavior of the simply supported cylinders just discussed was investigated under combinations of axial compression and thermal loads induced by heating the cylinder skin. Results of interaction studies are presented in figure 4, where the nondimensional mechanical buckling load $\hat{N}_{x_{cr}}/Et$ has been plotted against the thermal buckling load αT_{cr}. Buckling interaction curves are presented for cylinders of fixed overall geometry (see fig. 2) with three, five, and seven rings. The buckling loads shown for axial compression loading alone $\left(\alpha T_{cr} = 0\right)$ were compared with published results for isotropic cylinders having a similar value of Z (ref. 22). The comparison suggested that the rings of the present cylinders provide almost clamped supports for the skin bays when loaded in axial compression. A similar result has already been noted for thermal loading when Z is large. The interaction curves shown are very regular in shape with the exception of the case of three rings. Results of the interaction curves were compared with interactions suggested by reference 10 for clamped cylinders but no correlation was evident for the range of curvature parameter considered (Z = 8 to 30). In this range of Z, the results of reference 10 suggest that substantially larger thermal loads can be carried when axial compressive loads are present, whereas results from the present theory do not support this conclusion.

Stringer-Stiffened Cylinder

In order to investigate the thermal buckling behavior of longitudinally (stringer-) stiffened shells, the behavior of a large-diameter aluminum shell representative of proportions which might be considered for an interstage structure in a large launch vehicle

was investigated. The structure considered is an integrally stiffened shell which has been used in theoretical and experimental studies of stiffener and loading eccentricity effects. (See refs. 23 and 24.) The geometry and mechanical properties adopted for the present investigation are given in figure 5 and table I(b). Thermal buckling problems in interstage structures might conceivably arise from thermal gradients induced by rapid aerodynamic heating of the shell outer skin; as a result, thermal lags between stiffener and shell temperatures occur. For the present analysis, the skin was assumed to be heated whereas the stringers remained unheated. Bending and thrust loads are also present during flight; thus, it seemed desirable to investigate the interaction between axial compressive and thermal loads. For purposes of the investigation, the cylinder was assumed to be clamped at its ends $\left(N_{x_B} = v_B = w_B = w_{B,x} = 0\right)$. Local buckling of the skin was not considered.

Prebuckling stress distribution.- The stress distributions induced by combinations of axial compression and temperature were investigated by use of the results of the solution of the equations governing deformations and stresses prior to buckling. (See eq. (1).) Stress distributions in the skin and stringers of the interstage for three combinations of applied compressive load $\hat{N}_x$ and change in skin temperature T_{sk} are presented in figure 6 as functions of the distance x/a measured from the supported end of the shell. In figure 6(a) the axial stress at the skin middle surface is shown to increase in proportion to the applied axial load. The axial stress asymptotically approaches the membrane state of stress $\left(\sigma_x = \hat{N}_x/E\bar{t}\right)$ in the central areas of the shell. The higher values of stress near the ends of the shell ($x/a = 0$) are due to bending stresses developed from end constraints. In figure 6(b), the circumferential stresses at the skin middle surface shown increase roughly in proportion to skin-temperature changes. The circumferential stresses are small in the central regions of the cylinder and the stresses shown near the ends are largely due to restraints in expansion between the cold boundaries and cold stringers and the heated shell. A significant difference between circumferential stress variation in the present stiffened shell and results for unstiffened shells of similar geometry is that stresses decay much more rapidly in unstiffened shells. (See ref. 13.)

Stresses developed in the longitudinal stiffening for various combinations of axial compression and thermal load are shown in figure 6(c). The stress distribution in the stringer is plotted against the normal coordinate z nondimensionalized by the stringer height h for various longitudinal stations x/a. The origin of z was taken to be the surface of the stiffener in contact with the shell. The stress distributions shown in figure 6(c) indicate that bending stresses in the shell increase appreciably as the temperature difference between skin and stringers increases. For the case with no applied axial compression, the calculated stress in the outstanding flange of the stiffener actually exceeds the ultimate tensile strength of aluminum.

14

The results presented for the stress distribution in the interstage structure suggest that complex states of stress exist which depend on the relative magnitude of the applied axial compression and the differences in expansion between the boundaries and stringers, and the heated shell. Studies of the detailed stress distribution in skin and stiffeners indicate that intolerably large bending stresses exist in the stringers near the ends when only thermal loads are present. The results also indicate that thermal stresses are developed from boundary effects which appear to persist over relatively large sections of the longitudinally stiffened shell.

Buckling of stringer-stiffened cylinder.- The buckling behavior of the idealized interstage structure was investigated under combinations of axial compressive and thermal loads. Results of the investigation are presented in figure 7 as an interaction curve between the normalized axial compressive load at buckling $\hat{N}_{x_{cr}}/E\bar{t}$ and the change in skin temperature at buckling αT_{cr}. The three combinations of axial load and temperature change discussed in the section entitled "Prebuckling stress distribution" are shown as cross marks in figure 7. The buckling load shown for the clamped shell under axial compression alone $\left(\alpha T_{cr} \approx 0\right)$ was in good agreement with published results, the present calculation being about 2 percent higher than the result presented in reference 24.

In figure 7 it can be seen that the interaction curve has an unusual shape when small thermal loads are present. For temperature changes of about 50° F (28 K) in the skin, that is, $\alpha T_{cr} = 0.0007$, the shell buckling load actually increases to about 1.4 times the compressive buckling load of an unheated shell. It appears that small thermal loads can introduce favorable deformations prior to buckling which increase the shell's effective stiffness to resist axial compression. As can be seen from the interaction curve, however, when thermal loads became large, the longitudinally stiffened shell had little resistance to the circumferential thermal stresses so that buckling can occur by thermal loading alone $\left(\dfrac{\hat{N}_{x_{cr}}}{E\bar{t}} = 0\right)$. The temperature change corresponding to this case is about 130° F (72 K), and is well within a practical temperature range for aluminum. In interstage structures, when thermal environments are present, simple insulators such as cork are used to shield the outer skin of the structure. However, in many instances, the insulation is not adequate to eliminate all thermal gradients. The present results suggest that small gradients may be tolerated, but if large thermal gradients are present, the structure should be carefully considered with regard to the possibility of thermal buckling.

The normal component of the buckling mode shape for the interstage structure under thermal loading alone is shown in figure 8, where the normalized variation of the radial buckling displacements W/W_{max} is plotted against the length parameter x/a where a is the length of the shell. For comparison, prebuckling deformations at the onset of

buckling are shown in the inset in figure 8. The buckling wave pattern is characterized by a nearly sinusoidal wave along the length of the shell and many sinusoidal waves around the circumference (n = 65). Because the number of circumferential waves is large, the nodes in the buckle pattern in the circumferential direction are separated by distances which are about $1\frac{1}{2}$ times the stringer spacing. Since the stiffness properties of longitudinal stiffening are averaged in the present theory, the calculated circumferential mode shape is one which is near the limits of applicability of the theory.

Ring- and Stringer-Stiffened Cylinder

In order to investigate the thermal buckling behavior of ring- and stringer-stiffened shells, the behavior of a stiffened cylinder with geometry similar to that which might be considered in a preliminary design of a supersonic transport was investigated. A rather long, uniform, titanium fuselage section, bounded forward by a heavy bulkhead and aft by the wing-joint structure, was selected. The geometry and mechanical properties adopted for the present calculations are presented in figure 9 and table I. Studies of design loads and predicted thermal environment for this type of structure suggested the possibility of thermal buckling as a consequence of a rapid climb to altitude. In this maneuver there is a thermal lag between the skin and stiffening elements so that for a short period of time the skin is at elevated temperatures while both rings and stringers are unheated. Bending and pressurization loads on the fuselage are also present during the maneuver; therefore, it seemed desirable to investigate the interaction of axial compressive loads and thermal loads for various internal pressures. For purposes of the investigation, the cylinder was assumed to be simply supported at its ends $\left(N_{x_B} = v_B = w_B = M_{x_B} = 0\right)$ and the axial compression was introduced by means of a line load applied at the skin middle surface.

Prebuckling stress distribution.- The stress distribution induced by combinations of axial compression and temperature was investigated by using results based on the solution of equation (1). Stress distributions in the skin, stringers, and rings of the fuselage under an applied compressive load of 1650 lbf/in. (0.289 MN/m) and temperature difference of 360° F (200 K) between skin and stiffeners were obtained. Results are presented in figure 10. The diffusion of load into each element of the structure is illustrated by showing results for various stations near one of the supported ends of the cylinder. In figure 10(a) the stress distribution in the skin of the cylinder is shown as a function of length. At the end of the cylinder (x/a = 0), both axial and circumferential stresses are very high, but are still within the elastic range of titanium. The stresses are not nearly as large as those for the clamped interstage structure already discussed. Sharp peaks in stress occur at each of the 19 rings in the shell. The circumferential stress shown in bays that are distant from the boundary is a result of the differences in thermal expansion

16

between the rings and the shell. The curves shown in figure 10(a) indicate that the state of stress does not vary from bay to bay beyond the third bay (x/a ≈ 0.15).

Variations in the stress distribution in the stiffening elements are shown in figure 10(b). The assumptions of the present theory are such that the ring is in a state of uniform, uniaxial stress (in this case, tension). The ring stress variations shown in figure 10(b) indicate that the interior ring stresses are essentially constant in rings that are not adjacent to the boundary. The assumptions of the present theory are such that the stringers (longitudinal stiffening) are also in a state of uniaxial stress, although bending stresses through the depth of the stringers may exist. The magnitudes of these bending stresses are given in figure 10(b) by plotting stresses against the depth parameter z/h for various longitudinal stations. The bending stresses in the interior of the shell are mainly due to thermal stresses and restraints to expansion offered by the rings. The bending stresses near the ends of the cylinder also include the effects of introducing the applied axial compression load by means of a line load on the skin midplane. The edge moment introduced by the eccentricity of the line load with respect to the stringer-shell centroid has been noted in previous studies (ref. 23) and large effects on buckling predictions have been found. In the present case, the stress distributions shown in figure 10(b) suggest that this edge moment decays rapidly from the cylinder ends so that the state of stress in the stringers does not vary from bay to bay beyond the second ring.

The results presented for the stress distribution in this example indicate the complexity of the state of stress existing in a ring- and stringer-stiffened shell under combined mechanical and thermal loadings. Studies of the detailed stress distributions in skin and stiffening elements suggest that no large stresses exist that are not within the capabilities of the structural material. The effects of the boundaries of the stiffened shell on stress distribution appear to be negligible beyond the second bay of the cylinder.

Buckling of ring- and stringer-stiffened cylinder.- The buckling behavior of the idealized supersonic transport design was investigated under combinations of axial compressive and thermal loads. In addition, the effects of including cabin pressurization as an applied load were also included. The results of the investigation are summarized in figure 11 by means of interaction curves between axial compressive load at buckling $\hat{N}_{x_{cr}}/E\bar{t}$ and relative skin temperature at buckling αT_{cr}. The solid curves shown correspond to various values of internal pressure p normalized by sea-level atmospheric pressure p_0. The maximum value of p/p_0 shown is about that proposed for cruising altitude.

Results shown in figure 11 for $p/p_0 = 0$ indicate that the interaction between axial compressive and thermal loads is substantial. In fact, in the absence of axial compression, thermal loads are large enough to cause buckling in a practical temperature range. The value of αT_{cr} shown for this case corresponds to a temperature difference of about

17

525° F (292 K) between the skin and stiffening elements. Results shown in figure 11 for cases where internal pressurization exists $\left(p/p_o < 0\right)$ indicate that even small values of internal pressure are very beneficial in alleviating the problem of buckling under thermal loading alone. At cabin pressure at cruise $\left(p/p_o = -0.82\right)$, the interaction curve is nearly horizontal over a practical temperature range and the buckling load is roughly $1\frac{1}{2}$ times that of an unpressurized fuselage. In some aircraft design criteria for buckling, however, the beneficial effects of pressure are not included in buckling calculations; therefore, the fuselage structure is required to be stable even if all cabin pressure is accidentally lost. Under these circumstances, elimination of buckling under thermal and compressive loads or thermal loads alone may be a serious design consideration.

An additional effect shown in figure 11 by the dashed curve is that of introducing the axial compressive load at the neutral surface of the sheet-stringer combination $(\bar{e} = 0.13$ in. (0.33 cm)) rather than at the skin midplane $(\bar{e} = 0)$. The dashed curve suggests substantial improvement in buckling strength under axial compression alone due to the edge moment effect already mentioned. However, the interaction curve is unaffected when large thermal loadings are present.

The normal component of the buckling mode shape for the stiffened shell under thermal loading alone with no internal pressure is presented in figure 12, where the normalized variation of the radial buckling displacements W/W_{max} is plotted against length x/a for one-half of the cylinder. For comparison, prebuckling deformations at the onset of buckling are shown in the inset in figure 12. The wave shape shown in figure 12 is typical of a panel instability buckling pattern in that nodes occur at each of the rings. It can be seen that the amplitude of W decays in the interior bays so that in the central bays of the cylinder almost negligible deformation is present. The variation in amplitude from bay to bay suggests that buckling is a consequence of restraints at or near the boundaries of the cylinder. The presence of longitudinal stiffening apparently makes thermal edge effects persist over a large length as evidenced by the large amplitude of the buckle wave in the fifth bay of the cylinder $(0.20 \lesssim x/a \lesssim 0.25)$. As was the case with the interstage structure, a large number of circumferential waves (n = 57) occurred in the buckling mode when thermal loading predominated. In this case, however, at least three stringers are included in each circumferential half-wave. Thus, the buckling mode found appears to be a legitimate panel instability mode and is consistent with theory employing the average stiffness properties of longitudinal stiffening.

The present study of an idealized supersonic transport design indicates that a potential design problem exists in that temperature gradients which might be induced by a rapid climb to altitude were sufficient to buckle the shell in a practical temperature range. The presence of internal cabin pressure is sufficient to alleviate the thermal loads. If

18

internal cabin pressure is not available as a stabilizing force, additional reinforcement must be judiciously applied to the structure.

CONCLUDING REMARKS

An extension of the theory of NASA Technical Note D-4283 for buckling of stiffened cylindrical shells under combinations of mechanical and thermal loadings has been presented. It includes the effects of eccentricity in multilayered reinforcement, deformations prior to buckling, and discrete rings. The theory is sufficiently general to account for the averaged stiffnesses of stringers and multiple orthotropic shell layers as well as arbitrary temperature distributions through the thickness of the shell and depth of the stiffeners. Buckling solutions have been obtained by employing finite differences. Two computer programs from which buckling loads can be found (either by determinant plotting or modal iteration) have been developed.

Theoretical results for thermal buckling have been compared with existing solutions for unstiffened and ring-stiffened cylindrical shells. Results from the present theory for a simply supported unstiffened shell indicated that thermal buckling would not occur in a practical temperature range. Results for a clamped unstiffened shell were in agreement with published theoretical results. Buckling predictions for a ring-stiffened shell with various ring spacings were in agreement with existing theoretical results when the cylinder bay curvature parameter is large. In cases where large disparities between published theoretical results and those presented herein exist, differences are attributed to the effects of prebuckling deformations which have not been accounted for in previous theories.

The effects of interaction of thermal loading and axial compression on the buckling behavior of two types of contemporary stiffened shell structures have been investigated. Thermal loads were introduced by considering the skin of the structure to be heated, while the stiffening elements and shell boundaries remain unheated. The behavior of an aluminum, clamped, large-diameter longitudinally stiffened cylinder representative of a launch vehicle interstage structure was investigated. Stress distribution studies indicated that thermal stresses induced by moderate skin temperatures cause large bending stresses in the stiffeners near the ends. Buckling calculations suggest that the interstage structure may buckle under thermal loading alone at a realistic skin temperature.

The behavior of a titanium simply supported, ring- and stringer-stiffened cylinder representative of a preliminary design for a supersonic transport fuselage was also investigated. Stress distribution studies indicated that no large thermal stresses beyond

the capabilities of the shell material were present. Buckling calculations suggest that the fuselage also can buckle under thermal loading alone at a practical skin temperature.

Near the completion of this work, preliminary calculations for the ring-stiffened cylinders by another investigator suggested that thermal-buckling behavior could be influenced by the type of ring theory employed in the analysis. For the ring-stiffened cylinders, out-of-plane bending stiffness appeared to be an important parameter. To account for this effect, a ring theory which includes out-of-plane bending behavior was developed and is presented in appendix E. This ring theory was incorporated into one of the computer programs; however, no numerical results were available for this paper.

Langley Research Center,
    National Aeronautics and Space Administration,
        Hampton, Va., April 28, 1970.

APPENDIX A

CONVERSION OF U.S. CUSTOMARY UNITS TO SI UNITS

The International System of Units (SI) was adopted by the Eleventh General Conference on Weights and Measures in 1960. (See ref. 18.) Conversion factors for the units used in this report are given in the following table:

Physical quantity	U.S. Customary Unit	Conversion factor (*)	SI Unit (**)
Length	in.	0.0254	meters (m)
Stress modulus	ksi	6.895×10^6	newtons/meter^2 (N/m2)
Stress resultant	lbf/in.	175.1	newtons/meter (N/m)
Temperature change	$^\circ$F	5/9	Kelvin (K)

*Multiply value given in U.S. Customary Unit by conversion factor to obtain equivalent value in SI Units.

**Prefixes to indicate multiple of units are as follows:

Prefix	Multiple
giga (G)	10^9
mega (M)	10^6
kilo (k)	10^3
deci (d)	10^{-1}
centi (c)	10^{-2}
milli (m)	10^{-3}

APPENDIX B

DEVELOPMENT OF GOVERNING EQUATIONS

Stress-Strain Relations

In the ith layer of the shell, the stress-strain relations can be written as

$$\left.\begin{array}{l} \sigma_x^i = \dfrac{E_x^i}{1 - \mu_x^i \mu_y^i}\left[\epsilon_x^t + \mu_y^i \epsilon_y^t - \left(\alpha_x^i + \mu_y^i \alpha_y^i\right)T\right] \\[3ex] \sigma_y^i = \dfrac{E_y^i}{1 - \mu_x^i \mu_y^i}\left[\epsilon_y^t + \mu_x^i \epsilon_x^t - \left(\alpha_y^i + \mu_x^i \alpha_x^i\right)T\right] \\[3ex] \tau_{xy}^i = G_{xy}^i \gamma_{xy}^t \end{array}\right\} \tag{B1}$$

where α_x and α_y are coefficients of linear expansion associated with thermal elonga-tion in the axial and circumferential directions, respectively, T is a change in temper-ature relative to a thermal-stress-free state and the remaining quantities with the super-script i are orthotropic elastic constants associated with extension. The strains appearing in equation (B1) are related to the shell displacements u, v, and w by Donnell-von Karman relations having the form

$$\left.\begin{array}{l} \epsilon_x^t = \epsilon_x + z\kappa_x \\[2ex] \epsilon_y^t = \epsilon_y + z\kappa_y \\[2ex] \gamma_{xy}^t = \gamma_{xy} + z\kappa_{xy} \end{array}\right\} \tag{B2}$$

with

$$\epsilon_x = u_{,x} + \frac{1}{2}w_{,x}^2$$

$$\epsilon_y = v_{,y} + \frac{w}{R} + \frac{1}{2}w_{,y}^2$$

$$\gamma_{xy} = u_{,y} + v_{,x} + w_{,x}w_{,y}$$

$$\kappa_x = -w_{,xx}$$

22

$$\kappa_y = -w_{,yy}$$

$$\kappa_{xy} = -2w_{,xy}$$

In the stringers

$$\sigma_{x_S} = E_S\left(\epsilon_x^t - \alpha_S T\right) \tag{B3}$$

whereas in the rings

$$\sigma_{y_r} = E_r\left(\epsilon_y^t - \alpha_r T\right) \tag{B4}$$

To account for axisymmetric temperature variation along the length of the shell, the relative temperature of the shell is expressed as

$$T = T_{sk}\left(1 + \gamma_{sk}e^{gx/a}\right) \tag{B5}$$

where a is the length of the shell, and γ_{sk} and g are constants. Similarly, in the stringers,

$$T = T_s\left(1 + \gamma_s e^{gx/a}\right) \tag{B6}$$

and in the rings

$$T = T_r\left(1 + \gamma_r e^{gx/a}\right) \tag{B7}$$

where T_{sk}, T_s, and T_r are functions of z. By specifying temperature distributions with equations (B5) to (B7), the first-order effects of longitudinal variation in thermal distributions can be obtained. The present theory, however, does not consider the effects of variation of mechanical properties with the assumed longitudinal temperature distribution.

Potential Energy

The integration of the familiar strain energy expression

$$\Pi_s = \frac{1}{2} \iiint_{\text{Volume}} \left\{ \frac{E_x}{1 - \mu_x\mu_y}\left(\epsilon_x^t\right)^2 + \frac{2\mu_y E_x}{1 - \mu_x\mu_y}\epsilon_x^t\epsilon_y^t + \frac{E_y}{1 - \mu_x\mu_y}\left(\epsilon_y^t\right)^2 + G_{xy}\left(\gamma_{xy}^t\right)^2 - \frac{2}{1 - \mu_x\mu_y}\left[\left(\alpha_x + \mu_y\alpha_y\right)\epsilon_x^t + \left(\alpha_y + \mu_x\alpha_x\right)\epsilon_y^t\right]T \right\} dV$$

over the depth of the composite shell wall (shell plus stiffeners) yields the following expression:

$$\Pi_S = \frac{1}{2} \iint\limits_{Surface} \left\{ N_x \epsilon_x + N_y \epsilon_y + N_{xy}\gamma_{xy} + M_x \kappa_x + M_y \kappa_y + \left(M_{xy} - M_{yx}\right)\frac{\kappa_{xy}}{2} - \left[\left(N_{Tx} + N_{Ts}\right)\epsilon_x + \left(M_{Tx} + M_{Ts}\right)\kappa_x \right.\right.$$
$$\left.\left. + \left(N_{Ty} + N_{Tr}\right)\epsilon_y + \left(M_{Ty} + M_{Tr}\right)\kappa_y \right]\right\} dx\, dy \tag{B8}$$

where

$$\left.\begin{aligned}
N_x &= C_{11}\epsilon_x + C_{12}\epsilon_y + K_{11}\kappa_x + K_{12}\kappa_y - \left(N_{Tx} + N_{Ts}\right)\\[6pt]
N_y &= C_{12}\epsilon_x + C_{22}\epsilon_y + K_{12}\kappa_x + K_{22}\kappa_y - \left(N_{Ty} + N_{Tr}\right)\\[6pt]
N_{xy} &= C_{66}\gamma_{xy} + K_{66}\kappa_{xy}\\[6pt]
M_x &= K_{11}\epsilon_x + K_{12}\epsilon_y + D_{11}\kappa_x + D_{12}\kappa_y - \left(M_{Tx} + M_{Ts}\right)\\[6pt]
M_y &= K_{12}\epsilon_x + K_{22}\epsilon_y + D_{12}\kappa_x + D_{22}\kappa_y - \left(M_{Ty} + M_{Tr}\right)\\[6pt]
M_{xy} &= -\left(K_{66}\gamma_{xy} + D_{66}\kappa_{xy} + \frac{G_S J_S}{2d}\kappa_{xy}\right)\\[6pt]
M_{yx} &= K_{66}\gamma_{xy} + D_{66}\kappa_{xy} + \frac{1}{2}\sum_{j=1}^{N}\delta(x - j\ell)\, G_r J_r \kappa_{xy}
\end{aligned}\right\} \tag{B9}$$

where $\delta(x - j\ell)$ is the Dirac delta function associated with the N rings on the cylinder.

The quantities C_{ij}, D_{ij}, and K_{ij} appearing in equations (B9) are structural stiffnesses associated with extension, bending, and extension-bending coupling, respectively, and are given by the following integrals:

$$C_{11} = \int \frac{E_x}{1 - \mu_x\mu_y}\, dz + \frac{E_S A_S}{d} \tag{B10a}$$

$$C_{12} = \int \frac{\mu_x E_y}{1 - \mu_x\mu_y}\, dz \tag{B10b}$$

$$C_{22} = \int \frac{E_y}{1 - \mu_x\mu_y}\, dz + \sum_{j=1}^{N}\delta(x - j\ell)\, E_r A_r \tag{B10c}$$

$$C_{66} = \int G_{xy}\, dz \tag{B10d}$$

24

$$K_{11} = \int \frac{E_x}{1 - \mu_x \mu_y} z \, dz + \frac{E_s A_s \bar{z}_s}{d} \tag{B10e}$$

$$K_{12} = \int \frac{\mu_x E_y}{1 - \mu_x \mu_y} z \, dz \tag{B10f}$$

$$K_{22} = \int \frac{E_y}{1 - \mu_x \mu_y} z \, dz + \sum_{j=1}^{N} \delta(x - j\ell) E_r A_r \bar{z}_r \tag{B10g}$$

$$K_{66} = \int G_{xy} z \, dz \tag{B10h}$$

$$D_{11} = \int \frac{E_x}{1 - \mu_x \mu_y} z^2 dz + \frac{E_s I_s}{d} + \frac{E_s A_s \bar{z}_s^2}{d} \tag{B10i}$$

$$D_{12} = \int \frac{\mu_x E_y}{1 - \mu_x \mu_y} z^2 dz \tag{B10j}$$

$$D_{22} = \int \frac{E_y}{1 - \mu_x \mu_y} z^2 dz + \sum_{j=1}^{N} \delta(x - j\ell) \left(E_r I_r + E_r A_r \bar{z}_r^2 \right) \tag{B10k}$$

$$D_{66} = \int G_{xy} z^2 dz \tag{B10ℓ}$$

where the integration is to be performed over the multiple layers of the shell wall. A convenient numerical scheme for the integration for a specified reference surface can be found in equations (83) and (85) of reference 19 (p. 34). The properties associated with the stiffeners (location of the centroid of the stiffener $\bar{z}$, the moment of inertia I, the cross-sectional area A, and the torsional constant J) are also defined (when appropriate) with respect to an arbitrary reference surface. In specifying the structural stiffnesses, the dependence of the elastic constants upon temperature can be accounted for in the shell by analytically dividing the multilayered shell into thin layers and performing the required integration of equations (B10) numerically. In the stiffeners, the following sample definitions can be employed to perform a comparable integration through the depth of the stiffeners:

$$\frac{E_S A_S}{d} = \frac{1}{d} \int_{A_S} E_S(z) \, dA_S$$

$$\frac{z_S E_S A_S}{d} = \frac{1}{d} \int_{A_S} E_S(z) \, z \, dA_S$$

$$\cdot \qquad \cdot$$
$$\cdot \qquad \cdot$$
$$\cdot \qquad \cdot$$

The thermal moment M_T and thermal force terms N_T appearing in equations (B9) are

$$\left. \begin{aligned} N_{Tx} &= C_{Tx}\left(1 + \gamma_{sk} e^{gx/a}\right) \\[2mm] N_{Ty} &= C_{Ty}\left(1 + \gamma_{sk} e^{gx/a}\right) \\[2mm] N_{Ts} &= C_{Ts}\left(1 + \gamma_{s} e^{gx/a}\right) \\[2mm] N_{Tr} &= \sum_{j=1}^{N} \delta(x - j\ell)\, C_{Tr}\left(1 + \gamma_{r} e^{gx/a}\right) \end{aligned} \right\} \qquad \text{(B11)}$$

$$\left. \begin{aligned} M_{Tx} &= K_{Tx}\left(1 + \gamma_{sk} e^{gx/a}\right) \\[2mm] M_{Ty} &= K_{Ty}\left(1 + \gamma_{sk} e^{gx/a}\right) \\[2mm] M_{Ts} &= K_{Ts}\left(1 + \gamma_{s} e^{gx/a}\right) \\[2mm] M_{Tr} &= \sum_{j=1}^{N} \delta(x - j\ell)\, K_{Tr}\left(1 + \gamma_{r} e^{gx/a}\right) \end{aligned} \right\} \qquad \text{(B12)}$$

where

$$C_{Tx} = \int \left(\alpha_x + \mu_y\alpha_y\right)\frac{E_x}{1 - \mu_x\mu_y} T_{sk} \, dz$$

$$C_{Ty} = \int \left(\alpha_y + \mu_x\alpha_x\right)\frac{E_y}{1 - \mu_x\mu_y} T_{sk} \, dz$$

$$C_{Ts} = \frac{1}{d} \int_{A_s} \alpha_s E_s T_s \, dA_s$$

$$C_{Tr} = \int_{A_r} \alpha_r E_r T_r \, dA_r$$

$$K_{Tx} = \int \left(\alpha_x + \mu_y\alpha_y\right)\frac{E_x}{1 - \mu_x\mu_y} T_{sk} z \, dz$$

$$K_{Ty} = \int \left(\alpha_y + \mu_x\alpha_x\right)\frac{E_y}{1 - \mu_x\mu_y} T_{sk} z \, dz$$

$$K_{Ts} = \frac{1}{d} \int_{A_s} \alpha_s E_s T_s z \, dA_s$$

$$K_{Tr} = \int_{A_r} \alpha_r E_r T_r z \, dA_r$$

For C_{Tx}, C_{Ty}, K_{Tx}, and K_{Ty}, the integration is to be performed over the multiple layers of the shell wall and can be accomplished by the method suggested for equations (B10).

As in reference 17 the potential energy of mechanical loading for the case of an applied compression load $\hat{N}_x$, an applied shear load $\hat{N}_{xy}$, and an external pressure p is given by

$$\Pi_L = \int_0^{2\pi R} \int_0^a pw \, dx \, dy + \int_0^{2\pi R} \hat{N}_x\left(u - \bar{e}w_{,x}\right)\Big|_0^a \, dy + \int_0^{2\pi R} \hat{N}_{xy} v \Big|_0^a \, dy \qquad (B13)$$

where $\bar{e}$ is the distance from the arbitrary reference surface to the line on which the applied mechanical load resultant $\hat{N}_x$ acts.

Equilibrium Equations and Boundary Conditions

By the principle of minimum potential energy, the vanishing of the first variation of the total potential energy $\left(\delta\left(\Pi_S + \Pi_L\right) = 0\right)$ yields the equilibrium equations and appropriate boundary conditions. The first variation with respect to the displacement variables u, v, and w yields

$$\left. \begin{aligned} &N_{x,x} + N_{xy,y} = 0 \\[2mm] &N_{xy,x} + N_{y,y} = 0 \\[2mm] &-M_{x,xx} + \left(M_{xy} - M_{yx}\right)_{,xy} - M_{y,yy} + \frac{N_y}{R} - N_x w_{,xx} - N_y w_{,yy} - 2N_{xy} w_{,xy} + p = 0 \end{aligned} \right\} \quad \text{(B14)}$$

with the following boundary conditions to be specified at each end of the cylinder:

$$\left. \begin{aligned} &N_x + \hat{N}_x = 0 \\[2mm] &N_{xy} + \hat{N}_{xy} = 0 \\[2mm] &M_x + \hat{N}_x \bar{e} = 0 \\[2mm] &M_{x,x} - \left(M_{xy,y} - M_{yx,y}\right) + N_x w_{,x} + N_{xy} w_{,y} = 0 \end{aligned} \right\} \quad \text{or} \quad \left. \begin{aligned} &u = 0 \\[2mm] &v = 0 \\[2mm] &w_{,x} = 0 \\[2mm] &w = 0 \end{aligned} \right\} \quad \text{(B15)}$$

The nonlinear equilibrium equations and associated boundary conditions (eqs. (B14) and (B15)) are used to obtain equations governing the prebuckling and buckling states of the stiffened shell by taking the displacements u, v, and w to be

$$\left. \begin{aligned} &u(x,y) = u_A(x) + u_B(x,y) \\[2mm] &v(x,y) = v_A(x) + v_B(x,y) \\[2mm] &w(x,y) = w_A(x) + w_B(x,y) \end{aligned} \right\} \quad \text{(B16)}$$

In equations (B16) the subscript A denotes the axisymmetric, prebuckling displacements of the stiffened shell, and the subscript B denotes the infinitesimal nonaxisymmetric displacements that occur at buckling.

Prebuckling Equations

For axisymmetric prebuckling deformations, the equilibrium equations are found from equations (B14) by discarding terms which have derivatives of y. The resulting equations are

$$N_{x_{A,x}} = 0 \tag{B17a}$$

$$N_{xy_{A,x}} = 0 \tag{B17b}$$

$$-M_{x_{A,xx}} + \frac{N_{y_A}}{R} - N_{x_A} w_{A,xx} + p = 0 \tag{B17c}$$

with boundary conditions

$$N_{x_A} + \hat{N}_x = 0 \quad \text{or} \quad u_A = 0 \tag{B18a}$$

$$N_{xy_A} + \hat{N}_{xy} = 0 \quad \text{or} \quad v_A = 0 \tag{B18b}$$

$$M_{x_A} + \hat{N}_x \bar{e} = 0 \quad \text{or} \quad w_{A,x} = 0 \tag{B18c}$$

$$M_{x_{A,x}} + N_{x_A} w_{A,x} = 0 \quad \text{or} \quad w_A = 0 \tag{B18d}$$

where the subscript A terms are defined by inserting $u = u_A(x)$, $v = v_A(x)$, and $w = w_A(x)$ in the definitions of the stress resultants (eqs. (B2) and (B9)).

As discussed in the text, the cylinder was considered to be free to expand longitudinally $\left(u_A \neq 0 \right)$ so that integration of equation (B17a) yields

$$N_{x_A} = -\hat{N}_x \tag{B19}$$

where $\hat{N}_x$ is the applied compressive load at the boundary. From equation (B19) and the definition of N_{x_A},

$$\epsilon_{x_A} = \frac{N_{T_s} + N_{T_x}}{C_{11}} + \frac{K_{11}}{C_{11}} w_{A,xx} - \frac{C_{12}}{C_{11}} \frac{w_A}{R} - \frac{\hat{N}_x}{C_{11}} \tag{B20}$$

The use of the definitions of M_{x_A} and N_{y_A} together with equation (B20) in equation (B17c) yields the following equation in w_A:

$$\left(D_{11} - \frac{K_{11}^2}{C_{11}} \right) w_A'''' + \left[\frac{2}{R} \left(\frac{K_{11} C_{12}}{C_{11}} - K_{12} \right) + \hat{N}_x \right] w_A'' + \frac{1}{R^2} \left(C_{22} - \frac{C_{12}^2}{C_{11}} \right) w_A = \frac{1}{R} \left[N_{Ty} + N_{Tr} \right.$$

$$\left. + \frac{C_{12}}{C_{11}} \left(\hat{N}_x - N_{Ts} - N_{Tx} \right) \right] + N_T(x) - p \tag{B21}$$

with

$$N_T(x) = \frac{K_{11}}{C_{11}}\left(C_{Tx}\frac{\gamma_{sk}g^2}{a^2}e^{gx/a} + C_{Ts}\frac{\gamma_s g^2}{a^2}e^{gx/a}\right) - \left(K_{Tx}\frac{\gamma_{sk}g^2}{a^2}e^{gx/a} + K_{Ts}\frac{\gamma_s g^2}{a^2}e^{gx/a}\right)$$

where the primes denote total differentiation with respect to x.

Buckling Equations

The equilibrium equations and boundary equations which govern the buckling behavior of the stiffened cylinder are obtained by substituting equations (B16) into equations (B14) and (B15). If only linear terms in the buckling displacements (subscript B terms) are retained, and if equations (B17) are utilized, the following buckling equations are obtained:

$$\left.\begin{array}{l} N_{x_B,x} + N_{xy_B,y} = 0 \\[2ex] N_{xy_B,x} + N_{y_B,y} = 0 \\[2ex] -M_{x_B,xx} + M_{xy_B,xy} - M_{yx_B,xy} - M_{y_B,yy} + \dfrac{N_{y_B}}{R} + \hat{N}_x w_{B,xx} - N_{x_B}w''_A \\[2ex] -N_{y_A}w_{B,yy} + 2\hat{N}_{xy}w_{B,xy} = 0 \end{array}\right\} \quad (B22)$$

with the boundary conditions

$$\left.\begin{array}{ccc} N_{x_B} = 0 & & u_B = 0 \\[1ex] N_{xy_B} = 0 & & v_B = 0 \\[1ex] & \text{or} & \\[1ex] M_{x_B} = 0 & & w_{B,x} = 0 \\[1ex] M_{x_B,x} - \left(M_{xy_B,y} - M_{yx_B,y}\right) - \hat{N}_x w_{B,x} + N_{x_B}w'_A - \hat{N}_{xy}w_{B,y} = 0 & & w_B = 0 \end{array}\right\} \quad (B23)$$

where the stress resultants with the B subscript are given as in equation (B9) with the strains and curvatures defined as

$$\epsilon_{x_B} = u_{B,x} + w'_A w_{B,x}$$

$$\epsilon_{y_B} = v_{B,y} + \frac{w_B}{R}$$

$$\gamma_{xy_B} = u_{B,y} + v_{B,x} + w'_A w_{B,y} \qquad (B24)$$

$$\kappa_x = -w_{B,xx}$$

$$\kappa_y = -w_{B,yy}$$

$$\kappa_{xy} = -2w_{B,xy}$$

It is assumed that there are no additional thermal moments and thermal forces during the buckling process so that

$$N_{Tx_B} = N_{Ty_B} = N_{Ts_B} = N_{Tr_B} = M_{Tx_B} = M_{Ty_B} = M_{Ts_B} = M_{Tr_B} = 0$$

APPENDIX C

NUMERICAL SOLUTIONS

The solutions to the prebuckling and buckling equations were found by employing the finite-difference method. The equations were formed into a system of second-order difference equations. As shown in reference 25, this type of system can be easily solved by matrix algebra with a modified Gaussian elimination technique.

In many thermal buckling problems of technical interest, a knowledge of the interaction between thermal and mechanical loads is desired. Hence, for the present problem there are two possible choices for a buckling parameter: (1) the magnitude of the applied mechanical load (for example, the compressive load or external pressure) for a fixed temperature distribution or (2) the magnitude of a temperature change which determines thermal forces and moments for fixed mechanical loading. In the present study a solution was developed for each parameter. The solution using mechanical loading as the buckling parameter is similar in form to that of reference 17 so that the details are omitted herein. The solution with temperature as the buckling parameter is described in detail in the following sections.

To employ temperature as a buckling parameter, a scalar temperature change T_A is defined so that $T_{sk} = T_A \beta_{sk}$, $T_s = T_A \beta_s$, and $T_r = T_A \beta_r$; thus, in the shell

$$T = T_A \beta_{sk} \left(1 + \gamma_{sk} e^{gx/a} \right) \tag{C1a}$$

whereas in the stringers

$$T = T_A \beta_s \left(1 + \gamma_s e^{gx/a} \right) \tag{C1b}$$

and in the rings

$$T = T_A \beta_r \left(1 + \gamma_r e^{gx/a} \right) \tag{C1c}$$

Note that in the integrals associated with equations (B11) and (B12), T_A can be considered as a constant.

By virtue of equations (C1), the magnitude of the relative temperatures in the stiffened cylinder is linearly related to a scalar T_A. The shape of the temperature distribution is specified by the constants β, γ, and g. Thus, the problem to be solved is one in which the magnitude of the base temperature T_A may vary while the shape of the temperature distribution remains constant.

Prebuckling Solution

To formulate the prebuckling equations as a second-order finite-difference system, the variable ξ is introduced so that

$$w_A'' = \xi \tag{C2}$$

If the first and second derivatives at the ith station of the stiffened shell are approximated by central differences as

$$\left.\begin{array}{l} (f')_i = \dfrac{f_{i+1} - f_{i-1}}{2\Delta} \\[3ex] (f'')_i = \dfrac{f_{i+1} - 2f_i + f_{i-1}}{\Delta^2} \end{array}\right\} \tag{C3}$$

the prebuckling equilibrium equation (B21) and the definition of the variable ξ (eq. (C2)) can be written at the ith station as

$$\left.\begin{array}{l} \beta_1 \dfrac{\xi_{i+1} - 2\xi_i + \xi_{i-1}}{\Delta^2} + \beta_2 \xi_i + \beta_3(i)\left(w_A\right)_i = \beta_4 + T_A \beta_5(i) \\[3ex] \dfrac{\left(w_A\right)_{i+1} - 2\left(w_A\right)_i + \left(w_A\right)_{i-1}}{\Delta^2} - \xi_i = 0 \end{array}\right\} \tag{C4}$$

with

$$\beta_1 = D_{11} - \frac{K_{11}^2}{C_{11}}$$

$$\beta_2 = \frac{2}{R}\left(\frac{K_{11}C_{12}}{C_{11}} - K_{12}\right) + \hat{N}_x$$

$$\beta_3(i) = \frac{1}{R^2}\left[\overline{C}_{22}(i) - \frac{C_{12}^2}{C_{11}}\right]$$

$$\beta_4 = \frac{C_{12}}{C_{11}}\frac{\hat{N}_x}{R}$$

$$\beta_5(i) = \frac{1}{R}\left[\overline{N}_{Ty}(i) + \overline{N}_{Tr}(i) - \frac{C_{12}}{C_{11}}\left(\overline{N}_{Tx} + \overline{N}_{Ts}\right)\right] + \frac{K_{11}}{C_{11}}\left(\overline{C}_{Tx}\frac{\gamma_{sk}g^2}{a^2}e^{gx/a}\right.$$

$$\left. + \overline{C}_{Ts}\frac{\gamma_s g^2}{a^2}e^{gx/a}\right) - \left(\overline{K}_{Tx}\frac{\gamma_{sk}g^2}{a^2}e^{gx/a} + \overline{K}_{Ts}\frac{\gamma_s g^2}{a^2}e^{gx/a}\right)$$

where

$$\widetilde{C}_{22}(i) = \int \frac{E_y}{1 - \mu_x \mu_y} \, dz + \frac{\delta_{iH} E_r A_r}{\Delta}$$

$$\overline{N}_{Tr}(i) = \frac{\delta_{iH}}{\Delta} \overline{C}_{Tr}\left(1 + \gamma_r e^{gx/a}\right)$$

with the integration to be performed over the shell wall and

$$\delta_{iH} = 1 \qquad\qquad\qquad (i = H)$$

$$\delta_{iH} = 0 \qquad\qquad\qquad (i \neq H)$$

The subscript H denotes the difference station at which a ring is located. The barred thermal terms are found by considering a unit temperature change and letting

$$T_{sk} = \beta_{sk}$$

$$T_s = \beta_s$$

$$T_r = \beta_r$$

in equations (B11) and (B12).

In considering the boundary conditions associated with equation (C4), it was assumed that the cylinder was supported at each end (w = 0) and that the ends were free to expand longitudinally and a compressive load is prescribed at the boundary. Under these assumptions

$$N_{x_A} = -\hat{N}_x \qquad\qquad\qquad (C5)$$

where $\hat{N}_x$ is the magnitude of the applied compressive load. If the cylinder is supported so that $w_A = 0$ at the ends, the boundary conditions on w (eqs. (B18c) and (B18d)) can be stated in finite-difference form at stations $i = 0$ and $i = k$ (at the ends of the cylinder where $x = 0$ and $x = a$, respectively) as follows: For simply supported shells

$$\left.\begin{aligned} \beta_1 \xi_0 &= \beta_6 + T_A \beta_7(0) \\ \beta_1 \xi_k &= \beta_6 + T_A \beta_7(k) \end{aligned}\right\} \qquad\qquad (C6a)$$

and for clamped shells (by using the definition of ξ and eq. (C3))

$$\left.\begin{array}{l} \Delta^2 \xi_0 - 2\left(w_A\right)_1 = 0 \\ \Delta^2 \xi_k - 2\left(w_A\right)_{k-1} = 0 \end{array}\right\} \tag{C6b}$$

where

$$\beta_6 = \hat{N}_x\left(\bar{e} - \frac{K_{11}}{C_{11}}\right)$$

and

$$\beta_7(i) = \frac{K_{11}}{C_{11}}\left(\overline{N}_{Ts} + \overline{N}_{Tx}\right) - \left(\overline{M}_{Tx} + \overline{M}_{Ts}\right) \qquad (i = 0,k)$$

The governing equations (C4) and boundary conditions (C6) can be written in matrix form as

$$\begin{bmatrix} \overline{L} & \overline{K} & & & & & & \\ I & L_1 & I & & & & & \\ & I & L_2 & I & & & & \\ & & & \cdot & & & & \\ & & & & \cdot & & & \\ & & & & & \cdot & & \\ & & & & I & L_{k-1} & I \\ & & & & & \overline{K} & \overline{L} \end{bmatrix} \begin{bmatrix} \left(z_A\right)_0 \\ \left(z_A\right)_1 \\ \left(z_A\right)_2 \\ \cdot \\ \cdot \\ \cdot \\ \left(z_A\right)_{k-1} \\ \left(z_A\right)_k \end{bmatrix} = \begin{bmatrix} T_A R_0 + \overline{S} \\ T_A R_1 + S \\ T_A R_2 + S \\ \cdot \\ \cdot \\ \cdot \\ T_A R_{k-1} + S \\ T_A R_k + \overline{S} \end{bmatrix} \tag{C7}$$

where

$$\left(z_A\right)_i = \begin{bmatrix} \xi_i \\ \left(w_A\right)_i \end{bmatrix} \qquad (i = 0,1,2,\ .\ .\ .k)$$

$$L_i = \begin{bmatrix} -2 + \dfrac{\Delta^2 \beta_2}{\beta_1} & \dfrac{\Delta^2}{\beta_1}\,\beta_3(i) \\ -\Delta^2 & -2 \end{bmatrix} \qquad (i = 1,2,3,\ .\ .\ .k-1)$$

$\cdot$

$$R_i = \begin{bmatrix} \dfrac{\Delta^2}{\beta_1}\,\beta_5(i) \\[2ex] 0 \end{bmatrix} \qquad\qquad (i = 1,2,3,\ .\ .\ .k\text{-}1)$$

$$S = \begin{bmatrix} \dfrac{\Delta^2}{\beta_1}\,\beta_4 \\[2ex] 0 \end{bmatrix}$$

$$I = \begin{bmatrix} 1 & 0 \\ 0 & 1 \end{bmatrix}$$

For simple support boundary conditions

$$\overline{L} = I$$

$$\overline{K} = \begin{bmatrix} 0 & 0 \\ 0 & 0 \end{bmatrix}$$

$$\overline{S} = \begin{bmatrix} \dfrac{\beta_6}{\beta_1} \\[2ex] 0 \end{bmatrix}$$

$$R_0 = \begin{bmatrix} \dfrac{\beta_7(0)}{\beta_1} \\[2ex] 0 \end{bmatrix}$$

$$R_k = \begin{bmatrix} \dfrac{\beta_7(k)}{\beta_1} \\[2ex] 0 \end{bmatrix}$$

and for clamped boundary conditions

$$\overline{L} = \begin{bmatrix} \Delta^2 & 2 \\ 0 & 1 \end{bmatrix}$$

$$\overline{K} = \begin{bmatrix} 0 & -2 \\ 0 & 0 \end{bmatrix}$$

$$\overline{S} = R_0 = R_k = \begin{bmatrix} 0 \\ 0 \end{bmatrix}$$

Because equation (C7) contains a band matrix, to conserve computer storage it is convenient to solve for the unknowns $\left(z_A\right)_i$ by Gaussian elimination. By performing a series of elementary row operations (see ref. 17), equation (C7) can be written as

$$\begin{bmatrix} I & P_0 & & & & & \\ & I & P_1 & & & & \\ & & I & P_2 & & & \\ & & & \cdot & & & \\ & & & & \cdot & & \\ & & & & & \cdot & \\ & & & & & I & P_{k-1} \\ & & & & & & I \end{bmatrix} \begin{bmatrix} \left(z_A\right)_0 \\ \left(z_A\right)_1 \\ \left(z_A\right)_2 \\ \cdot \\ \cdot \\ \cdot \\ \left(z_A\right)_{k-1} \\ \left(z_A\right)_k \end{bmatrix} = T_A \begin{bmatrix} \left(Q_T\right)_0 \\ \left(Q_T\right)_1 \\ \left(Q_T\right)_2 \\ \cdot \\ \cdot \\ \cdot \\ \left(Q_T\right)_{k-1} \\ \left(Q_T\right)_k \end{bmatrix} + \begin{bmatrix} Q_0 \\ Q_1 \\ Q_2 \\ \cdot \\ \cdot \\ \cdot \\ Q_{k-1} \\ Q_k \end{bmatrix} \qquad (C8)$$

where

$$\left.\begin{aligned} P_0 &= \overline{L}^{-1}\overline{K} \\ P_i &= \left(L_i - P_{i-1}\right)^{-1} \end{aligned} \qquad (i = 1,2,\ldots k-1)\right\} \quad (C9)$$

$$\left.\begin{aligned} Q_0 &= \overline{S}\,\overline{L}^{-1} = Q_k \\ Q_i &= P_i\left(S - Q_{i-1}\right) \end{aligned} \qquad (i = 1,2,\ldots k-1)\right\} \quad (C10)$$

and

$$\left.\begin{aligned} \left(Q_T\right)_0 &= R_0\overline{L}^{-1} \\ \left(Q_T\right)_i &= P_i\left[R_i - \left(Q_T\right)_{i-1}\right] \qquad (i = 1,2,\ldots k-1) \\ \left(Q_T\right)_k &= R_k\overline{L}^{-1} \end{aligned}\right\} \quad (C11)$$

The unknowns $(z_A)_i$ are determined by finding P_i, Q_i, and $(Q_T)_i$ from equations (C9), (C10), and (C11) and solving successively for $(z_A)_{k-1}$, $(z_A)_{k-2}$, . . . from equations (C8).

It should be noted from equations (C8) that the prebuckling radial displacements w_A are linear with T_A so that

$$(z_A)_i = (z_{A_M})_i + T_A(z_{A_T})_i = \begin{bmatrix} (\xi_M)_i \\ (w_{A_M})_i \end{bmatrix} + T_A \begin{bmatrix} (\xi_T)_i \\ (w_{A_T})_i \end{bmatrix} \tag{C12}$$

where $(z_{A_M})_i$ are the variables associated with deformation resulting from mechanical loading whereas $(z_{A_T})_i$ are the variables associated with deformation resulting from thermal loading. Deformations associated with mechanical loading are found by setting T_A equal to zero in equation (C8) and solving for $(z_A)_i$. Deformations associated with thermal loadings are obtained by deleting the Q_i column from the right-hand side of equation (C8) and solving for $(z_A)_i$ corresponding to a unit base temperature change $(T_A = 1)$.

Buckling Solution

If torsional loading is neglected $(\hat{N}_{xy} = 0)$, the partial differential equations governing buckling of a stiffened cylinder (eqs. (B22) and (B23)) can be uncoupled into a set of ordinary differential equations by assuming the following relations:

$$\left.\begin{aligned} u_B &= U(x) \cos \frac{ny}{R} \\[2ex] v_B &= V(x) \sin \frac{ny}{R} \\[2ex] w_B &= W(x) \cos \frac{ny}{R} \\[2ex] M_{x_B} &= M(x) \cos \frac{ny}{R} \end{aligned}\right\} \tag{C13}$$

where n, the number of circumferential buckling waves, is an integer. The substitution of equations (C13) into equations (B22) together with the definition of M_{x_B} yields four ordinary differential equations in u, v, w, and M. To eliminate derivatives of higher order than 2, equation (B20) was employed together with the expression

$$w_{B,xxx} = -\frac{M_{x_{B,x}}}{D_{11}} + \frac{K_{11}}{D_{11}}u_{B,xx} + \frac{K_{12}}{D_{11}}v_{B,xy} + \frac{1}{R}\frac{K_{12}}{D_{11}}w_{B,x} + \frac{K_{11}}{D_{11}}\left(w_{A,x}w_{B,x}\right)_{,x} - \frac{D_{12}}{D_{11}}w_{B,xyy}$$

$$(C14)$$

obtained from the derivative of M_{x_B}. The resulting buckling equations can be written as

$$\Lambda_{11}U'' + \Lambda_{12}U + \Lambda_{13}V' + \left(\Lambda_{14} - T_A\Lambda_{15}\right)W'' + \left(\Lambda_{16} - T_A\Lambda_{17}\right)W'$$
$$+ \left(\Lambda_{18} - T_A\Lambda_{19}\right)W + \Lambda_{110}M' = 0 \qquad (C15a)$$

$$\Lambda_{21}U' + \Lambda_{22}V'' + \Lambda_{23}V + \Lambda_{24}W'' + \left(\Lambda_{25} - T_A\Lambda_{26}\right)W' + \left(\Lambda_{27} - T_A\Lambda_{28}\right)W = 0 \quad (C15b)$$

$$\left(\Lambda_{31} - T_A\Lambda_{32}\right)U' + \Lambda_{33}V'' + \left(\Lambda_{34} - T_A\Lambda_{35}\right)V + \left(\Lambda_{36} - T_A\Lambda_{37}\right)W'' + \left(\Lambda_{38} - T_A\Lambda_{39}\right.$$
$$\left. - T_A^2\Lambda_{310}\right)W' + \left(\Lambda_{311} - T_A\Lambda_{312}\right)W - M'' = 0 \qquad (C15c)$$

$$\Lambda_{41}U' + \Lambda_{42}V + \Lambda_{43}W'' + \left(\Lambda_{44} - T_A\Lambda_{45}\right)W' + \Lambda_{46}W + M = 0 \qquad (C15d)$$

where

$$\Lambda_{11} = C_{11} - \frac{K_{11}^2}{D_{11}}$$

$$\Lambda_{12} = -C_{66}\left(\frac{n}{R}\right)^2$$

$$\Lambda_{13} = \left(C_{12} + C_{66} - \frac{K_{12}K_{11}}{D_{11}}\right)\frac{n}{R}$$

$$\Lambda_{14} = \Lambda_{11}w'_{A_M}$$

$$\Lambda_{15} = -\Lambda_{11}w'_{A_T}$$

$$\Lambda_{16} = \Lambda_{11}w''_{A_M} + \frac{1}{R}\left(C_{12} - \frac{K_{11}K_{12}}{D_{11}}\right) + \left(K_{12} + 2K_{66} - \frac{K_{11}D_{12}}{D_{11}}\right)\left(\frac{n}{R}\right)^2$$

$$\Lambda_{17} = -\Lambda_{11} w''_{A_T}$$

$$\Lambda_{18} = -C_{66}\left(\frac{n}{R}\right)^2 w'_{A_M}$$

$$\Lambda_{19} = C_{66}\left(\frac{n}{R}\right)^2 w'_{A_T}$$

$$\Lambda_{110} = \frac{K_{11}}{D_{11}}$$

$$\Lambda_{21} = -\left(C_{12} + C_{66}\right)\frac{n}{R}$$

$$\Lambda_{22} = C_{66}$$

$$\Lambda_{23} = -C_{22}\left(\frac{n}{R}\right)^2$$

$$\Lambda_{24} = \left(K_{12} + 2K_{66}\right)\frac{n}{R}$$

$$\Lambda_{25} = \Lambda_{21} w'_{A_M}$$

$$\Lambda_{26} = -\Lambda_{21} w'_{A_T}$$

$$\Lambda_{27} = -C_{66}\frac{n}{R} w''_{A_M} - \frac{C_{22}n}{R^2} - K_{22}\left(\frac{n}{R}\right)^3$$

$$\Lambda_{28} = C_{66}\frac{n}{R} w''_{A_T}$$

$$\Lambda_{31} = \frac{C_{12}}{R} + \left(K_{12} + 2K_{66}\right)\left(\frac{n}{R}\right)^2 - C_{11} w''_{A_M}$$

$$\Lambda_{32} = C_{11} w''_{A_T}$$

$$\Lambda_{33} = -2K_{66}\frac{n}{R}$$

$$\Lambda_{34} = \frac{C_{22}n}{R^2} + K_{22}\left(\frac{n}{R}\right)^3 - C_{12}\frac{n}{R}w''_{A_M}$$

$$\Lambda_{35} = C_{12}\frac{n}{R}w''_{A_T}$$

$$\Lambda_{36} = K_{11}w''_{A_M} - \left[4D_{66} + \frac{G_S J_S}{d} + \sum_{j=1}^{N} \delta(x - j\ell) G_r J_r + D_{12}\right]\left(\frac{n}{R}\right)^2$$

$$- \frac{K_{12}}{R} + \hat{N}_x$$

$$\Lambda_{37} = -K_{11}w''_{A_T}$$

$$\Lambda_{38} = \left[\frac{C_{12}}{R} + \left(K_{12} + 2K_{66}\right)\left(\frac{n}{R}\right)^2\right]w'_{A_M} - C_{11}w'_{A_M}w''_{A_M}$$

$$- \sum_{j=1}^{N} \delta'(x - j\ell) G_r J_r\left(\frac{n}{R}\right)^2$$

$$\Lambda_{39} = -\left[\frac{C_{12}}{R} + \left(K_{12} + 2K_{66}\right)\left(\frac{n}{R}\right)^2\right]w'_{A_T} + C_{11}\left(w''_{A_M}w'_{A_T} + w'_{A_M}w''_{A_T}\right)$$

$$\Lambda_{310} = C_{11}w'_{A_T}w''_{A_T}$$

$$\Lambda_{311} = \left\{\left[\frac{C_{12}K_{11}}{C_{11}} - 2\left(K_{12} - K_{66}\right)\right]\left(\frac{n}{R}\right)^2 - \frac{C_{12}}{R}\right\}w''_{A_M} + \frac{1}{R}\left(C_{22}\right.$$

$$\left. - \frac{C_{12}^2}{C_{11}}\right)\left(\frac{n}{R}\right)^2 w_{A_M} + D_{22}\left(\frac{n}{R}\right)^4 + \frac{2K_{22}}{R}\left(\frac{n}{R}\right)^2 + \frac{C_{22}}{R^2} - \frac{C_{12}}{C_{11}}\left(\frac{n}{R}\right)^2\hat{N}_x$$

$$\Lambda_{312} = \left\{\left[2\left(K_{12} - K_{66}\right) - \frac{C_{12}K_{11}}{C_{11}}\right]\left(\frac{n}{R}\right)^2 + \frac{C_{12}}{R}\right\}w''_{A_T} - \frac{1}{R}\left(C_{22}\right.$$

$$\left. - \frac{C_{12}^2}{C_{11}}\right)\left(\frac{n}{R}\right)^2 w_{A_T} + \left[\overline{N}_{Tr} + \overline{N}_{Ty} - \frac{C_{12}}{C_{11}}\left(\overline{N}_{Ts} + \overline{N}_{Tx}\right)\right]\left(\frac{n}{R}\right)^2$$

$$\Lambda_{41} = -K_{11}$$

$$\Lambda_{42} = -K_{12}\frac{n}{R}$$

$$\Lambda_{43} = D_{11}$$

$$\Lambda_{44} = -K_{11}w'_{A_M}$$

$$\Lambda_{45} = K_{11}w'_{A_T}$$

$$\Lambda_{46} = -\left[D_{12}\left(\frac{n}{R}\right)^2 + \frac{K_{12}}{R}\right]$$

To represent the Dirac delta and doublet functions appearing in the coefficients of equation (C15), the following finite-difference approximations were employed:

$$\delta(x - j\ell)\,f = \delta_{iH}\frac{f}{\Delta}$$

$$\delta'(x - j\ell)\,f = \delta_{(i-1)H}\frac{f}{2\Delta^2} - \delta_{(i+1)H}\frac{f}{2\Delta^2}$$

In this form, equations (C15) are the analogs of equations (36) of reference 17. As outlined in that reference, equations of this form can be cast into matrix form, and buckling loads can be found by examination of a simple determinant resulting from a Gaussian elimination procedure similar to that previously described herein. A solution of this type was obtained in the present study by using the determinant plotting method described in reference 17.

Modal Iteration Scheme

If the central difference formula (eqs. (C3)) are employed for the first and second derivatives of U, V, W, and M in equations (C15), the equilibrium equations can be written at the interior stations of the shell as

$$A_i Z_{i-1} + B_i Z_i + C_i Z_{i+1} = T_A\left(D_i Z_{i-1} + E_i Z_i + F_i Z_{i+1}\right)$$
$$+ T_A^2\left(G_i Z_{i-1} + H_i Z_{i+1}\right) \qquad (i = 1,2,\ldots k-1) \quad (C16)$$

where

$$A_i = \begin{bmatrix} \Lambda_{11} & -\dfrac{\Delta}{2}\Lambda_{13} & \Lambda_{14} - \dfrac{\Delta}{2}\Lambda_{16} & -\dfrac{\Delta}{2}\Lambda_{110} \\[2ex] -\dfrac{\Delta}{2}\Lambda_{21} & \Lambda_{22} & \Lambda_{24} - \dfrac{\Delta}{2}\Lambda_{25} & 0 \\[2ex] -\dfrac{\Delta}{2}\Lambda_{31} & \Lambda_{33} & \overline{\Lambda}_{36} - \dfrac{\Delta}{2}\overline{\Lambda}_{38} & -1 \\[2ex] -\dfrac{\Delta}{2}\Lambda_{41} & 0 & \Lambda_{43} - \dfrac{\Delta}{2}\Lambda_{44} & 0 \end{bmatrix}$$

$$B_i = \begin{bmatrix} -2\Lambda_{11} + \Delta^2\Lambda_{12} & 0 & -2\Lambda_{14} + \Delta^2\Lambda_{18} & 0 \\[2ex] 0 & -2\Lambda_{22} + \Delta^2\overline{\Lambda}_{23} & -2\Lambda_{24} + \Delta^2\overline{\Lambda}_{27} & 0 \\[2ex] 0 & -2\Lambda_{33} + \Delta^2\overline{\Lambda}_{34} & -2\overline{\Lambda}_{36} + \Delta^2\overline{\Lambda}_{311} & 2 \\[2ex] 0 & \Delta^2\Lambda_{42} & -2\Lambda_{43} + \Lambda^2\Lambda_{46} & \Delta^2 \end{bmatrix}$$

$$C_i = \begin{bmatrix} \Lambda_{11} & \dfrac{\Delta}{2}\Lambda_{13} & \Lambda_{14} + \dfrac{\Delta}{2}\Lambda_{16} & \dfrac{\Delta}{2}\Lambda_{110} \\[2ex] \dfrac{\Delta}{2}\Lambda_{21} & \Lambda_{22} & \Lambda_{24} + \dfrac{\Delta}{2}\Lambda_{25} & 0 \\[2ex] \dfrac{\Delta}{2}\Lambda_{31} & \Lambda_{33} & \overline{\Lambda}_{36} + \dfrac{\Delta}{2}\overline{\Lambda}_{38} & -1 \\[2ex] \dfrac{\Delta}{2}\Lambda_{41} & 0 & \Lambda_{43} + \dfrac{\Delta}{2}\Lambda_{44} & 0 \end{bmatrix}$$

$$D_i = \begin{bmatrix} 0 & 0 & \Lambda_{15} - \dfrac{\Delta}{2}\Lambda_{17} & 0 \\[2ex] 0 & 0 & -\dfrac{\Delta}{2}\Lambda_{26} & 0 \\[2ex] -\dfrac{\Delta}{2}\Lambda_{32} & 0 & \Lambda_{37} - \dfrac{\Delta}{2}\Lambda_{39} & 0 \\[2ex] 0 & 0 & -\dfrac{\Delta}{2}\Lambda_{45} & 0 \end{bmatrix}$$

$$E_i = \begin{bmatrix} 0 & 0 & -2\Lambda_{15} + \Delta^2\Lambda_{19} & 0 \\ 0 & 0 & \Delta^2\Lambda_{28} & 0 \\ 0 & \Delta^2\Lambda_{35} & -2\Lambda_{37} + \Delta^2\overline{\Lambda}_{312} & 0 \\ 0 & 0 & 0 & 0 \end{bmatrix}$$

$$F_i = \begin{bmatrix} 0 & 0 & \Lambda_{15} + \frac{\Delta}{2}\Lambda_{17} & 0 \\ 0 & 0 & \frac{\Delta}{2}\Lambda_{26} & 0 \\ \frac{\Delta}{2}\Lambda_{32} & 0 & \Lambda_{37} + \frac{\Delta}{2}\Lambda_{39} & 0 \\ 0 & 0 & \frac{\Delta}{2}\Lambda_{45} & 0 \end{bmatrix}$$

$$G_i = \begin{bmatrix} 0 & 0 & 0 & 0 \\ 0 & 0 & 0 & 0 \\ 0 & 0 & -\frac{\Delta}{2}\Lambda_{310} & 0 \\ 0 & 0 & 0 & 0 \end{bmatrix}$$

$$H_i = \begin{bmatrix} 0 & 0 & 0 & 0 \\ 0 & 0 & 0 & 0 \\ 0 & 0 & \frac{\Delta}{2}\Lambda_{310} & 0 \\ 0 & 0 & 0 & 0 \end{bmatrix}$$

with

$$\overline{\Lambda}_{23} = -\overline{C}_{22}\left(\frac{n}{R}\right)^2$$

$$\overline{\Lambda}_{27} = -C_{66}\frac{n}{R}w''_{A_M} - \overline{C}_{22}\frac{n}{R^2} - \overline{K}_{22}\left(\frac{n}{R}\right)^3$$

$$\overline{\Lambda}_{34} = \overline{C}_{22}\frac{n}{R^2} + \overline{K}_{22}\left(\frac{n}{R}\right)^3 - C_{12}\frac{n}{R}w''_{A_M}$$

$$\overline{\Lambda}_{36} = K_{11}w''_{A_M} - \left(4D_{66} + \frac{G_sJ_s}{d} + \delta_{iH}\frac{G_rJ_r}{\Delta} + D_{12}\right)\left(\frac{n}{R}\right)^2 + \frac{K_{12}}{R} + \hat{N}_x$$

$$\overline{\Lambda}_{38} = \left[\frac{C_{12}}{R} + \left(K_{12} + 2K_{66}\right)\left(\frac{n}{R}\right)^2\right]w'_{A_M} - C_{11}w'_{A_M}w''_{A_M} + \frac{1}{2\Delta^2}G_rJ_r\left(\frac{n}{R}\right)^2\left[\delta_{(i-1)H} - \delta_{(i+1)H}\right]$$

$$\overline{\Lambda}_{311} = \left\{\left[\frac{C_{12}K_{11}}{C_{11}} - 2\left(K_{12} - K_{66}\right)\right]\left(\frac{n}{R}\right)^2 - \frac{C_{12}}{R}\right\}w''_{A_M} + \frac{1}{R}\left(\overline{C}_{22} - \frac{C_{12}^2}{C_{11}}\right)\left(\frac{n}{R}\right)^2 w_{A_M} + \overline{D}_{22}\left(\frac{n}{R}\right)^4$$

$$+ \frac{2\overline{K}_{22}}{R}\left(\frac{n}{R}\right)^2 + \frac{\overline{C}_{22}}{R^2} - \frac{C_{12}}{C_{11}}\left(\frac{n}{R}\right)^2\hat{N}_x$$

$$\overline{\Lambda}_{312} = \left\{\left[2\left(K_{12} - K_{66}\right) - \frac{C_{12}K_{11}}{C_{11}}\right]\left(\frac{n}{R}\right)^2 + \frac{C_{12}}{R}\right\}w''_{A_T} - \frac{1}{R}\left(\overline{C}_{22} - \frac{C_{12}^2}{C_{11}}\right)\left(\frac{n}{R}\right)^2 w_{A_T} + \left[\overline{N}_{Tr} + \overline{N}_{Ty}\right.$$

$$\left. - \frac{C_{12}}{C_{11}}\left(\overline{N}_{Ts} + \overline{N}_{Tx}\right)\right]\left(\frac{n}{R}\right)^2$$

in which

$$\overline{C}_{22} = \int\frac{E_y}{1 - \mu_x\mu_y}\,dz + \delta_{iH}\frac{E_rA_r}{\Delta}$$

$$\overline{K}_{22} = \int\frac{E_y}{1 - \mu_x\mu_y}\,z\,dz + \delta_{iH}\frac{E_rA_r\overline{z}_r}{\Delta}$$

$$\overline{D}_{22} = \int\frac{E_y}{1 - \mu_x\mu_y}\,z^2dz + \delta_{iH}\left(\frac{E_rI_r}{\Delta} + \frac{E_rA_r\overline{z}_r^2}{\Delta}\right)$$

In order to develop a modal iteration solution, the following forward and backward difference formulas are introduced at ends of the cylinder (finite-difference stations 0 and k)

$$\left.\begin{aligned} f_0' &= \frac{1}{\Delta}\left(f_1 - f_0\right) \\ f_k' &= \frac{1}{\Delta}\left(f_k - f_{k-1}\right) \end{aligned}\right\} \tag{C17}$$

The cylinder was assumed to be supported at the ends so that $w_B = 0$. The eight possible boundary conditions for buckling in equations (B23) can be written in matrix form as

$$\left.\begin{aligned} B_0 Z_0 + C_0 Z_1 &= T_A E_0 Z_1 \\ A_k Z_{k-1} + B_k Z_k &= T_A E_k Z_{k-1} \end{aligned}\right\} \tag{C18}$$

with

$$B_0 = \bar{\alpha}\begin{bmatrix} -\Lambda_{11} & \frac{\Delta n}{R}\left(C_{12} - \frac{K_{11}K_{12}}{D_{11}}\right) & 0 & \Delta\frac{K_{11}}{D_{11}} \\ -C_{66}\frac{n}{R}\Delta & -C_{66} & 0 & 0 \\ 0 & 0 & 0 & 0 \\ 0 & 0 & -1 & 0 \end{bmatrix} + \begin{bmatrix} 1 - \bar{\alpha}_{11} & 0 & 0 & 0 \\ 0 & 1 - \bar{\alpha}_{22} & 0 & 0 \\ 0 & 0 & 1 & 0 \\ 0 & 0 & 0 & 1 - \bar{\alpha}_{44} \end{bmatrix}$$

$$\tag{C19a}$$

$$C_0 = \bar{\alpha}\begin{bmatrix} \Lambda_{11} & 0 & \Lambda_{11}w'_{A_M}(0) & 0 \\ 0 & C_{66} & 2K_{66}\frac{n}{R} & 0 \\ 0 & 0 & 0 & 0 \\ 0 & 0 & 1 & 0 \end{bmatrix} \tag{C19b}$$

$$E_0 = \bar{\alpha} \begin{bmatrix} 0 & 0 & -\Lambda_{11} w'_{A_T}(0) & 0 \\ 0 & 0 & 0 & 0 \\ 0 & 0 & 0 & 0 \\ 0 & 0 & 0 & 0 \end{bmatrix} \qquad (C19c)$$

where

$$\bar{\alpha} = \begin{bmatrix} \bar{\alpha}_{11} & 0 & 0 & 0 \\ 0 & \bar{\alpha}_{22} & 0 & 0 \\ 0 & 0 & 0 & 0 \\ 0 & 0 & 0 & \bar{\alpha}_{44} \end{bmatrix}$$

and

$$\left. \begin{array}{l} A_k = C_0 \\ B_k = B_0 \\ E_k = -E_0 \end{array} \right\} \qquad (C20)$$

where in equations (C20) w'_A terms are to be evaluated at $x = a$ rather than at $x = 0$. The elements of the selection matrix $\bar{\alpha}$ are defined as follows:

Element	Value	Boundary condition
$\bar{\alpha}_{11}$	0	$u_B = 0$
	1	$N_{x_B} = 0$
$\bar{\alpha}_{22}$	0	$v_B = 0$
	1	$N_{xy_B} = 0$
$\bar{\alpha}_{44}$	0	$M_{x_B} = 0$
	1	$v_B = 0$

The equilibrium equations (C16) and boundary conditions (C18) can now be written in matrix form as

$$AX = T_A BX + T_A^2 CX \qquad (C21)$$

where T_A is a scalar, X is a vector, and A, B, and C are matrices. In order to perform modal iteration, let

$$\lambda = \frac{1}{T_A} \qquad (C22)$$

so that equation (C21) can be written as

$$\lambda AX = BX + \frac{1}{\lambda} CX \qquad (C23)$$

To start the iteration process assume that $X = X^O$ where X^O is a trial eigenvector. Substitute X^O into the right-hand side of the approximate equation

$$\lambda AX \approx BX$$

and solve

$$A\lambda X = BX^O \qquad (C24)$$

by treating λX as the unknown variable. In finding the solution to equation (C24), Gaussian elimination (Potter's method) is employed to avoid having to find the inverse of A. The resulting approximate eigenvalue λ_1 and normalized eigenvector X^1 can be taken as

$$\lambda_1 = |\lambda X|$$

$$X^1 = \frac{\lambda X}{\lambda_1} \qquad (C25)$$

For subsequent iterations the equation

$$A\lambda X = BX^i + \frac{1}{\lambda_i} CX^i \qquad (i = 1,2,. . .) \qquad (C26)$$
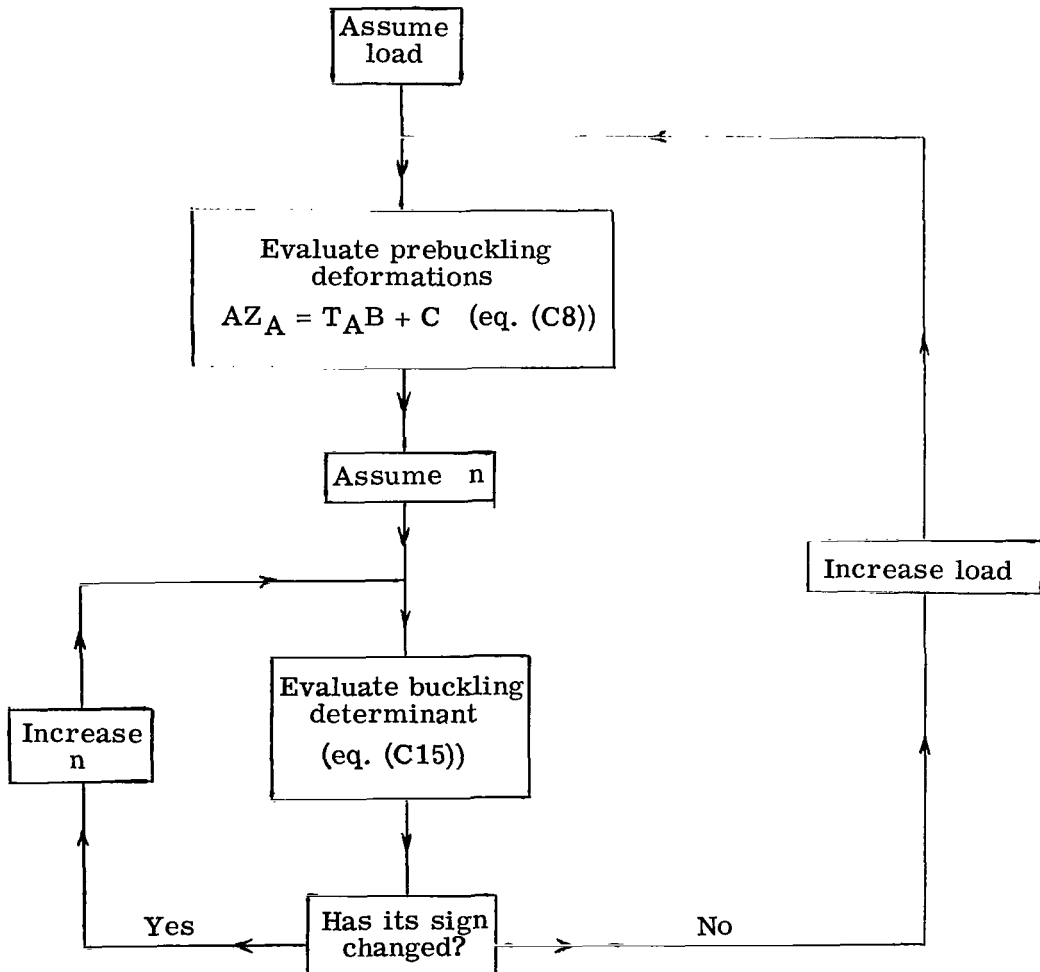
must be solved to find more accurate solutions to equation (C23). The iteration process converges to the largest characteristic value of λ (lowest T_A) provided $\frac{1}{\lambda} CX$ is small compared with BX. Thus the temperature T_A can be found for a specified number of circumferential waves n. The lowest value of T_A found is then the buckling temperature.

APPENDIX D

COMPUTER PROGRAMS

BAMSOC I

The computer program BAMSOC I finds the buckling load for a stiffened cylindrical shell subjected to mechanical and thermal loadings by using determinant plotting. The programed solution is similar to that developed in reference 17 and differs only in that the present solution considers thermal effects in a multilayered orthotropic cylinder. Buckling loads or buckling temperatures can be selected as the buckling parameter, and critical values are found by determinant plotting over user-specified ranges of circumferential wave number n and the buckling parameter. For a specified n, the program seeks a change in sign in a determinant or "modified residual" by varying the buckling parameter. A flow diagram for BAMSOC I (determinant plotting solution) follows:

```
                        ┌──────────┐
                        │ Assume   │
                        │  load    │
                        └────┬─────┘
                             │              ┌─ ──< ─── ──────────────┐
                             │                                       │
                             ▼                                       │
              ┌──────────────────────────────┐                      │
              │   Evaluate prebuckling        │                      │
              │     deformations              │                      │
              │  AZ_A = T_A B + C  (eq. (C8)) │                      │
              └───────────────┬──────────────┘                      │
                              ▼                                      │
                        ┌──────────┐                                 │
                        │Assume  n │                       ┌──────────────────┐
                        └────┬─────┘                       │  Increase load   │
                             │                             └──────────────────┘
              ┌──────────────┤                                       ▲
              │              ▼                                       │
       ┌──────────┐   ┌──────────────────┐                          │
       │ Increase │   │ Evaluate buckling│                          │
       │    n     │   │   determinant    │                          │
       └──────────┘   │   (eq. (C15))    │                          │
              ▲       └────────┬─────────┘                          │
              │                ▼                                     │
              │         ┌──────────────┐                            │
     Yes      │         │ Has its sign │    No                      │
       ◄──────┴─────────│  changed?    │──── > ──────────────────────
                        └──────────────┘
```

$$AZ_A = T_A B + C \quad \text{(eq. (C8))}$$

49

The program is written in **FORTRAN IV** and will run on the Control Data 6000 series computer with the Scope 3.0 operating system. The program elements were over-layed so that a maximum of 200 finite-difference intervals could be used on a remote computer terminal with 70 000 octal storage units. A maximum of 20 layers can be used in the shell. Input required by the program is contained in the following namelists:

$ CON

NI	initial value of n to be investigated
NF	final value of n
DELN	increment in n
NBARXI	initial or fixed value of $\hat{N}_x$, axial compressive load
NBARXF	final value of $\hat{N}_x$
DELNX	increment in $\hat{N}_x$
PINIT	initial or fixed value of p or q, lateral or hydrostatic pressure
PFIN	final value of p or q
DELP	increment in p or q
TAI	initial or fixed value of T_A, base temperature (see eq. (C1))
TAF	final value of T_A
DELTA	increment in T_A
KASE = 1	axial compression with fixed temperature and lateral pressure
= 2	lateral pressure with fixed temperature and axial compression
= 3	hydrostatic pressure with fixed temperature and axial compression
= 4	thermal loads corresponding to T_A with fixed mechanical loads

$ (end of CON)

$ NANCY

R	radius to reference surface
A	cylinder length
DELBAR	distance from inner wall surface to reference surface
BC = 1	simply supported for prebuckling analysis .
= 2	clamped for prebuckling analysis
ER	Young's modulus for ring
AR	area of ring
IR	moment of inertia of ring about its centroid
ZR	distance of centroid of ring to reference surface (positive, external rings)
GRJR	ring torsional stiffness, GJ
NRING	number of rings
NRSPACE	number of finite-difference intervals between adjacent rings (no more than 200 stations along cylinder length)
ES	Young's modulus for stringer
AS	area of stringer
IS	moment of inertia of stringer about its centroid
ZS	distance from centroid of stringer to reference surface (positive, external stringers)
GSJS	stringer torsional stiffness, GJ
D	stringer spacing

ECC   distance from reference surface to surface on which $\hat{N}_x$ acts

GAMS   stringer temperature shape parameter, γ_s (see eq. (C1b))

GAMR   ring temperature shape parameter, γ_r (see eq. (C1c))

TAUS $\int \alpha_s \beta_s(z) dA_s$

TAUR $\int \alpha_r \beta_r(z) dA_r$ where β is temperature shape parameter in equation (C1)

TAUSPR $\int \alpha_s \beta_s(z) z\, dA_s$

TAURPR $\int \alpha_r \beta_r(z) z\, dA_r$

G   exponential temperature shape factor, g (see eq. (C1))

EX(I) E_x of ith layer of shell (first layer lies on inner surface of shell; no more than 20 layers)

EY(I) E_y

NUX(I) μ_x

NUY(I) μ_y

GXY(I) G_{xy}

H(I)   thickness of layer

GAMMA(I)   layer temperature shape factor γ_{sk} (see eq. (C1a))

BETA(I)   layer temperature shape factor β_{sk} (see eq. (C1a))

ALPHAX(I) α_x

ALPHAY(I) α_y

LAYER   number of layers ($\leqq 20$)

$ (end of NANCY)

$ CORNIE

IALF = 1 $N_{x_B} = 0$, $v_B = 0$, $w_B = 0$, $M_{x_B} = 0$

= 2 $U_B = 0$, $v_B = 0$, $w_B = 0$, $M_{x_B} = 0$

= 3 $N_{x_B} = 0$, $N_{xy_B} = 0$, $w_B = 0$, $M_{x_B} = 0$

= 4 $U_B = 0$, $N_{xy_B} = 0$, $w_B = 0$, $M_{x_B} = 0$

= 5 $U_B = 0$, $N_{xy_B} = 0$, $w_B = 0$, $w_{B,x} = 0$

= 6 $N_{x_B} = 0$, $N_{xy_B} = 0$, $w_B = 0$, $w_{B,x} = 0$

= 7 $N_{x_B} = 0$, $v_B = 0$, $w_B = 0$, $w_{B,x} = 0$

= 8 $U_B = 0$, $v_B = 0$, $w_B = 0$, $w_{B,x} = 0$

MODE = 0   calculation of buckling mode shape is not required

$\neq 0$ calculation of buckling mode shape is required

IRING = 1   simplified ring theory described in appendixes A, B, and C

= 2   more accurate ring theory described in appendix E

$ (end of CORNIE)

$ RING (required only if IRING = 2)

IX I_x, moment of inertia for out-of-plane bending of ring (eq. (E11))

IOXZ $I_{o\bar{x}z}$, cross product of inertia for out-of-plane bending of ring (eq. (E11))

$ (end of RING)

A sample output listing for BAMSOC I follows. The case shown is the ring- and stringer-stiffened cylinder loaded by thermal loading alone. (See text.) The parameter

T_A has been selected as the change in temperature of the heated skin. Experience with determinant plotting solutions has shown that it is possible to miss sign changes in the determinant by taking too large an increment in the load parameter. As a safeguard against this possibility, the present program examines small loading increments, when unusual trends in the determinant are detected.

In the sample problem, for $N = 51$ or 52, the modified residual value was found to increase in value after a steady decline. The irregularity was detected and finer load increments were employed in the calculations and a change in the sign of the determinant was found. Note, however, that no irregularities were found for $N = 53$, and as a consequence, sign changes were found at higher temperatures. Further investigation with finer load increments in calculations not presented established a buckling temperature of about 525° F (292 K) for $N = 57$.

NAMELIST INPUT FOR BAMSOC I

```
$CON NI=50., NF=53., DELN=1., NBARXI=0., NBARXF=0., DELNX=1.,
PINIT=0., PFIN=0., DELP=1., TAI=450., TAF=600., DELTA=20., KASE=4$

$NANCY R=65., A=300., DELBAR=.03, BC=1, ER=16.4E6, AR=.246, IR=.1377,
ZR=-1.992, GRJR=3477., NRING=19, NRSPACE=10, ES=16.4E6, AS=.0495, IS=.004082,
ZS=-.342, GSJS=93., D=1.35, ECC=0., GAMS=0., GAMR=0., TAUS=0., TAUR=0.,
TAUSPR=0., TAURPR=0., G=0., EX(1)=14.5E6, EY(1)=14.5E6, NUX(1)=.3, NUY(1)=.3,
GXY(1)=5.580E6, H(1)=.06, GAMMA(1)=0., BETA(1)=1.,

ALPHAX(1)=5.E-6, ALPHAY(1)=5.E-6, LAYER=1$
$CORNIE IALF=1, MODE=0, IRING=1$
```

BAMSOC I

CALCULATION OF BUCKLING LOAD FOR THERMALLY STRESSED, STIFFENED, MULTI-LAYERED CYLINDER USING DETERMINANT PLOTTING
         CHANG-CARD   RDF364   NASA LANGLEY RESEARCH CENTER   1968

DATE 03/27/69

```
    NI= 5.0000E+01        NF= 5.3000E+01        DELN= 1.0000E+00
   TAI= 4.5000E+02       TAF= 6.0000E+02       DELTA= 2.0000E+01
 NBARX= 0.
     P= 0.
```

INPUT FOR PROGRAM THERMUL   CHANG-CARD   A2031   RDF364   JANUARY,1968

```
GEOMETRY PARAMETERS          LOADINGS                TEMPERATURE PARAMETERS
      R= 6.5000E+01                                       TAUS= 0.          GAMS= 0.
      A= 3.0000E+02                                       TAUR= 0.          GAMR= 0.
 DELBAR= 3.0000E-02          ECC= 0.                    TAUSPR= 0.             G= 0.
                                                        TAURPR= 0.
```

```
RING PROPERTIES                  STRINGER PROPERTIES
ER= 1.6400E+07   ZR=-1.9920E+00       ES= 1.6400E+07      ZS=-3.4200E-01
AR= 2.4600E-01   GRJR= 3.4770E+03     AS= 4.9500E-02    GSJS= 9.3000E+01
IR= 1.3770E-01                        IS= 4.0820E-03       D= 1.3500E+00
```

NUMBER OF RINGS=   19
NUMBER OF FINITE DIFFERENCE SPACES BETWEEN RINGS=   10

GEOMETRY AND TEMPERATURE PROPERTIES FOR LAYERS

LAYER	EX	EY	NUX	NUY	GXY	H	GAMMA	BETA	ALPHA X	ALPHA Y
1	1.450E+07	1.450E+07	3.000E-01	3.000E-01	5.580E+06	6.000E-02	0.	1.000E+00	5.000E-06	5.000E-06

SIMPLE SUPPORT BOUNDARY CONDITIONS

	11	12	22	66	13	23
B 1	1.59340659E+07	4.78021978E+06	1.59340659E+07	5.58000000E+06	-1.03571429E+02	-1.03571429E+02
C	9.56043956E+05	2.86813187E+05	9.56043956E+05	3.34800000E+05		
D	2.86813187E+02	8.60439560E+01	2.86813187E+02	1.00440000E+02		
K	0.	0.	0.	0.		
L					-6.21428571E+00	-6.21428571E+00
M					0.	0.

INPUT FOR CALCULATION OF MODIFIED RESIDUAL   CHANG—CARD   RDF364   FEBRUARY,1968

IALF= 1

N= 5.0000E+01

TA	MODIFIED RESIDUAL
4.50000000E+02	−7.79225885E+05
4.70000000E+02	−7.75252974E+05
4.90000000E+02	−7.65576851E+05
5.10000000E+02	−7.60571046E+05
5.30000000E+02	−7.42188514E+05
5.50000000E+02	6.79009921E+05
5.40000000E+02	−7.14898570E+05
5.40000000E+02	CROSSING FOUND WITHIN 1. PERCENT

N= 5.1000E+01

TA	MODIFIED RESIDUAL
4.50000000E+02	−7.88803726E+05
4.70000000E+02	−7.84474819E+05
4.90000000E+02	−7.78172671E+05
5.10000000E+02	−7.67786896E+05
5.30000000E+02	−7.43541985E+05
5.50000000E+02	−9.24281493E+05
OPEN UP INTERVAL IN SEARCH OF CROSSING	
5.30000000E+02	−7.43541985E+05
5.32000000E+02	−7.38292392E+05
5.34C00000E+02	−7.31168334E+05
5.36000000E+02	−7.19848153E+05
5.38000000E+02	−6.91640017E+05
5.40000000E+02	9.03024088E+05
5.39000000E+02	−6.24795117E+05
5.39000000E+02	CROSSING FOUND WITHIN 1. PERCENT

N= 5.20C0E+01

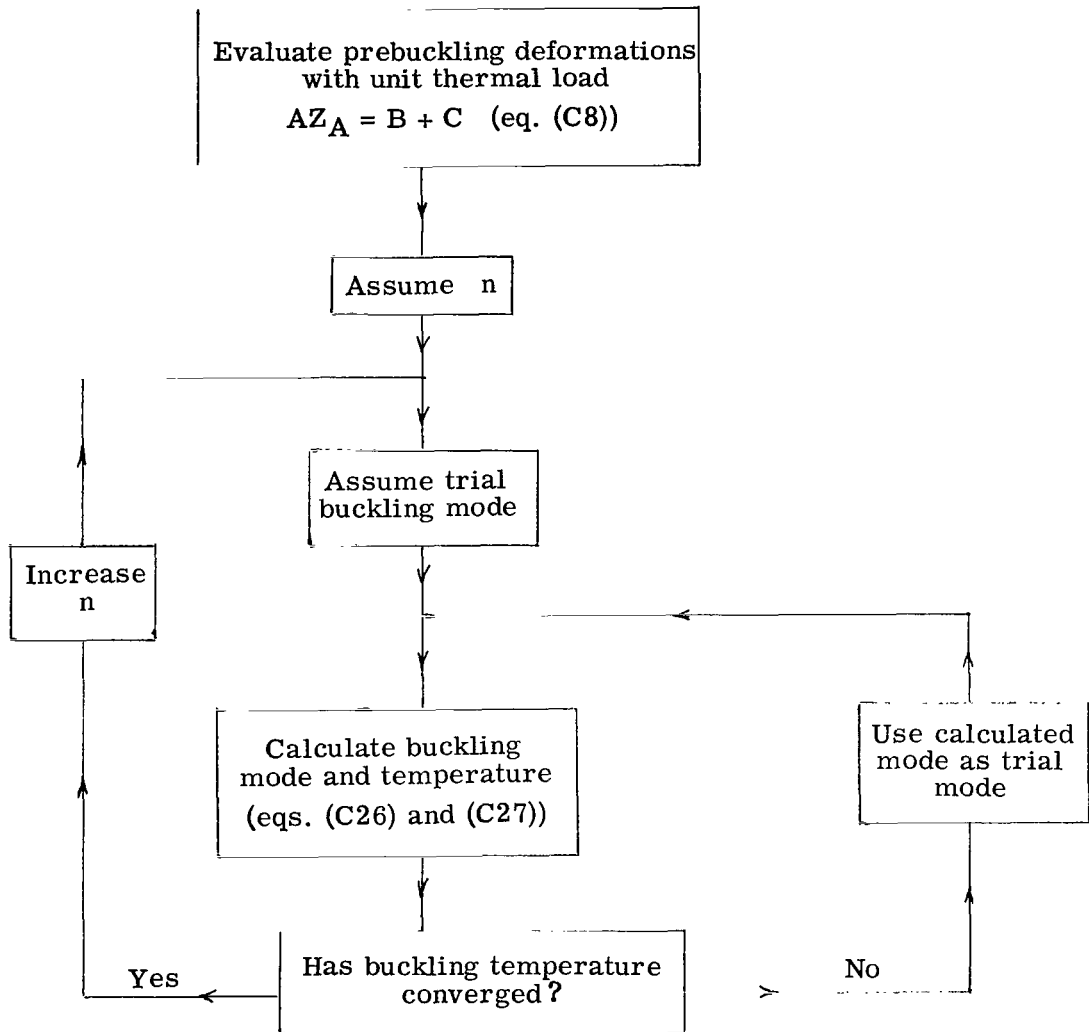| TA	MODIFIED RESIDUAL
4.50000000E+02	−7.98256606E+05
4.70000000E+02	−7.93594324E+05
4.90000000E+02	−7.86682408E+05
5.10000000E+02	−7.74838733E+05
5.30000000E+02	−7.41093951E+05
5.50000000E+02	−7.61622322E+05
OPEN UP INTERVAL IN SEARCH OF CROSSING	
5.30C00000E+02	−7.41093951E+05
5.32000000E+02	−7.29620508E+05
5.34000000E+02	−6.99861698E+05
5.36000000E+02	8.61174311E+05
5.35000000E+02	−6.16100274E+05
5.35000000E+02	CROSSING FOUND WITHIN 1. PERCENT

N= 5.3000E+01

TA	MODIFIED RESIDUAL
4.50000000E+02	−8.07594308E+05
4.70000000E+02	−8.02630842E+05
4.9C000000E+02	−7.95147042E+05
5.10C00000E+02	−7.81817375E+05
5.30000000E+02	−7.24361857E+05
5.50000000E+02	−7.05664617E+05
5.70000000E+02	6.79333836E+05
5.60000000E+02	8.50808776E+05
5.60000000E+02	CROSSING FOUND WITHIN 1. PERCENT

MINIMUM TA= 5.35000000E+02   N= 5.20000000E+01

BAMSOC II

The computer program BAMSOC II finds the buckling load for a stiffened cylindrical shell subjected to mechanical and thermal loadings by using modal iteration. The solution corresponds to equations (C16), (C18), and (C27) of the present text. A flow diagram for BAMSOC II (modal iteration solution) follows:

Evaluate prebuckling deformations
with unit thermal load
$$AZ_A = B + C \quad (\text{eq. (C8)})$$

Assume n

Assume trial
buckling mode

Increase
n

Use calculated
mode as trial
mode

Calculate buckling
mode and temperature
(eqs. (C26) and (C27))

Yes

Has buckling temperature
converged?

No

Buckling temperatures are found for specified ranges of the circumferential wave number n. If the solution is well behaved, the program will converge to the candidate buckling temperature after several iterations. The program is overlayed to permit a maximum of 200 finite-difference intervals and requires 150 000 octal storage units.

The input required by the modal iteration solution is similar to that for BAMSOC I except that loading ranges and increments are not specified and the solution is valid only for simply supported boundary conditions. The following modifications are required for the three namelists presented for BAMSOC I:

    (1) in namelist CON, retain only NI, NF, DELN, NBARXI, and PINIT

    (2) retain namelist NANCY

    (3) in namelist CORNIE, permissible values of IALF are from 1 to 4. Delete
         MODE and IRING.

The convergence criteria (see eq. (C27)) is specified internally for the ith iteration as

$$\frac{\left|\left(T_A\right)_i - \left(T_A\right)_{i-1}\right|}{\left|\left(T_A\right)_i\right|} = 0.001$$

A sample output listing for BAMSOC II follows. The case is the same case as for BAMSOC I except that only 100 finite-difference intervals were employed to condense the output.

APPENDIX D — Continued

NAMELIST INPUT FOR BAMSOC II

$CON NI=57., NF=57., DELN=1., NBARXI=0., PINIT=0.$

$NANCY P=65., A=300., DELBAR=.03, BC=1, ER=16.4E6, AR=.246, IR=.1377,
ZR=-1.992, GRJR=3477., NRING=19, NRSPACE= 5, ES=16.4E6, AS=.0495, IS=.004082,
ZS=-.342, GSJS=93., D=1.35, ECC=0., GAMS=0., GAMR=0., TAUS=0., TAUR=0.,
TAUSPR=0., TAURPR=0., G=0., GXY(1)=5.580E6, H(1)=.06, GAMMA(1)=0., BETA(1)=1.,
EX(1)=14.5E6, EY(1)=14.5E6, NUX(1)=.30, NUY(1)=.30, ALPHAX(1)=5.E-6,
ALPHAY(1)=5.E-6, LAYER=1$

$CORNIE IALF=1$

BAMSOC II

CALCULATION OF BUCKLING LOAD FOR THERMALLY STRESSED, STIFFENED, MULTI-LAYER CYLINDER BY MODAL ITERATION
CHANG-CARD   RDF364   NASA LANGLEY RESEARCH CENTER   1968

DATE 03/27/69

NI= 5.7000E+01   NF= 5.7000E+01   DELN= 1.0000E+00

INITIAL Z VECTOR (UNSCALED)

	UB	VB	WB	MB
1	0.	0.	1.00000000E+00	0.
21	0.	0.	1.00000000E+00	0.
41	0.	0.	1.00000000E+00	0.
61	0.	0.	1.00000000E+00	0.
81	0.	0.	1.00000000E+00	0.
101	0.	0.	1.00000000E+00	0.

ITERATION NUMBER   1

TEMPERATURE TA= 1.63659058E-01   CORRESPONDING SCALED Z VECTOR

	UB	VB	WB	MB
1	-7.76570953E-07	0.	0.	0.
21	-1.91130069E-10	1.83146093E-08	7.35752664E-09	-1.83573040E-01
41	-7.01489655E-14	1.83760317E-08	7.39760844E-09	-1.83772776E-01
61	7.01489688E-14	1.83760317E-08	7.39760844E-09	-1.83772776E-01
81	1.91130069E-10	1.83146093E-08	7.35752664E-09	-1.83573040E-01
101	7.76570953E-07	0.	0.	0.

ITERATION NUMBER   2

TEMPERATURE TA= 1.17890697E+03   CORRESPONDING SCALED Z VECTOR

	UB	VB	WB	MB
1	7.27927938E-07	0.	0.	0.
21	-1.57725826E-09	5.04390724E-08	3.52955211E-08	-1.52729564E-01
41	-1.20398426E-12	5.07973257E-08	3.55277678E-08	-1.53943644E-01
61	1.20398423E-12	5.07973257E-08	3.55277678E-08	-1.53943644E-01
81	1.57725826E-09	5.04390724E-08	3.52955211E-08	-1.52729564E-01
101	-7.27927938E-07	0.	0.	0.

ITERATION NUMBER   25

TEMPERATURE TA= 5.37719505E+02   CORRESPONDING SCALED Z VECTOR

	UB	VB	WB	MB
1	4.58064816E-07	0.	0.	0.
21	-2.87625169E-07	-9.81722985E-09	-6.56022956E-09	3.23334452E-02
41	-4.84982682E-08	-4.40150651E-09	-2.92732002E-09	1.45714341E-02
61	4.84982682E-08	-4.40150651E-09	-2.92732002E-09	1.45714341E-02
81	2.87625169E-07	-9.81722985E-09	-6.56022956E-09	3.23334452E-02
101	-4.58064816E-07	0.	0.	0.

59

ITERATION NUMBER   26

    TEMPERATURE TA= 5.37123003E+02   CORRESPONDING SCALED Z VECTOR

	UB	VB	WB	MB
1	4.46578687E-07	0.	0.	0.
21	-2.93047826E-07	-9.38196491E-09	-6.26962170E-09	3.08988773E-02
41	-5.29982857E-08	-4.69946566E-09	-3.12613561E-09	1.55542013E-02
61	5.29982857E-08	-4.69946566E-09	-3.12613561E-09	1.55542013E-02
81	2.93047826E-07	-9.38196491E-09	-6.26962170E-09	3.08988773E-02
101	-4.46578687E-07	0.	0.	0.

ITERATION NUMBER   27

    TEMPERATURE TA= 5.36575924E+02   CORRESPONDING SCALED Z VECTOR

	UB	VB	WB	MB
1	4.35668C83E-07	0.	0.	0.
21	-2.97920426E-07	-8.94910655E-09	-5.98057394E-09	2.94725094E-02
41	-5.75110986E-08	-4.98896109E-09	-3.31932851E-09	1.65089071E-02
61	5.75110986E-08	-4.98896109E-09	-3.31932851E-09	1.65089071E-02
81	2.97920426E-07	-8.94910655E-09	-5.98057394E-09	2.94725094E-02
101	-4.35668C83E-07	0.	0.	0.

ITERATION NUMBER   28

    CONVERGED TEMPERATURE TA= 5.36074232E+02   CORRESPONDING SCALED Z VECTOR

	UB	VB	WB	MB
1	4.25301149E-07	0.	0.	0.
2	-7.59850632E-07	-4.59625262E-07	2.88703579E-05	1.97151230E-01
3	-5.21414819E-07	-7.71134756E-07	4.27008188E-05	2.03472475E-01
4	7.46228255E-11	-7.28756070E-07	3.92369407E-05	1.45920054E-01
5	2.70353608E-07	-4.41484170E-07	2.31230666E-05	8.13483855E-02
6	2.99574280E-07	-9.37078924E-09	-5.52645553E-09	-6.63765673E-04
7	2.81086829E-07	4.28726627E-07	-2.32819862E-05	-1.08527967E-01
8	1.11722331E-07	6.97014670E-07	-3.79640995E-05	-1.76416032E-01
9	-1.45090817E-07	7.09547922E-07	-3.85226372E-05	-1.84431761E-01
10	-3.27532512E-07	4.55146445E-07	-2.42795296E-05	-1.24870198E-01
11	-3.62973005E-07	2.43286648E-09	1.72226769E-09	-9.63841827E-03
12	-3.44911857E-07	-4.67981720E-07	2.50584371E-05	1.20262254E-01
13	-1.44970992E-07	-7.46556218E-07	4.04388090E-05	1.92473613E-01
14	1.49747724E-07	-7.43563747E-07	4.02956732E-05	1.90551988E-01
15	3.45113853E-07	-4.61421596E-07	2.47843487E-05	1.15363571E-01
16	3.53028614E-07	4.79054708E-07	3.21738900E-05	-1.57017051E-02
17	3.03512382E-07	4.42124012E-07	-2.34938675E-05	-1.23089686E-01
18	1.11311952E-07	6.84191543E-07	-3.70558546E-05	-1.78314582E-01
19	-1.52077748E-07	6.67749535E-07	-3.62463455E-05	-1.68109183E-01
20	-3.16278412E-07	4.04730815E-07	-2.18899554E-05	-9.40429520E-02
21	-3.02289280E-07	-8.52149244E-09	-5.69499266E-09	2.80636251E-02
22	-2.40603980E-07	-3.70626319E-07	1.95833395E-05	1.08943509E-01
23	-7.79210795E-08	-5.60691973E-07	3.03633453E-05	1.47419054E-01
24	1.33393533E-07	-5.38503291E-07	2.92702575E-05	1.33661345E-01
25	2.58710335E-07	-3.20106295E-07	1.74149936E-05	6.96391649E-02
26	2.34182913E-07	9.58375632E-08	6.39701604E-06	-3.15968803E-02
27	1.73529469E-07	2.81843089E-07	-1.48179466E-05	-8.67100390E-02
28	4.90093406E-08	4.17721507E-07	-2.26210193E-05	-1.10635773E-01
29	-1.05031425E-C7	3.95379757E-07	-2.15199960E-05	-9.67952493E-02
30	-1.92160659E-07	2.30933170E-07	-1.26321987E-05	-4.70731332E-02
31	-1.66745567E-07	-8.73802977E-09	-5.82660431E-09	2.88428069E-02
32	-1.14405427E-07	-1.96104461E-07	1.02615469E-05	6.28887408E-02
33	-2.73157633E-08	-2.84928388E-07	1.54304282E-05	7.59949709E-02
34	7.54101910E-08	-2.65806306E-07	1.44877480E-05	6.41582849E-02
35	1.30679669E-07	-1.52498812E-07	8.38882829E-06	2.89144603E-02
36	1.07290082E-07	7.01425061E-09	4.67248845E-09	-2.31792101E-02
37	6.81917701E-08	1.24588002E-07	-6.48369788E-06	-4.18076618E-02
38	1.24C77770E-08	1.76889287E-07	-9.57824365E-06	-4.76148396E-02
39	-4.98547675E-08	1.62C46387E-07	-8.84625794E-06	-3.84342699E-02
40	-8.10843369E-08	9.07149850E-08	-5.02850473E-06	-1.53969322E-02

41	-6.20122302E-08	-5.26917618E-09	-3.50634900E-09	1.74328862E-02
42	-3.40867935E-08	-6.97854476E-08	3.59568563E-06	2.52369502E-02
43	-2.04212480E-09	-9.50531674E-08	5.14159204E-06	2.61273885E-02
44	3.04004734E-08	-8.38477792E-08	4.58879044E-06	1.92021907E-02
45	4.40193554E-08	-4.41941266E-08	2.49591889E-06	5.26846401E-03
46	2.79055634E-08	4.04701034E-09	2.69043138E-09	-1.34039223E-02
47	7.88264544E-09	2.81461217E-08	-1.39425150E-06	-1.29366908E-02
48	-6.66980972E-09	3.22525792E-08	-1.73154237E-06	-9.83661853E-03
49	-1.66255869E-08	2.30691997E-08	-1.27836897E-06	-4.16443057E-03
50	-1.61454443E-08	7.16082486E-09	-4.92203515E-07	3.44703134E-03
51	-5.11607606E-20	-3.61446716E-09	-2.40179628E-09	1.19772649E-02
52	1.61454443E-08	7.16082486E-09	-4.92203515E-07	3.44703134E-03
53	1.66255869E-08	2.30691997E-08	-1.27836897E-06	-4.16443057E-03
54	6.66980972E-09	3.22525792E-08	-1.73154237E-06	-9.83661853E-03
55	-7.88264544E-09	2.81461217E-08	-1.39425150E-06	-1.29366908E-02
56	-2.79055634E-08	4.04701034E-09	2.69043138E-09	-1.34039223E-02
57	-4.40193554E-08	-4.41941266E-08	2.49591889E-06	5.26846401E-03
58	-3.04004734E-08	-8.38477792E-08	4.58879044E-06	1.92021907E-02
59	2.04212480E-09	-9.50531674E-08	5.14159204E-06	2.61273885E-02
60	3.40867935E-08	-6.97854476E-08	3.59568563E-06	2.52369502E-02
61	6.20122302E-08	-5.26917618E-09	-3.50634900E-09	1.74328862E-02
62	8.10843369E-08	9.07149850E-08	-5.02850473E-06	-1.53969322E-02
63	4.98547675E-08	1.62046387E-07	-8.84625794E-06	-3.84342699E-02
64	-1.24077770E-08	1.76889287E-07	-9.57824345E-06	-4.76148396E-02
65	-6.81917701E-08	1.24588002E-07	-6.48369788E-06	-4.18076618E-02
66	-1.07290082E-07	7.01425061E-09	4.67248845E-09	-2.31792101E-02
67	-1.30679669E-07	-1.52498812E-07	8.38882829E-06	2.89144603E-02
68	-7.54101910E-08	-2.65806306E-07	1.44877480E-05	6.41582849E-02
69	2.73157633E-08	-2.84928388E-07	1.54304282E-05	7.59949709E-02
70	1.14405427E-07	-1.96104461E-07	1.02615469E-05	6.28887408E-02
71	1.65745567E-07	-8.73802977E-09	-5.82660431E-09	2.88428069E-02
72	1.92160659E-07	2.30933170E-07	-1.26321987E-05	-4.70731332E-02
73	1.05031425E-07	3.95379757E-07	-2.15199960E-05	-9.67952493E-02
74	-4.90093406E-08	4.17721507E-07	-2.26210193E-05	-1.10635773E-01
75	-1.73529469E-07	2.81843089E-07	-1.48179466E-05	-8.67100390E-02
76	-2.34182913E-07	9.58375632E-08	6.39701603E-09	-3.15968803E-02
77	-2.58710335E-07	-3.20106295E-07	1.74149936E-05	6.96391649E-02
78	-1.33393533E-07	-5.38503291E-07	2.92702575E-05	1.33661345E-01
79	7.79210795E-08	-5.60691973E-07	3.03063453E-05	1.47419064E-01
80	2.40603980E-07	-3.70626319E-07	1.95833395E-05	1.08943509E-01
81	3.02289280E-07	-8.52149244E-09	-5.69499266E-09	2.80636251E-02
82	3.16278412E-07	4.04730815E-07	-2.18899554E-05	-9.40429520E-02
83	1.52077748E-07	6.67749535E-07	-3.62463455E-05	-1.68109183E-01
84	-1.11311952E-07	6.84191543E-07	-3.70558546E-05	-1.78314582E-01
85	-3.03512382E-07	4.42124012E-07	-2.34938675E-05	-1.23089686E-01
86	-3.53028614E-07	4.79054708E-07	3.21738908E-09	-1.57017051E-02
87	-3.45113853E-07	-4.61421596E-07	2.47834487E-05	1.15363571E-01
88	-1.49747724E-07	-7.43563747E-07	4.02956732E-05	1.90551988E-01
89	1.44970992E-07	-7.46556218E-07	4.04388090E-05	1.92473613E-01
90	3.44911857E-07	-4.67981720E-07	2.50584371E-05	1.20262254E-01
91	3.62973005E-07	2.43286648E-09	1.72226769E-09	-9.63841827E-03
92	3.27532512E-07	4.55146445E-07	-2.42795296E-05	-1.24870198E-01
93	1.45090817E-07	7.09547922E-07	-3.85226372E-05	-1.84431761E-01
94	-1.11722331E-07	6.97014670E-07	-3.79640995E-05	-1.76416032E-01
95	-2.81086829E-07	4.28726627E-07	-2.32819862E-05	-1.08527967E-01
96	-2.99574280E-07	-9.37078924E-09	-5.52645553E-09	-6.63765673E-04
97	-2.70353608E-07	-4.41484170E-07	2.31230666E-05	8.13483855E-02
98	-7.46228255E-11	-7.28756070E-07	3.92369407E-05	1.45920054E-01
99	5.21414819E-07	-7.71134756E-07	4.27008188E-05	2.03472475E-01
100	7.59850632E-07	-4.59625262E-07	2.88703579E-05	1.97151230E-01
101	-4.25301149E-07	0.	0.	0.

NUMBER OF ITERATIONS= 28

MINIMUM   TA= 5.36074232E+02   N= 5.70000000E+01

RUNNING TIME APPROXIMATELY 72 SECONDS

APPENDIX E

DEVELOPMENT OF MORE ACCURATE RING THEORY

Near the completion of this investigation, Dr. David Bushnell of the Lockheed Missiles and Space Company verified the results of some of the present calculations by using a newly developed program for shells of revolution (ref. 26). In doing so, he obtained results which indicated that the thermal-buckling behavior of the ring-stiffened shells investigated herein could be influenced by the type of ring theory employed in the analysis. Preliminary results suggested that the out-of-plane ring bending stiffness during buckling was especially important.

The purpose of this appendix is to present an extension of the present analysis to include the first-order effects of out-of-plane deformations in the rings during buckling. The ring theory is developed by a method proposed in reference 27 to obtain a consistent theory for sturdy rings attached firmly to a shell. A key assumption in the development is that compatibility of the ring and shell deformations is enforced along a normal passing through the centroid of the ring. Thus, local deformations of the ring elements are ignored and the ring behaves as a rigid beam. More exact models for rings which enforce compatibility only at the point of attachment have been proposed. (See, for example, ref. 28.) However, these models lead to extremely complex, unwieldy equations.

Ring Displacements

The ring center of shear and centroid are assumed to coincide. The ring displacements u_r^t, v_r^t, and w_r^t are specified in local ring coordinates $\bar{x}$, $\bar{y}$, and $\bar{z}$, which are parallel to the coordinates of figure 1 but have their origin at the ring centroid. The ring displacements u_r^t, v_r^t, and w_r^t are expressed (ref. 28) as

$$\left.\begin{array}{l} u_r^t = u_c + \bar{z}\beta_1 \\[10pt] v_r^t = v_c + \bar{z}\beta_2 - \bar{x}u_{c,\bar{y}} \\[10pt] w_r^t = w_c - \bar{x}\beta_1 \end{array}\right\} \tag{E1}$$

with $\beta_1 = -w_{c,\bar{x}}$ and $\beta_2 = -w_{c,\bar{y}} + \dfrac{v_c}{R_c}$ where the subscript c denotes the ring centroid.

The ring coordinates $\bar{y}$ and $\bar{z}$ are related to the shell coordinates y and z by

$$\left.\begin{array}{c} \bar{y} = \left(1 + \dfrac{\bar{z}_r}{R}\right)y \\[2mm] \bar{z} = z - \bar{z}_r \end{array}\right\} \tag{E2}$$

The displacements in the shell in the vicinity of the ring are assumed to be

$$\left.\begin{array}{c} u^t_{sk} = u - zw,_x \\[2mm] v^t_{sk} = v - z\left(w,_y - \dfrac{v}{R}\right) \\[2mm] w^t_{sk} = w \end{array}\right\} \tag{E3}$$

To develop a ring theory for sturdy stiffeners, compatibility of shell and ring deformation is enforced along a shell normal passing through the centroid of the ring. Matching ring and shell displacements along $\bar{x} = 0$ $\left(\text{that is, } u^t_{sk} = u^t_r\big|_{\bar{x}=0}, \text{ and so forth}\right)$ yields

$$\left.\begin{array}{c} u_c = u - \bar{z}_r w,_{\bar{x}} \\[2mm] v_c = v\left(1 + \dfrac{\bar{z}_r}{R}\right) - \bar{z}_r w,_y + 0\left(\dfrac{z}{R}\right)^2 \\[2mm] w_c = w \end{array}\right\} \tag{E4}$$

and

$$\left.\begin{array}{c} u^t_r = u - zw,_{\bar{x}} \\[2mm] v^t_r = v\left(1 + \dfrac{z}{R}\right) - zw,_y - \bar{x}\left(1 - \dfrac{\bar{z}_r}{R}\right)\left(u,_y - \bar{z}_r w,_{\bar{x}y}\right) + 0\left(\dfrac{z}{R}\right)^2 \\[2mm] w^t_r = w + \bar{x}w,_{\bar{x}} \end{array}\right\} \tag{E5}$$

Strain Energy

The strain energy in the N interior rings on the shell is approximated as

$$\Pi_r = \frac{1}{2}\sum_{j=1}^{N}\int_0^{2\pi R}\int_0^a\left[\int E_r\left(\epsilon^t_r\right)^2 dA_r + G_r J_r \beta^2_{1,y} - E_r \alpha_r T \epsilon^t_r\right]\delta(x - j\ell)dx\, dy \tag{E6}$$

with

$$\epsilon_r^t = v_{r,y}^t + \frac{w_r^t}{R} + \frac{1}{2}\left(w_r^t\right)_{,y}^2 \tag{E7}$$

where the introduction of the Dirac delta function permits the replacement of $\bar{x}$ by x in the derivatives appearing in equation (E5).

Buckling Strain Energy

By following the procedures outlined in appendix B, the total potential energy of the shell, its stiffening elements, and the external loading can be formed, and the principle of minimum potential energy ($\delta\Pi = 0$) can be used to obtain nonlinear equilibrium equations. The equations governing prebuckling and buckling can be derived by separating displacements into axisymmetric and small asymmetric parts (for example, $u = u_A + u_B$). For the more accurate ring theory, the prebuckling equations obtained are the same as those developed as equation (1) or equation (B21) in appendix B. Thus, the new terms of the more accurate ring theory appear only in the buckling equations.

In order to make a comparison of the present theory with existing ring theories, the strain energy during buckling can be written as

$$\Pi_{rB} = \frac{1}{2} \sum_{j=1}^{N} \int_0^{2\pi R} \int_0^a \left[\int E_r \left(\epsilon_{rB}^t\right)^2 dA_r + G_r J_r \left(\beta_{B,y}\right)^2 \right] \delta(x - j\ell) dx \, dy \tag{E8}$$

where

$$\epsilon_{rB}^t = v_{B,y}\left(1 + \frac{z}{R}\right) - zw_{B,yy} - \bar{x}\left(1 - \frac{\bar{z}_r}{R}\right)\left(u_{B,yy} - \bar{z}_r w_{B,xyy}\right) + \frac{1}{R}\left(w_B + \bar{x}w_{B,x}\right) \tag{E9}$$

$$\beta_B = -w_{B,x} \tag{E10}$$

To express the energy as a function of the buckling displacement variables U, V, and W, equations (C13)

$$u_B = U \cos \frac{ny}{R}$$

$$v_B = V \sin \frac{ny}{R}$$

$$w_B = W \cos \frac{ny}{R}$$

are employed. The integration over the ring area can be accomplished with the following definitions:

$$\left.\begin{array}{ll} \int E_r \, dA_r = E_r A_r & \int E_r \bar{x} \, dA_r = 0 \qquad \left(\because \bar{x}_r = 0\right) \\[2ex] \int E_r z \, dA_r = \bar{z}_r E_r A_r & \int E_r \bar{x} z \, dA_r = E_r I_{o\bar{x}z} \\[2ex] \int E_r z^2 dA_r = E_r I_{oz} & \int E_r \bar{x}^2 dA_r = E_r I_{\bar{x}} \end{array}\right\} \qquad (E11)$$

where the subscript o is used to denote that the inertias I_{oz} and $I_{o\bar{x}z}$ are to be computed about the shell reference surface, $z = 0$.

After integration, equation (E8) can be written in matrix form as

$$\Pi_{rB} = \frac{\pi R}{2} \int_0^a \bar{Z}_B^T G \bar{Z}_B \, dx \qquad (E12)$$

in which

$$\bar{Z}_B = \begin{Bmatrix} U \\ V \\ W \\ W' \end{Bmatrix} \qquad (E13)$$

and

$$G = \begin{bmatrix} G_{11} & G_{12} & G_{13} & G_{14} \\ & G_{22} & G_{23} & G_{24} \\ & & G_{33} & G_{34} \\ \text{Symmetric} & & & G_{44} \end{bmatrix} \qquad (E14)$$

with

$$G_{11} = \sum_{j=1}^{N} \delta(x - j\ell) \eta^2 E_r I_{\bar{x}} \left(\frac{n}{R}\right)^4$$

$$G_{12} = \sum_{j=1}^{N} \delta(x - j\ell) \eta E_r I_{o\bar{x}z} \frac{n^3}{R^4}$$

$$G_{13} = \sum_{j=1}^{N} \delta(x - j\ell) \eta E_r I_{o\bar{x}z} \left(\frac{n}{R}\right)^4$$

$$G_{14} = \sum_{j=1}^{N} \delta(x - j\ell) \left[\eta E_r I_{\bar{x}} \frac{n^2}{R^3} - \eta^2 \bar{z}_r E_r I_{\bar{x}} \left(\frac{n}{R}\right)^4 \right]$$

$$G_{22} = \sum_{j=1}^{N} \delta(x - j\ell) \left[E_r A_r \left(\frac{n}{R}\right)^2 + 2\bar{z}_r E_r A_r \frac{n^2}{R^3} + E_r I_{oz} \frac{n^2}{R^4} \right]$$

$$G_{23} = \sum_{j=1}^{N} \delta(x - j\ell) \left[E_r A_r \frac{n}{R^2} + \bar{z}_r E_r A_r \left(\frac{n + n^3}{R^3}\right) + E_r I_{oz} \frac{n^3}{R^4} \right]$$

$$G_{24} = \sum_{j=1}^{N} \delta(x - j\ell) \left(E_r I_{o\bar{x}z} \frac{n}{R^3} - \bar{z}_r \eta E_r I_{o\bar{x}z} \frac{n^3}{R^4} \right)$$

$$G_{33} = \sum_{j=1}^{N} \delta(x - j\ell) \left[\frac{E_r A_r}{R^2} + 2\bar{z}_r E_r A_r \frac{n^2}{R^3} + E_r I_{oz} \left(\frac{n}{R}\right)^4 \right]$$

$$G_{34} = \sum_{j=1}^{N} \delta(x - j\ell) \left[E_r I_{o\bar{x}z} \frac{n^2}{R^3} - \bar{z}_r \eta E_r I_{o\bar{x}z} \left(\frac{n}{R}\right)^4 \right]$$

$$G_{44} = \sum_{j=1}^{N} \delta(x - j\ell) \left[\frac{E_r I_{\bar{x}}}{R^2} + \bar{z}_r^2 \eta^2 E_r I_{\bar{x}} \left(\frac{n}{R}\right)^4 - 2\bar{z}_r \eta E_r I_{\bar{x}} \frac{n^2}{R^3} + G_r J_r \left(\frac{n}{R}\right)^2 \right]$$

(E15)

where

$$\eta = 1 - \frac{\bar{z}_r}{R} \qquad \left(\text{Note that } E_r I_{oz} = E_r I_r + \bar{z}_r^2 E_r A_r\right)$$

In this form, the elements of the ring stiffness matrix G can be compared with results obtained in other buckling studies of ring-stiffened shells. (See refs. 28 to 30.)

Equilibrium Equations

The condition for vanishing of the first variation of the ring energy $\left(\delta\Pi_{rB} = 0\right)$ yields the contribution of the more accurate ring theory to the buckling equilibrium equations. If the terms in δU, δV, and δW are collected, the set of buckling equations which are the counterpart of equations (C15) with a more accurate ring theory can be written as:

$$\Lambda_{11}U'' + \left(\Lambda_{12} - G_{11}\right)U + \Lambda_{13}V' - G_{12}V + \left(\Lambda_{14} - T_A\Lambda_{15}\right)W'' + \left(\Lambda_{16} - G_{14} - T_A\Lambda_{17}\right)W'$$

$$+ \left(\Lambda_{18} - G_{13} - T_A\Lambda_{19}\right)W + \Lambda_{110}M' = 0 \tag{E16a}$$

$$\Lambda_{21}U' - G_{12}U + \Lambda_{22}V'' + \left(\Lambda_{23} - \Gamma_{21}\right)V + \Lambda_{24}W'' + \left(\Lambda_{25} - G_{24} - T_A\Lambda_{26}\right)W'$$

$$+ \left(\Lambda_{27} - \Gamma_{22} - T_A\Lambda_{28}\right)W = 0 \tag{E16b}$$

$$\left(\Lambda_{31} - G_{14} - T_A\Lambda_{32}\right)U' + \Gamma_{31}U + \Lambda_{33}V'' - G_{24}V' + \left(\Lambda_{34} + \Gamma_{32} - T_A\Lambda_{35}\right)V$$

$$+ \left(\Lambda_{36} - \Gamma_{33} - T_A\Lambda_{37}\right)W'' + \left(\Lambda_{38} - \Gamma_{34} - T_A\Lambda_{39} - T_A^2\Lambda_{310}\right)W'$$

$$+ \left(\Lambda_{311} - G_{34}' - T_A\Lambda_{312}\right)W - M'' = 0 \tag{E16c}$$

$$\Lambda_{41}U' + \Lambda_{42}V + \Lambda_{43}W'' + \left(\Lambda_{44} - T_A\Lambda_{45}\right)W' + \Lambda_{46}W + M = 0 \tag{E16d}$$

where

$$\Gamma_{21} = G_{22} - \sum_{j=1}^{N} \delta(x - j\ell)E_r A_r\left(\frac{n}{R}\right)^2$$

$$\Gamma_{22} = G_{23} - \sum_{j=1}^{N} \delta(x - j\ell)\left[E_r A_r \frac{n}{R^2} + \bar{z}_r E_r A_r\left(\frac{n}{R}\right)^3\right]$$

$$\Gamma_{31} = G_{13} - G'_{14}$$

$$\Gamma_{32} = G_{23} - G'_{24} - \sum_{j=1}^{N} \delta(x - j\ell)\left[E_r A_r \frac{n}{R^2} + z_r E_r A_r \left(\frac{n}{R}\right)^3\right]$$

$$\Gamma_{33} = G_{44} - \sum_{j=1}^{N} \delta(x - j\ell)G_r J_r \left(\frac{n}{R}\right)^2$$

$$\Gamma_{34} = G'_{44} - \sum_{j=1}^{N} \delta(x - j\ell)G_r J_r \left(\frac{n}{R}\right)^2$$

Equations (E16) were cast in finite-difference form using the techniques described in appendix C and reference 17; the results were programed as part of the determinant plotting solution in the computer program entitled BAMSOC I (see appendix D). However, numerical results employing the more accurate ring theory are not available.

REFERENCES

1. Hoff, N. J.: Buckling of Thin Cylindrical Shells Under Hoop Stresses Varying in Axial Direction. J. Appl. Mech., vol. 24, no. 3, Sept. 1957, pp. 405-412.

2. Zuk, William: Thermal Buckling of Clamped Cylindrical Shells. J. Aeronaut. Sci., vol. 24, no. 5, May 1957, p. 389.

3. Abir, David; Hoff, N. J.; Nardo, S. V.; Pohle, Frederick V.; Vafakos, William; and Wan, Koon-Sang: Thermal Buckling of Circular Cylindrical and Conical Thin-Walled Shells. WADC Tech. Rep. 58-104, ASTIA Doc No. AD151068, U.S. Air Force, Apr. 1958.

4. Baruch, Menahem; and Frum, Joseph: Experimental Study of the Thermal Buckling of Cylindrical Shells. TAE Rep. No. 92 (Contract AF 61(052)-905), Technion — Israel Inst. Technol., Sept. 1969.

5. Hoff, Nicholas J.; Chao, Chi Chang; and Madsen, Wayne A.: Buckling of Thin-Walled Circular Cylindrical Shell Heated Along an Axial Strip. SUDAER No. 142 (Grant AF-AFOSR-62-146), Stanford Univ., Sept. 1962.

6. Sunakawa, Megumi: Deformation and Buckling of Cylindrical Shells Subjected to Heating. Rep. No. 370, Aeronaut. Res. Inst., Univ. of Tokyo, July 1962.

7. Lu, S. Y.; and Chang, L. K.: Thermal Buckling of Conical Shells. AIAA J., vol. 5, no. 10, Oct. 1967, pp. 1877-1882.

8. Chang, L. K.; and Lu, S. Y.: Nonlinear Thermal Elastic Buckling of Conical Shells. Nucl. Eng. Design, vol. 7, no. 2, Feb. 1968, pp. 159-169.

9. Pride, Richard A.; Hall, John B., Jr.; and Anderson, Melvin S.: Effects of Rapid Heating on Strength of Airframe Components. NACA TN 4051, 1957.

10. Anderson, Melvin S.: Combinations of Temperature and Axial Compression Required for Buckling of a Ring-Stiffened Cylinder. NASA TN D-1224, 1962.

11. Anderson, Melvin S.; and Card, Michael F.: Buckling of Ring-Stiffened Cylinders Under a Pure Bending Moment and a Non-Uniform Temperature Distribution. NASA TN D-1513, 1962.

12. Gellatly, R. A.; Bijlaard, P. P.; and Gallagher, R. H.: Thermal Stress and Instability of Sandwich Cylinders on Rigid Supports. J. Aircraft, vol. 2, no. 1, Jan.-Feb. 1965, pp. 44-48.

13. Johns, D. J.: Thermal Stress Analyses. Pergamon Press, Inc., c.1965.

14. Stein, Manuel: Some Recent Advances in the Investigation of Shell Buckling. AIAA J., vol. 6, no. 12, Dec. 1968, pp. 2339-2345.

15. Cohen, Gerald A.: Computer Analysis of Asymmetric Buckling of Ring-Stiffened Orthotropic Shells of Revolution. AIAA J., vol. 6, no. 1, Jan. 1968, pp. 141-149.

16. Bushnell, D.; Almroth, B. O.; and Sobel, L. H.: Buckling of Shells of Revolution With Various Wall Constructions. Vol. 2 — Basic Equations and Method of Solution. NASA CR-1050, 1968.

17. Block, David L.: Influence of Discrete Ring Stiffeners and Prebuckling Deformations on the Buckling of Eccentrically Stiffened Orthotropic Cylinders. NASA TN D-4283, 1968.

18. Comm. on Metric Pract.: ASTM Metric Practice Guide. NBS Handbook 102, U.S. Dep. Com., Mar. 10, 1967.

19. Ambartsumyan, S. A.: Theory of Anisotropic Shells. NASA TT F-118, 1964.

20. Batdorf, S. B.; and Schildcrout, Murry: Critical Axial-Compressive Stress of a Curved Rectangular Panel With a Central Chordwise Stiffener. NACA TN 1661, 1948.

21. Jones, Robert M.: Buckling of Circular Cylindrical Shells With Multiple Orthotropic Layers and Eccentric Stiffeners. AIAA J., vol. 6, no. 12, Dec. 1968, pp. 2301-2305.

22. Almroth, B. O.: Influence of Edge Conditions on the Stability of Axially Compressed Cylindrical Shells. NASA CR-161, 1965.

23. Stuhlman, C.; Deluzio, A.; and Almroth, B.: Influence of Stiffener Eccentricity and End Moment on Stability of Cylinders in Compression. AIAA J., vol. 4, no. 5, May 1966, pp. 872-877. (Also presented in proceedings of the AIAA 6th Structures and Materials Conference (Palm Springs, Calif.), Apr. 1965, pp. 117-125.)

24. Almroth, B. O.; Bushnell, D.; and Sobel, L. H.: Buckling of Shells of Revolution With Various Wall Constructions. Vol. 1 — Numerical Results. NASA CR-1049, 1968.

25. Budiansky, Bernard; and Radkowski, Peter P.: Numerical Analysis of Unsymmetrical Bending of Shells of Revolution. AIAA J., vol. 1, no. 8, Aug. 1963, pp. 1833-1842.

26. Bushnell, David: Analysis of Ring-Stiffened Shells of Revolution Under Combined Thermal and Mechanical Loading. AIAA/ASME 11th Structures, Structural Dynamics, and Materials Conference, Apr. 1970, pp. 196-210.

27. McElman, John A.: Eccentrically Stiffened Shallow Shells. Ph. D. Thesis, Virginia Polytech. Inst., 1966.

28. Weeks, George E.; and Walz, Joseph E.: Generalized Ring Stiffness Matrix for Ring-Stiffened Shells of Revolution. NASA TN D-5701, 1970.

29. Bushnell, David: Analysis of Buckling and Vibration of Ring-Stiffened, Segmented Shells of Revolution. Int. J. Solid Structures, vol. 6, no. 1, Jan. 1970, pp. 157-181.

30. Cohen, Gerald A.: Computer Analysis of Asymmetric Free Vibrations of Ring-Stiffened Orthotropic Shells of Revolution. AIAA J., vol. 3, no. 12, Dec. 1965, pp. 2305-2312.

TABLE I.- STRUCTURAL PROPERTIES FOR BUCKLING CALCULATIONS

(a) SI Units

Type of cylinder	E_{sk} GN/m²	μ_{sk}	α_{sk} Per K	E_r GN/m²	A_r cm²	I_r cm⁴	$*\bar{z}_r$ cm	$G_r J_r$ N-m²	E_s GN/m²	A_s cm²	I_s cm⁴	$*\bar{z}_s$ cm	$G_s J_s$ N-m²
Ring-stiffened	183	0.3	1.43×10^{-5}	183	0.626	1.228	-1.364	0					
Stringer-stiffened	72.4	.32	2.52						72.4	2.394	3.663	-2.344	68.44
Ring- and stringer-stiffened	100	.30	0.9	113	1.587	5.732	-5.060	9.999	113	.319	.1699	-.864	0

(b) U.S. Customary Units

Type of cylinder	E_{sk} psi	μ_{sk}	α_{sk} Per °F	E_r psi	A_r in²	I_r in⁴	$*\bar{z}_r$ in.	$G_r J_r$ lb-in²	E_s psi	A_s in²	I_s in⁴	$*\bar{z}_s$ in.	$G_s J_s$ lb-in²
Ring-stiffened	26.5×10^6	0.3	7.95×10^{-6}	26.5×10^6	0.097	0.0295	-0.537	0					
Stringer-stiffened	10.5	.32	14						10.5×10^6	0.371	0.088	-0.923	23 800
Ring- and stringer-stiffened	14.5	.30	5	16.4	.246	.1377	-1.992	3477	16.4	.0495	.004082	-.342	0

*Based on reference surface at skin middle surface.
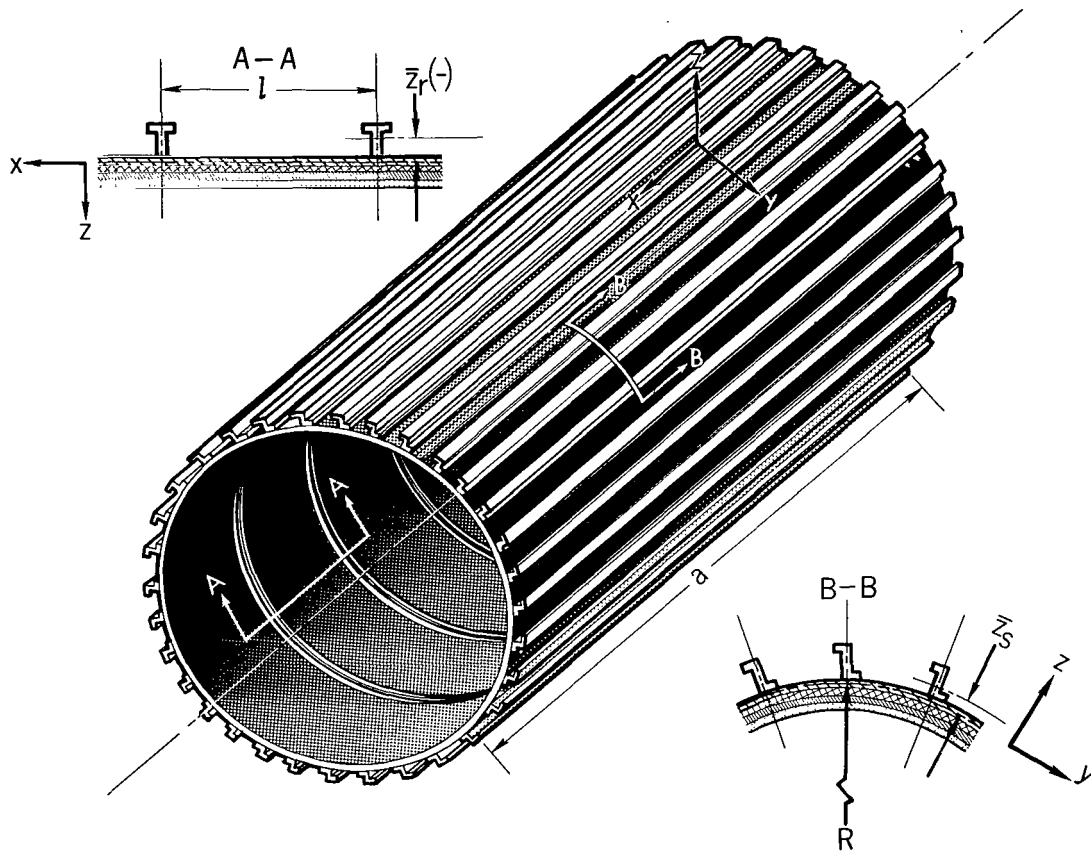
Figure 1.- Geometry of stiffened multilayered cylinder.

12.3
(31.2)

INTERNAL
RINGS

19.02
(48.56)

OVERALL GEOMETRY

0.50
(1.27)

1.25
(3.18)

0.05 TYP.
(0.13)

0.75
(1.91)

l
(VARIABLE)

R = 9.56 (24.28)

0.030
(0.076)

RING DETAIL
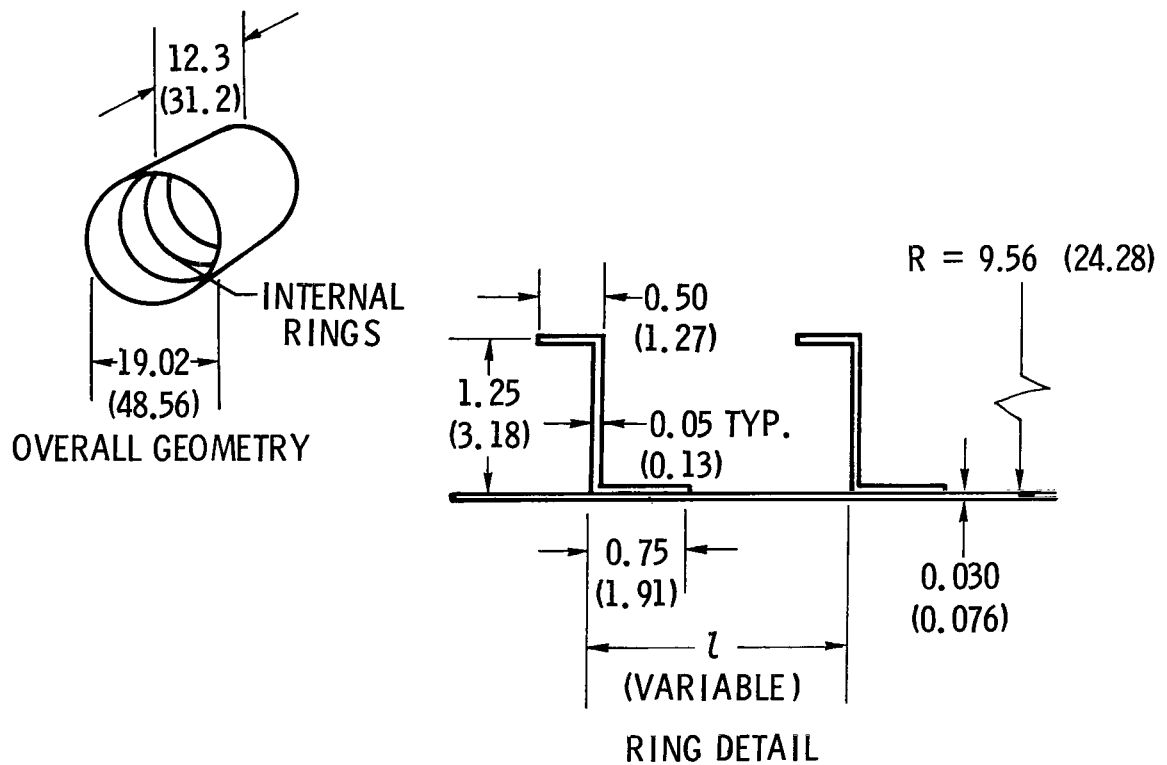
Figure 2.- Geometry of ring-stiffened cylindrical shells from reference 11.
Dimensions are in inches (cm).
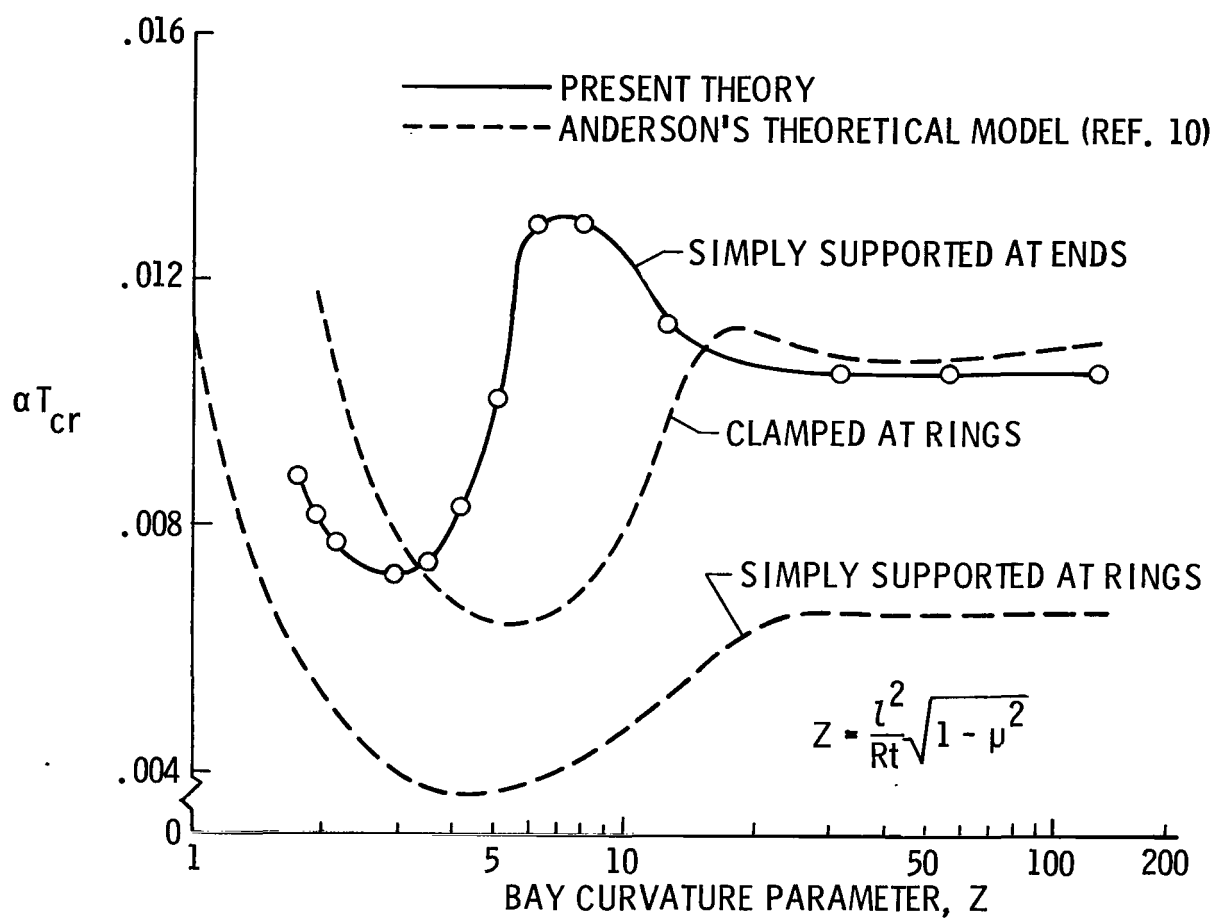
Figure 3.- Thermal buckling predictions for ring-stiffened cylinders.
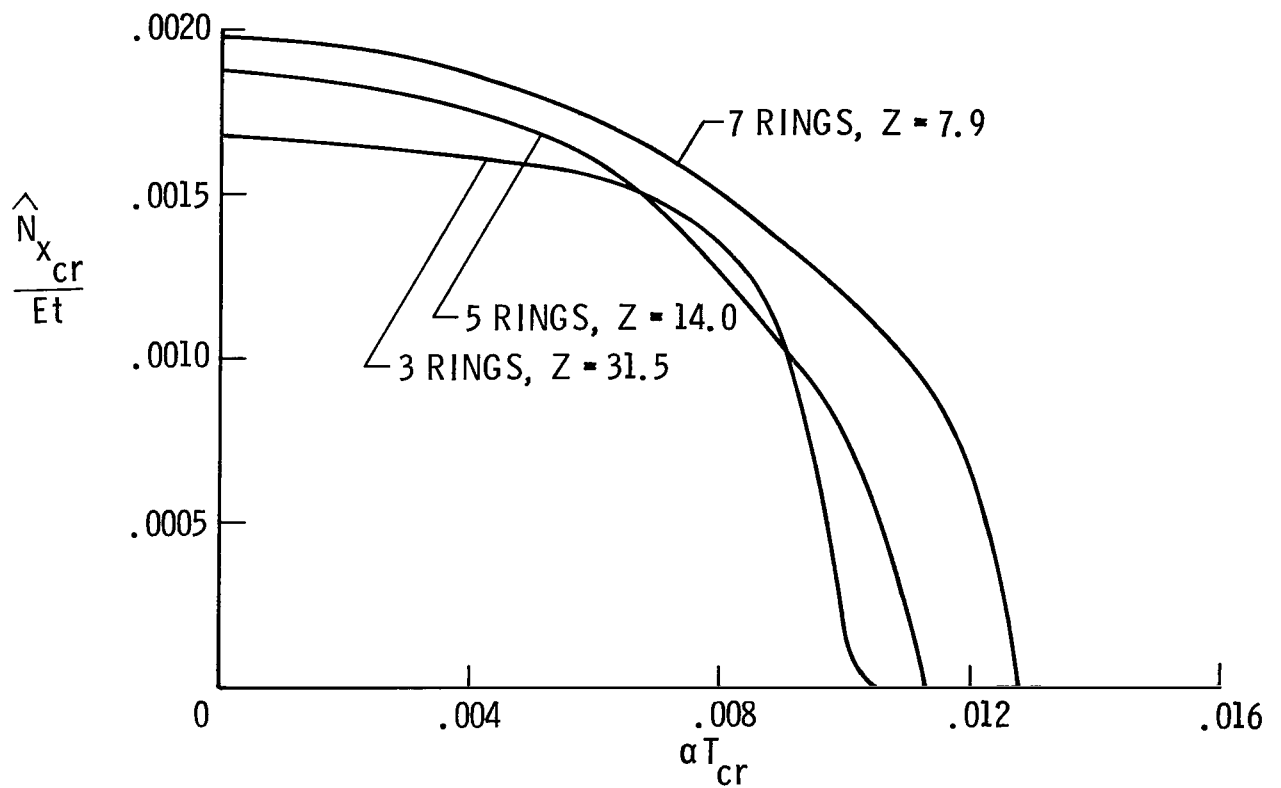
Figure 4.- Buckling interaction curve for ring-stiffened cylinders under combinations of axial, compressive, and thermal loadings.

INTERNAL STRINGERS

95
(241)

396
(1006)

OVERALL GEOMETRY

R = 198 (503)

6.25
(15.88)

0.22
(0.56)

0.163
(0.414)

1.687
(4.285)

STRINGER DETAIL
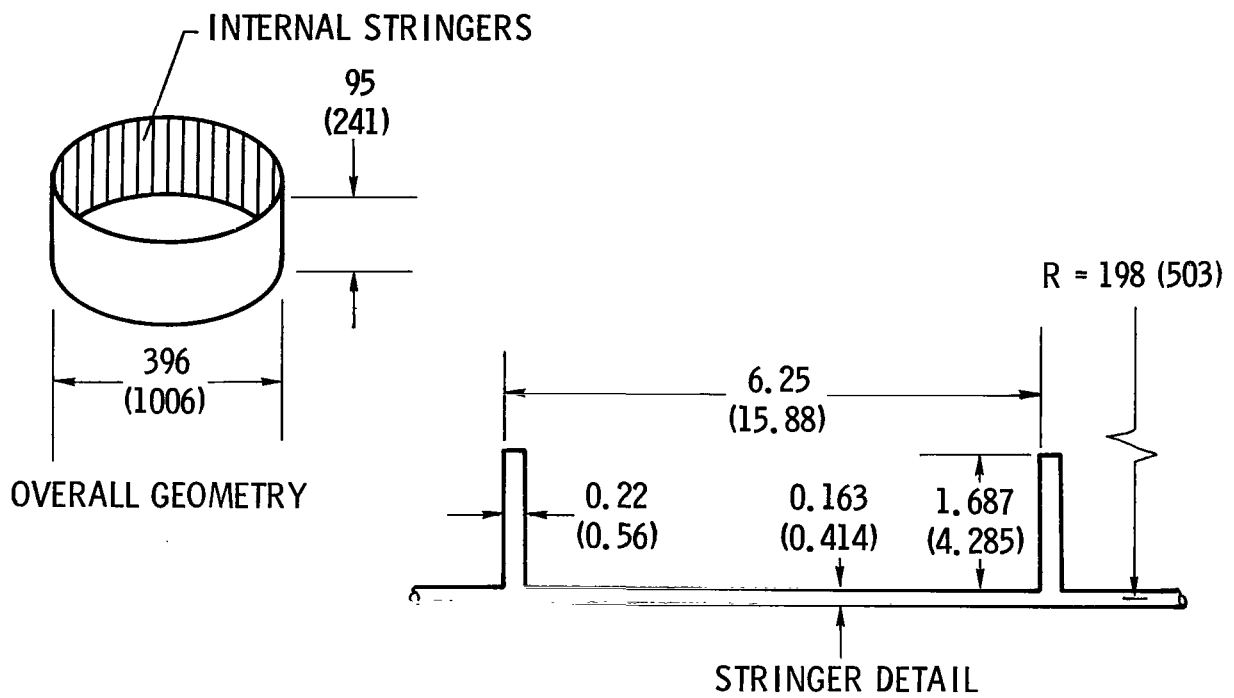
Figure 5.- Geometry of stringer-stiffened cylinder from references 23 and 24.
Dimensions are in inches (cm).
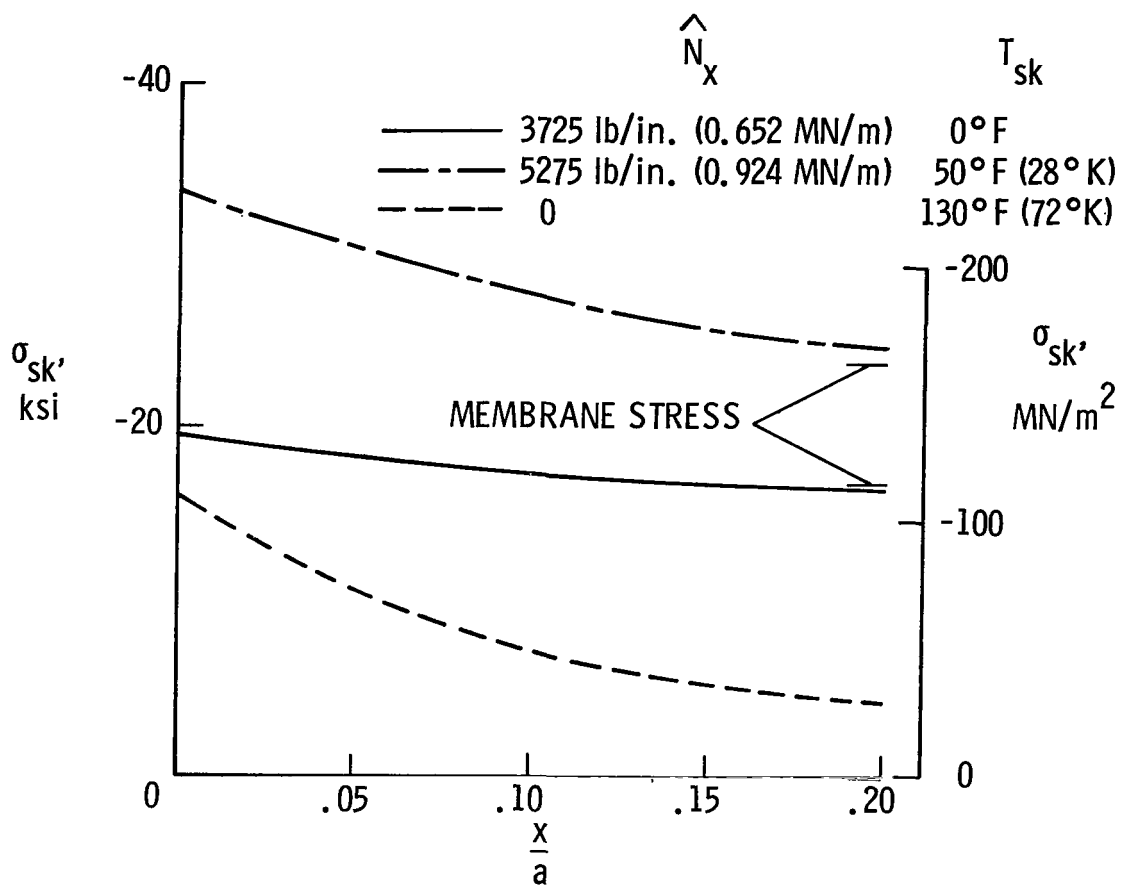
(a) Longitudinal skin stress.

Figure 6.- Stress distribution in clamped stringer-stiffened cylinder under
combinations of axial compression and thermal loadings. (Negative sign
on stresses denotes compression.)
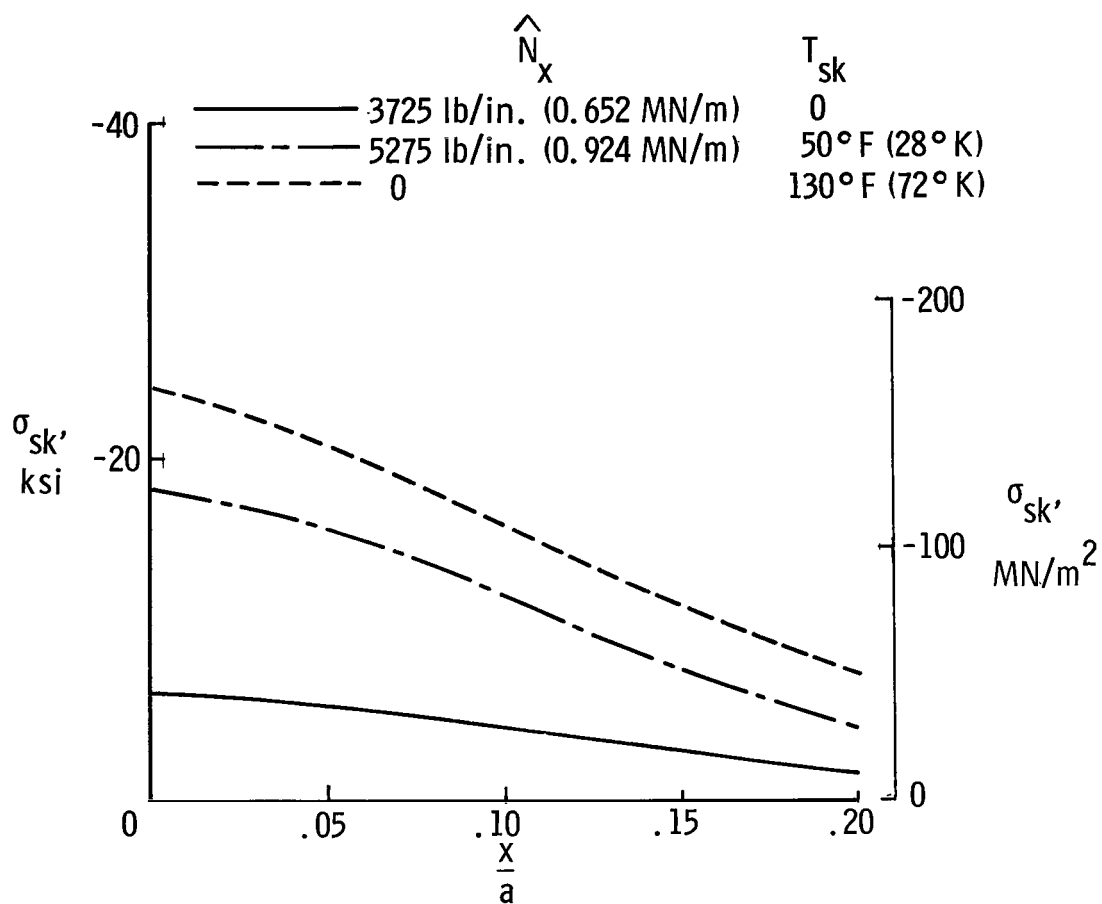
(b) Circumferential skin stresses.

Figure 6.- Continued.
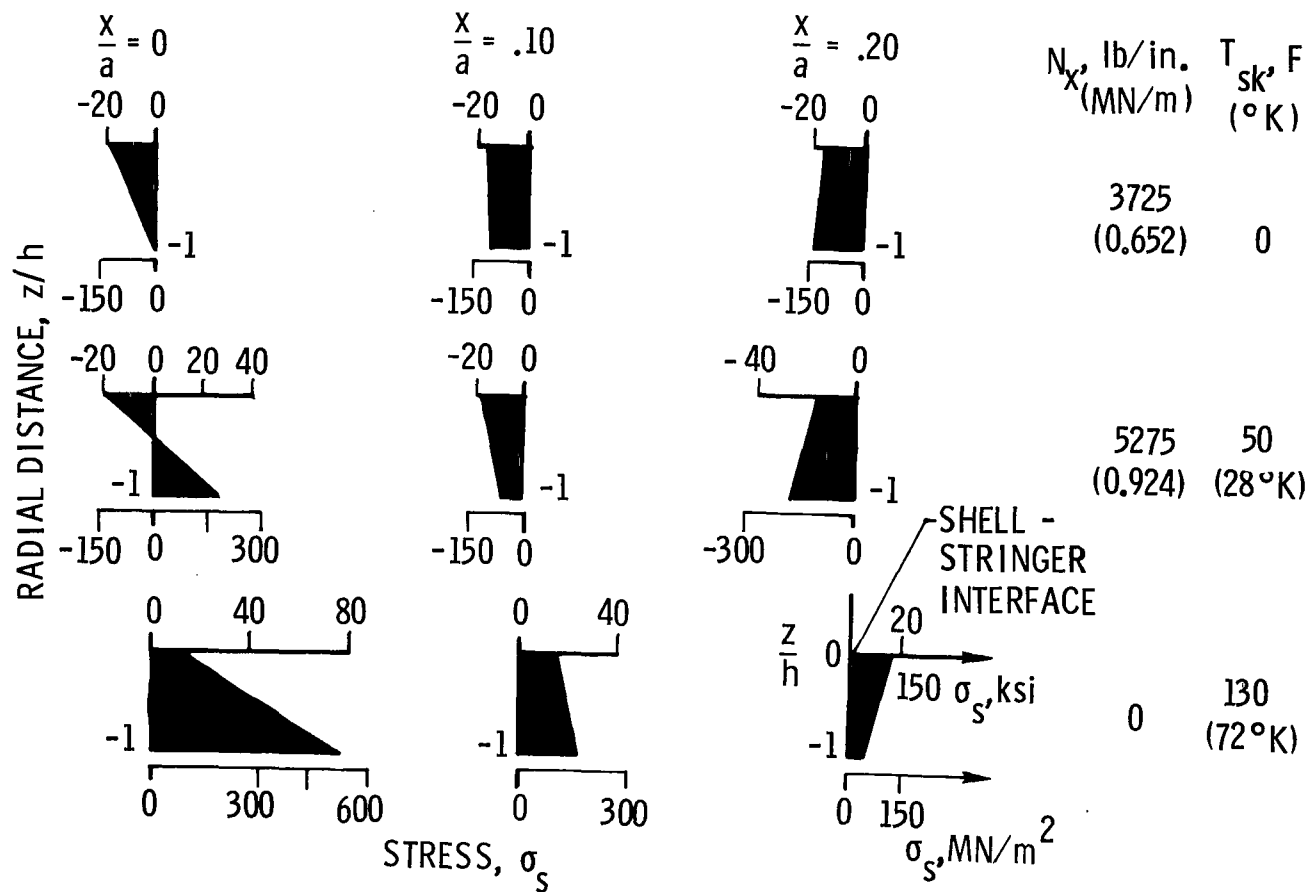
(c) Stringer stresses.

Figure 6.- Concluded.
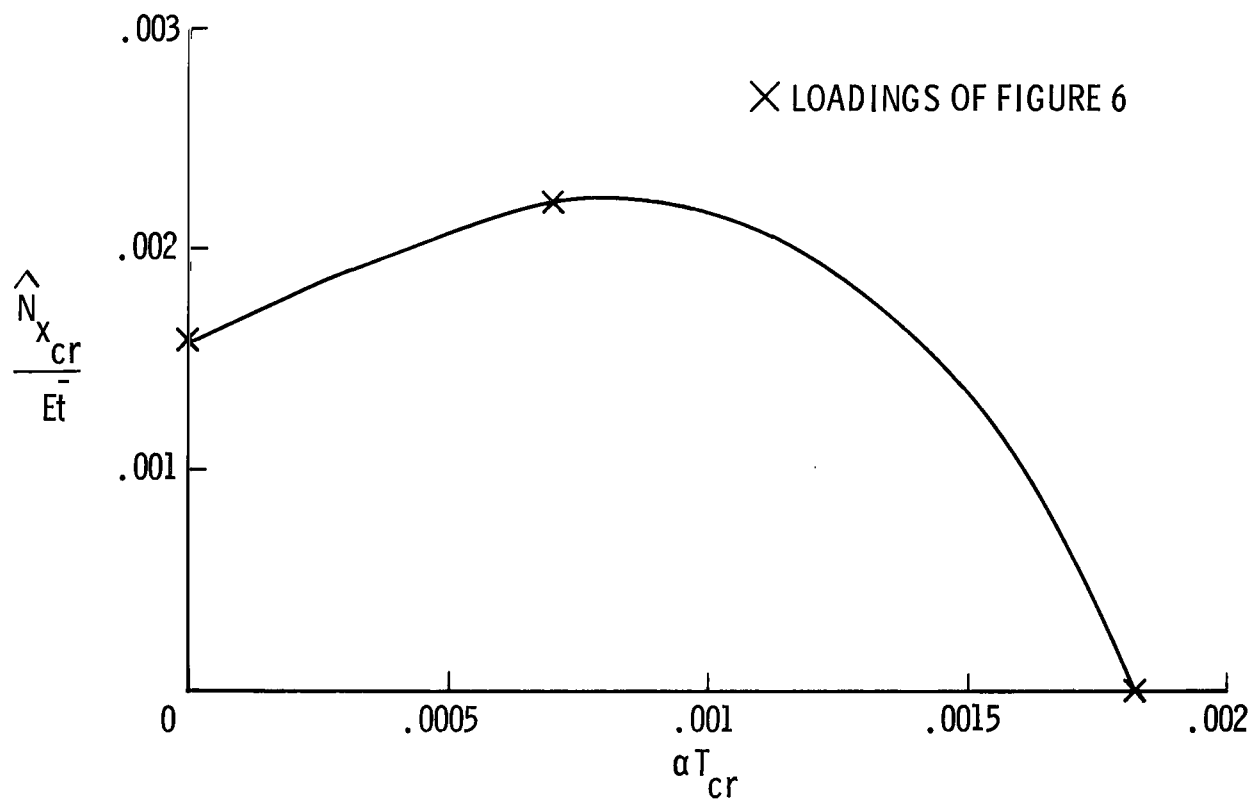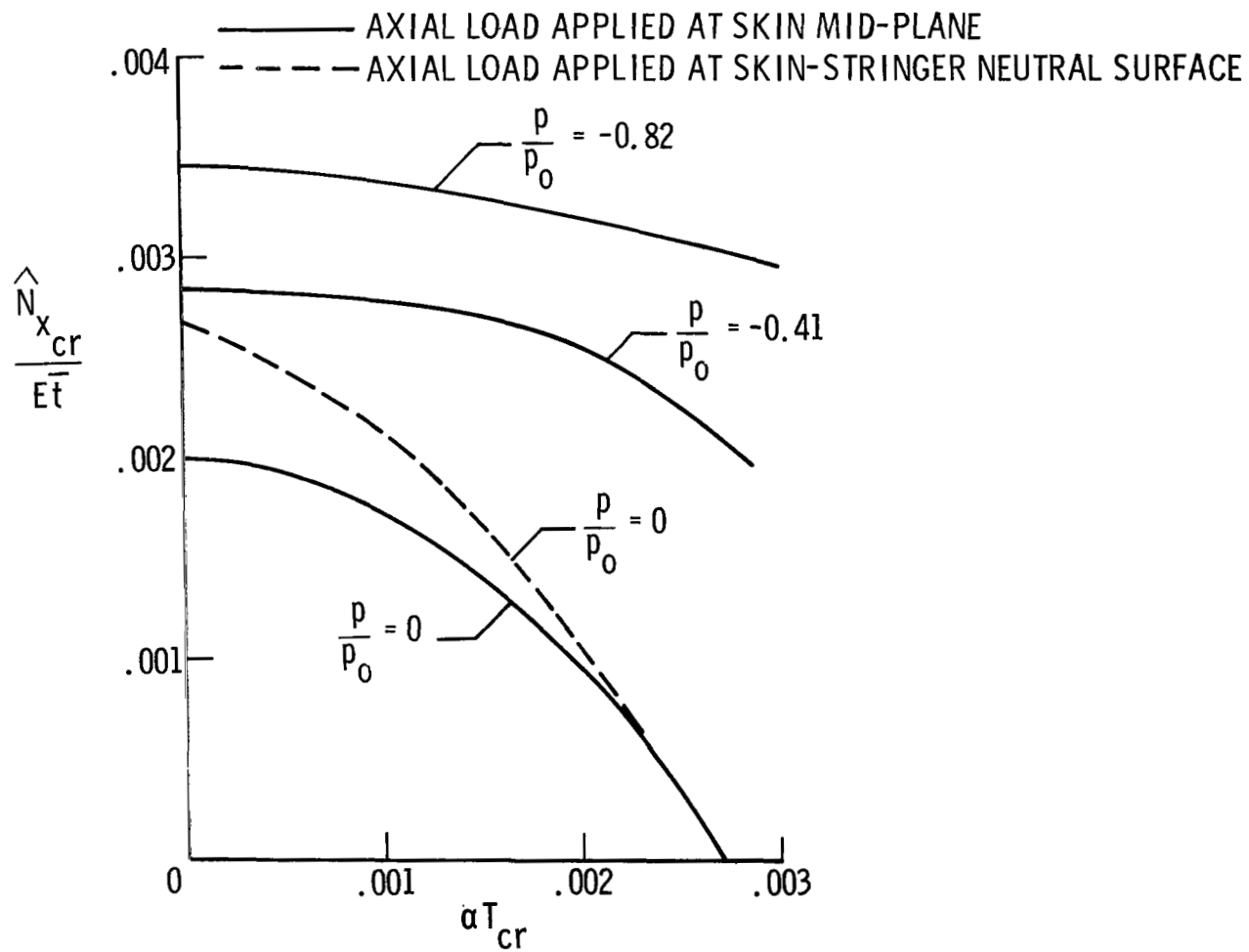
Figure 7.- Buckling interaction curve for clamped stringer-stiffened cylinder under combinations of axial, compressive, and thermal loadings.
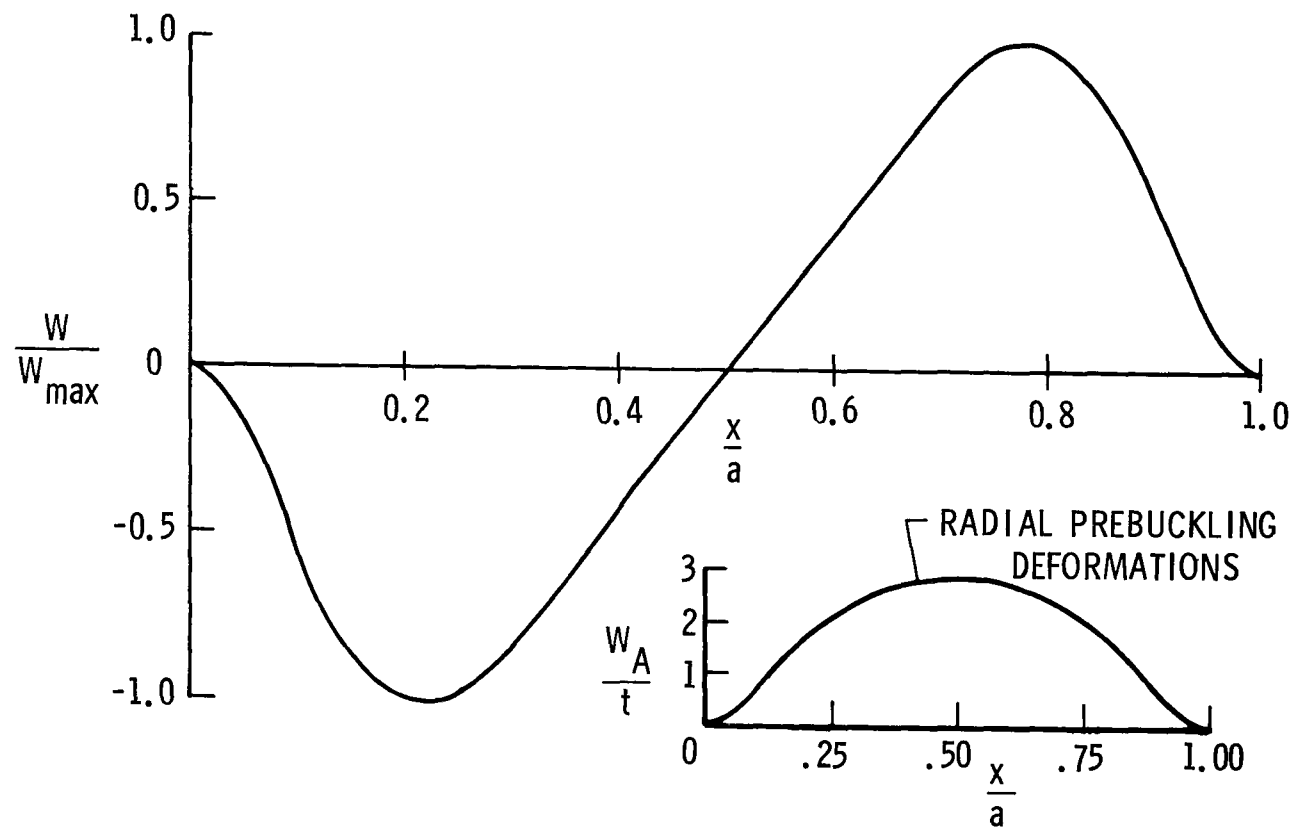
Figure 8.- Radial buckling deformation for thermally loaded stringer-stiffened cylinder.
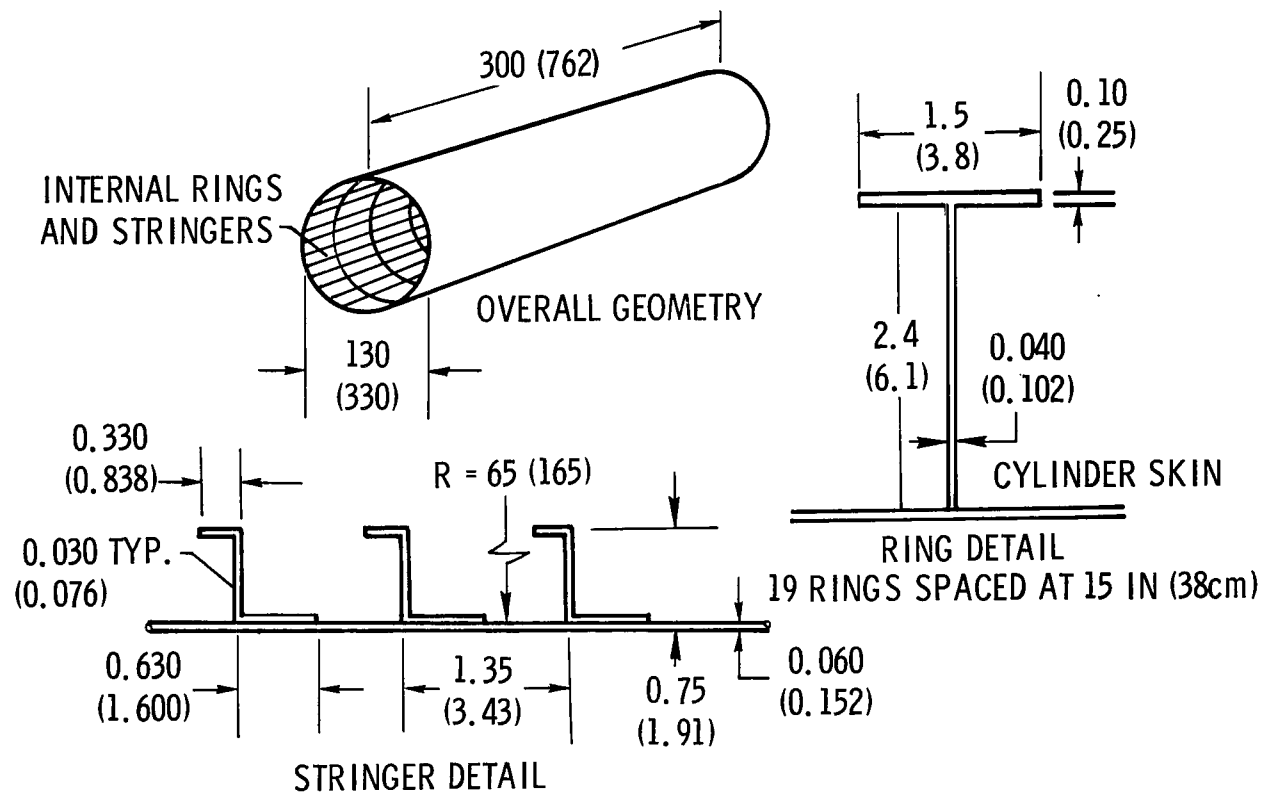
Figure 9.- Geometry of ring- and stringer-stiffened cylinder. Dimensions are in inches (cm).
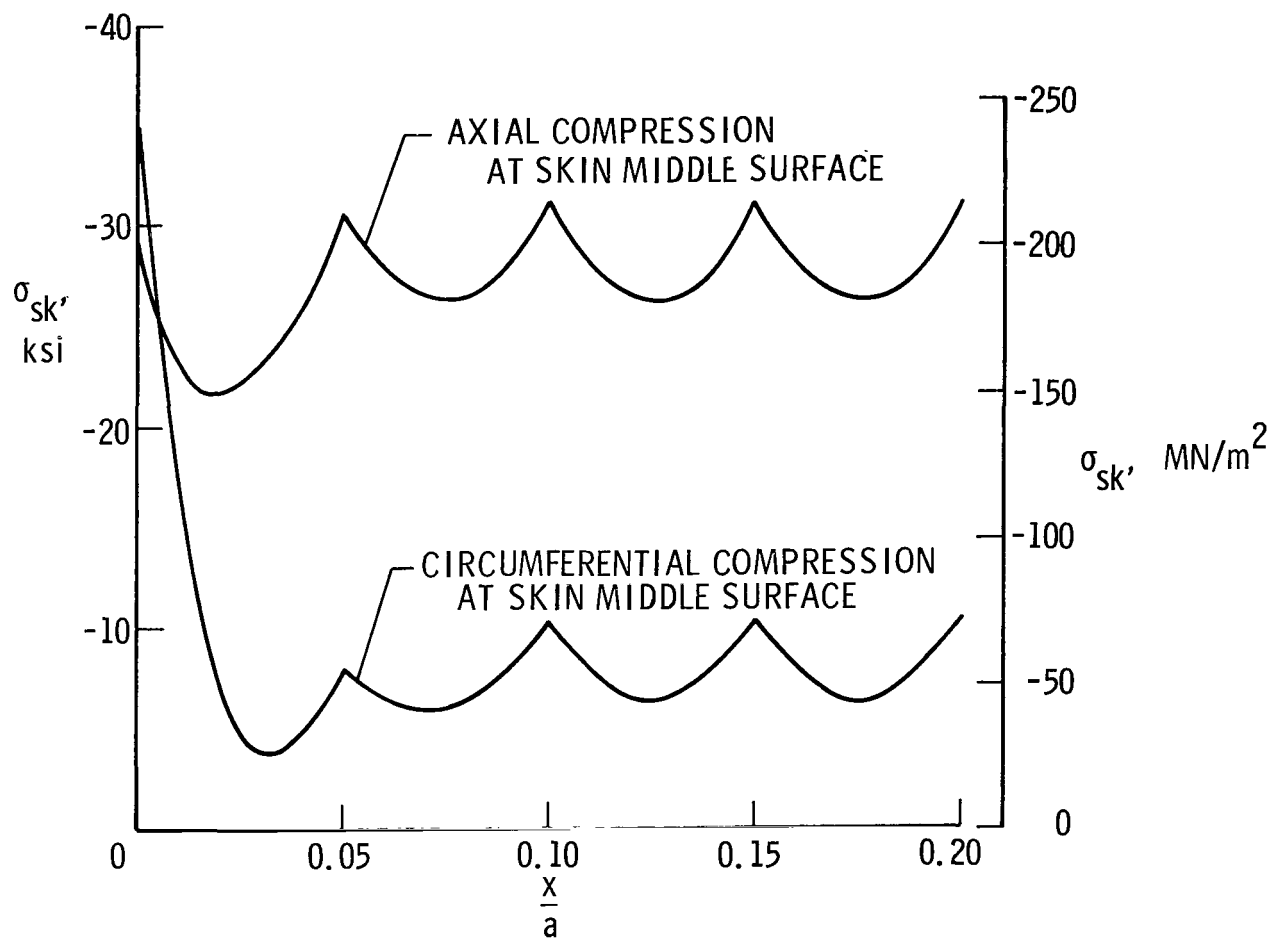
(a) Skin stresses.

Figure 10.- Stress distribution in simply supported ring- and stringer-stiffened cylinder under a combination of axial compression and temperature $\left(\hat{N}_x = 1650 \text{ lb/in., } 0.289 \text{ MN/m}; \quad T_{sk} = 360^{\circ} \text{ F, } 200 \text{ K}\right).$
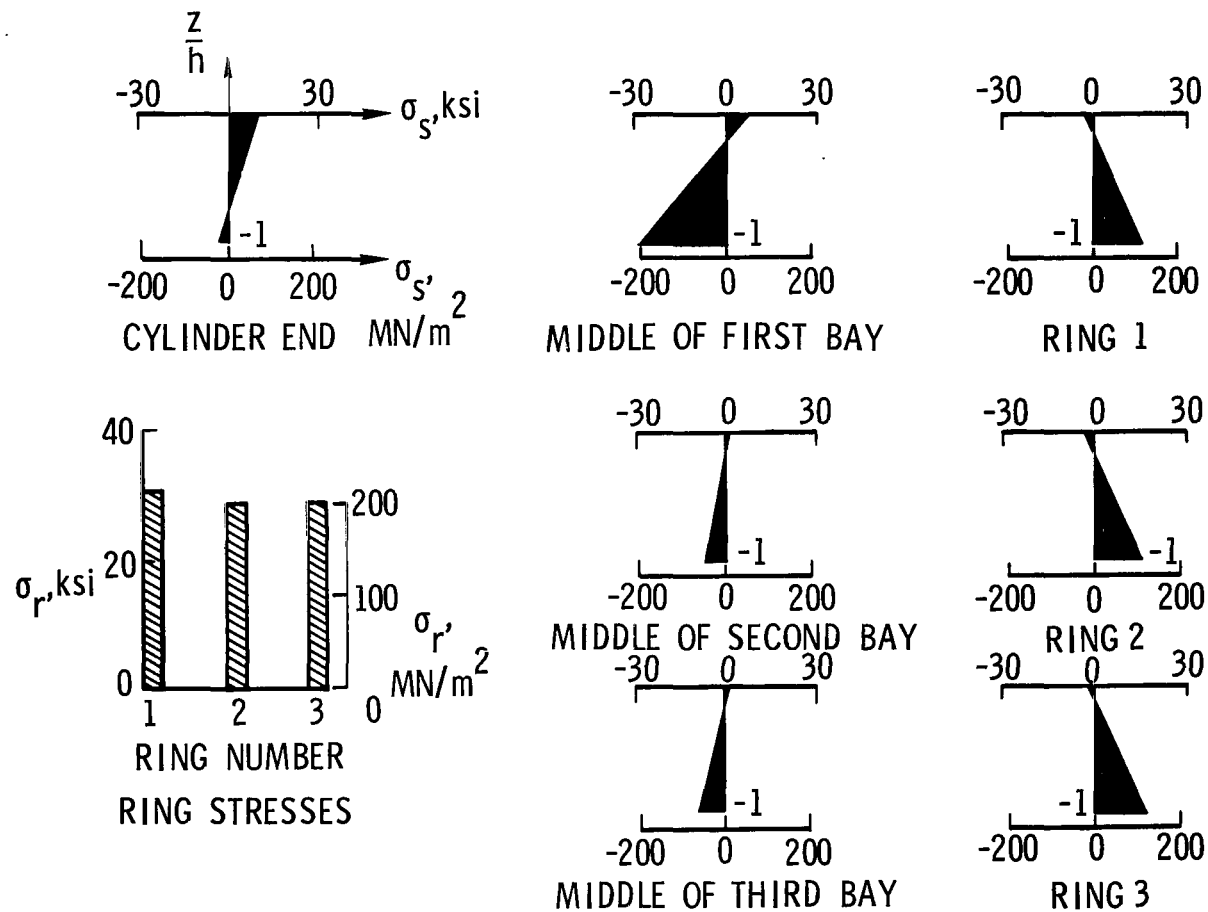
(b) Stiffener stresses.

Figure 10.- Concluded.

Figure 11.- Buckling interaction curve for simply supported ring- and stringer-stiffened cylinder under combinations of axial compressive, thermal, and pressure loadings.
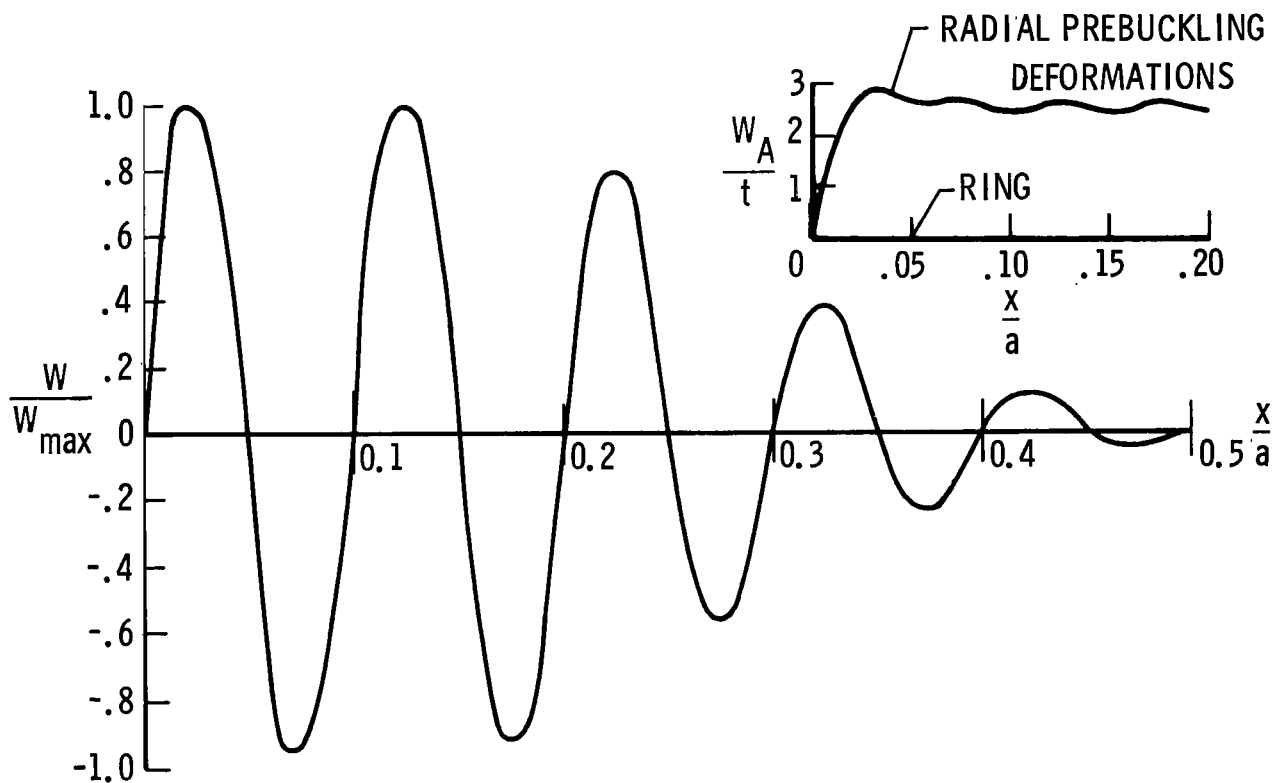
Figure 12.- Radial buckling deformation in thermally loaded ring- and stringer-stiffened cylinder.

11U 001 57 51 3DS   71.10   00903
AIR FORCE WEAPCNS LABORATCRY /WLOL/
KIRTLAND AFB, NEW MEXICO   87117

ATT E. LOU BOWMAN, CHIEF,TECH. LIBRARY

"The aeronautical and space activities of the United States shall be conducted so as to contribute . . . to the expansion of human knowledge of phenomena in the atmosphere and space. The Administration shall provide for the widest practicable and appropriate dissemination of information concerning its activities and the results thereof."

— NATIONAL AERONAUTICS AND SPACE ACT OF 1958

NASA SCIENTIFIC AND TECHNICAL PUBLICATIONS

TECHNICAL REPORTS: Scientific and technical information considered important, complete, and a lasting contribution to existing knowledge.

TECHNICAL NOTES: Information less broad in scope but nevertheless of importance as a contribution to existing knowledge.

TECHNICAL MEMORANDUMS: Information receiving limited distribution because of preliminary data, security classification, or other reasons.

CONTRACTOR REPORTS: Scientific and technical information generated under a NASA contract or grant and considered an important contribution to existing knowledge.

TECHNICAL TRANSLATIONS: Information published in a foreign language considered to merit NASA distribution in English.

SPECIAL PUBLICATIONS: Information derived from or of value to NASA activities. Publications include conference proceedings, monographs, data compilations, handbooks, sourcebooks, and special bibliographies.

TECHNOLOGY UTILIZATION PUBLICATIONS: Information on technology used by NASA that may be of particular interest in commercial and other non-aerospace applications. Publications include Tech Briefs, Technology Utilization Reports and Technology Surveys.

Details on the availability of these publications may be obtained from:

SCIENTIFIC AND TECHNICAL INFORMATION OFFICE

NATIONAL AERONAUTICS AND SPACE ADMINISTRATION
Washington, D.C. 20546